

Riikka Korpi

NANOPARTICLES AS MAGNETIC RESONANCE IMAGING CONTRAST AGENTS

*FEASIBILITY STUDIES ON CELL LABELLING, ACUTE
MYOCARDIAL INFARCT IMAGING AND ARTICULAR
CARTILAGE IMAGING*

UNIVERSITY OF OULU;
UNIVERSITY OF OULU, FACULTY OF MEDICINE;
MEDICAL RESEARCH CENTER OULU;
OULU UNIVERSITY HOSPITAL;
ÅBO AKADEMI UNIVERSITY



ACTA UNIVERSITATIS OULUENSIS
D Medica 1572

RIIKKA KORPI

**NANOPARTICLES AS MAGNETIC
RESONANCE IMAGING CONTRAST
AGENTS**

Feasibility studies on cell labelling, acute myocardial
infarct imaging and articular cartilage imaging

Academic dissertation to be presented with the assent
of the Doctoral Training Committee of Health and
Biosciences of the University of Oulu for public defence
in the Helene Schjerfbeck auditorium (Hotel Kämp,
Helsinki) on 22 May 2020, at 12 noon

UNIVERSITY OF OULU, OULU 2020

Copyright © 2020
Acta Univ. Oul. D 1572, 2020

Supervised by
Professor Roberto Blanco Sequeiros
Professor Miika Nieminen
Professor Petri Lehenkari

Reviewed by
Docent Mikko Kettunen
Docent Pekka Niemi

Opponent
Sami Kajander

ISBN 978-952-62-2612-5 (Paperback)
ISBN 978-952-62-2613-2 (PDF)

ISSN 0355-3221 (Printed)
ISSN 1796-2234 (Online)

Cover Design
Raimo Ahonen

PUNAMUSTA
TAMPERE 2020

Korpi, Riikka, Nanoparticles as magnetic resonance imaging contrast agents. Feasibility studies on cell labelling, acute myocardial infarct imaging and articular cartilage imaging

University of Oulu; University of Oulu, Faculty of Medicine; Medical Research Center Oulu; Oulu University Hospital; Åbo Akademi University

Acta Univ. Oul. D 1572, 2020

University of Oulu, P.O. Box 8000, FI-90014 University of Oulu, Finland

Abstract

Acute myocardial infarction (AMI) and osteoarthritis (OA) are both diseases of tissues with poor regenerative capacities. Stem cell therapies administered post-AMI have shown therapeutic potential. With the previously used approaches, the engraftment of the cells in the myocardium has been low and the mechanisms behind the observed therapeutic effects are thought to involve multifactorial processes. It has been hypothesized that the earliest biochemical changes, mainly proteoglycan depletion, of OA, might be reversible. Delayed gadolinium-enhanced magnetic resonance imaging of cartilage (dGEMRIC) has been shown to be a sensitive way to assess proteoglycan depletion in OA, however the use of gadolinium has now raised safety concerns.

Magnetic resonance (MR) imaging is currently the preferred method for assessing the label *in vivo*. The label contrast is attributable to the high magnetic moment of the label which shortens the T_1 and T_2 relaxation times. Superparamagnetic iron oxide (SPIO) nanoparticles have shown some potential for stem cell labelling however there are interpretational challenges with the contrast and those labelling methods that are considered to be safe are time consuming.

The object of the present work was to develop labels and labelling methods for cellular MR imaging. The usability of a novel fast rotation incubation SPIO labelling method for labelling bone marrow mononuclear cells (BMMNC) and the evaluation of cell homing in an experimental AMI model were studied. The labelling method appeared to be feasible for acute phase cell tracking. The transplantation of BMMNCs seemed to improve the ejection fraction at three weeks' post-AMI.

Novel manganese oxide (MnO) labels were developed to overcome the signal interpretational problems associated with the SPIO label. Amorphous MnO (MnOx) was observed to have better relaxometric properties than crystalline MnO, although both compounds appeared to be safe, high in relaxivity and suitable for cellular imaging *in vitro*. The usability of MnOx in assessing the proteoglycan content in OA was investigated. The relaxation of MnOx seemed higher than the corresponding phenomenon with gadolinium and the behavior of MnOx was observed to mimic that of dGEMRIC.

In conclusion, both the novel fast labelling method and the novel label were demonstrated to be feasible and functional in these experimental models.

Keywords: acute myocardial infarction, articular cartilage, cell labeling, magnetic resonance imaging, nanoparticles, stem cell transplantation

Korpi, Riikka, Nanopartikkelit magneettikuvauksen varjoaineina. Käytettävyys solujen leimauksessa, akuutin sydänlihassinfarktin kuvantamisessa ja nivelruston kuvantamisessa

Oulun yliopisto; Oulun yliopisto, Lääketieteellinen tiedekunta; Medical Research Center Oulu; Oulun yliopistollinen sairaala; Åbo Akademi

Acta Univ. Oul. D 1572, 2020

Oulun yliopisto, PL 8000, 90014 Oulun yliopisto

Tiivistelmä

Akuutti sydäninfarkti ja artroosi ovat molemmat huonosti uusiutumiskykyisissä kudoksissa ilmeneviä tauteja. Kantasoluhoidot sydänlihassinfarktin jälkeen ovat osoittautuneet terapeuttisiksi. Solujen kudostegraation sijaan terapeuttinen vaikutus näyttää kuitenkin olevan monitekijäinen ja edelleen solujen kohtalo tunnetaan huonosti. Artroosin mekaaniset muutokset rustossa ovat palautumattomia, mutta on esitetty hypoteesi, että näitä edeltävät biokemialliset muutokset, pääasiassa proteoglykaanipitoisuuden lasku, olisi mahdollista parantaa. Magneettikuvaus käyttäen myöhäistä gadolinium-tehostusta on osoittautunut herkäksi menetelmäksi määrittää proteoglykaanipitoisuus rustossa. Nykykäsitetyksen mukaan lineaariset gadoliniumia sisältävät varjoaineet ovat kuitenkin myrkyllisiä.

Magneettikuvaus on käytetty solukuvantamismenetelmä. Varjoaineen kontrasti perustuu aineen korkeaan magneettiseen momenttiin, mikä lyhentää T_1 ja T_2 aikaa. Rautaa sisältävät nanopartikkelit ovat osoittautuneet lupaavaksi varjoaineeksi, vaikkakin niiden tiedetään aiheuttavan tulkinnan vaikeutta T_2 relaksaatioaikaa lyhentävien elimistön omien prosessien kanssa. Lisäksi, leimamenetelmät ovat aikaa vieviä.

Työn tavoitteena oli kehittää solukuvantamisen varjoaineita ja leimausmenetelmiä. Uuden nopean leimausmenetelmän käytettävyyttä kantasolujen leimaukseen ja käytettävyyteen kokeellisessa sydäninfarktimallassa tutkittiin. Menetelmä vaikutti turvalliselta ja näytti soveltuvan akuuttivaiheen siirrettyjen solujen havainnointiin. Soluhoidetuilla eläimillä sydämen iskutilavuus parani kolmen viikon kohdalla sydäninfarktista.

Uusi mangaania sisältävä varjoaine kehitettiin tarkoituksena voittaa rautaa sisältävän varjoaineen tulkinnan päällekkäisyydet. Amorfinen mangaanioksidi vaikutti relaksaatiometrisiltä ominaisuuksilta käytetympää kiteistä muotoa paremmalta, relaksiivisuudeltaan korkealta ja turvalliselta. Leimatut solut olivat havaittavissa sekä 3 T että 7.1 T. Amorfisen mangaanioksidin käytettävyyttä proteoglykaanimäärän arvioimiseksi nivelrustossa tutkittiin. Mangaanin relaksiivisuus oli korkeampi kuin gadoliniumin ja käyttäytyminen muistutti gadolinium-mallin käytöstä nivelrustossa.

Molemmat kehitellyt leima-aine ja leimamenetelmä vaikuttivat lupaavilta soluleimaukseen ja molemmat vaikuttivat turvallisilta ja käyttökelpoisilta käytetyissä koasetelmissa.

Asiasanat: akuutti sydäninfarkti, kantasolusiirto, magneettikuvaus, nanopartikkeli, nivelrusto, soluleimaus

To P.K. and J.K.

Acknowledgements

The study was carried out at the department of Radiology, Institute of Medicine, University of Oulu, Finland, during the years 2008-2019.

I wish to express my most sincere gratitude to my supervisor Prof. Roberto Blanco Sequeiros, M.D., Ph.D. for his guidance, valuable advice and support. Not once during all these years did he discourage me. For the positive example he has shown I am the most thankful. To my co-supervisors Prof. Miika Nieminen, Ph.D. and Prof. Petri Lehenkari, M.D., Ph.D., thank you for jumping in during the late stage and thank you for the support, valuable advice, and challenges.

Thank you to the official reviewers of the thesis, Dos. Pekka Niemi, M.D., Ph.D. and Dos. Mikko Kettunen, Ph.D. for the careful revision of the manuscript, valuable comments and good discussion, and to Ewen MacDonald for his careful revision of the language. Thank you to my follow-up group members Dos. Jaakko Niinimäki, M.D., Ph.D. and Dos. Risto Ojala, M.D., Ph.D. for the time and effort you put into helping me to complete this thesis.

Sincere thank you to Dos. Ville Telkki, Ph.D. for the good advice, valuable comments and pure help. Thank you to the research group of Dos. Tatu Juvonen, M.D., Ph.D. and Dos. Vesa Anttila, M.D., Ph.D. for assistance and support, and for letting me to sneak in a bit. My most sincere thank you there is assigned to Kirsi Kujanpää, M.D., Ph.D. for sharing the struggles during the years. Sincere thank you to Prof. Jessica Rosenholm, Ph.D. and to Eveliina Lammentausta, Ph.D. for the endless help and high expertise. Sincere thank you to Elisa Lappi-Blanco, M.D., Ph.D. and Siri Lehtonen, Ph.D. for their expertise and assistance. All co-authors and collaborators are gratefully acknowledged for their contribution to this project. I wish to thank the Department of Radiology for providing such excellent research facilities.

I wish to thank the research group of Prof. George Sandor, M.D., D.D.S., Ph.D. for the joint research unfortunately on topics outside this thesis in the end, and for the high spirits. Sincere thank you to the previous and current colleagues in Helsinki for support, and also for understanding with extended specialization studies and multiple research vacations.

I wish to express my warmest gratitude to my family. Thank you to my dear mother and father, who share the silent understanding to the difficulties, aches, and the beauty of this profession, for the support during the journey of making this thesis. For the example they have shown me and the quiet support, I am beyond thankful. Thank you to my dear older siblings for support, and for making the

academic world as a norm. Thank you to my dear in-laws for listening and support. Thank you to our dear friends, who I am afraid are treated as an extended family in both good and bad, for sharing the pieces of our lives and theirs with us. To my dear husband and to our dear daughter, the deepest thank you. Thank you Jarkko for your love, understanding, and for oh so many good advice. You Pippa, are the most charming being, the beauty of my life. With you, I have paused to smell each flower on our way home and built a snowman when the snow has hardly touched the ground. You have taught *mamma* more than *mamma* ever has for you. Always be my dearest girl and the best friend. I love the two of you.

This study was financially supported by the Finnish Medical Foundation, The Finnish Association of Radiologists, and the Medical Faculty of the University of Oulu.

Helsinki, March 2020

Riikka Korpi

Abbreviations

AMI	acute myocardial infarction
BMMNC	bone marrow mononuclear cell
CLIO	cross-linked iron oxide
CX	circumflex coronary artery
DE	delayed enhancement
dGEMRIC	delayed gadolinium-enhanced magnetic resonance imaging of articular cartilage
EF	ejection fraction
FDA	U.S. Food and Drug Administration
Fe ³⁺	iron
FLAIR	fluid-attenuated inversion recovery
FOV	field of view
FSE	fast spin echo
GBCA	gadolinium based contrast agent
G-CSF	granulocyte colony-stimulating factor
Gd-DOTA	gadoterate
Gd-DTPA	gadopentetate dimeglumine
Gd ³⁺	gadolinium
GFP	green fluorescent protein
HE	hematoxylin-eosin
HEPES	4-(2-hydroxyethyl)piperazine-1-ethanesulfonic acid
HGF	hepatocyte growth factor
IFN- γ	interferon gamma
IGF-1	insulin-like growth factor-1
IL-1Ra	interleukin-1 receptor antagonist
iPSC	induced pluripotent stem cell
LV	left ventricular
MES	morpholine-4-ethanesulfonic acid
MI	myocardial infarction
MION	monocrystalline iron oxide nanoparticle
MnCl ₂	manganese chloride
Mn ²⁺	manganese
MnO	manganese oxide
MnOc	crystalline manganese oxide
MnOx	amorphous manganese oxide

MPIO	micron-sized paramagnetic iron oxide
MR	magnetic resonance
MSC	mesenchymal stem cell
NMR	nuclear magnetic resonance
NSF	nephrogenic systemic fibrosis
OA	osteoarthritis
OARSI	Osteoarthritis Research Society International
OD	optical density
PAA	poly(acrylic acid)
PBS	phosphate-buffered saline
PDGF	platelet-derived growth factor
PEG	polyethylene glycol
PG	proteoglycan
PMO	persistent microvascular obstruction
PVP	poly(vinyl pyrrolidone)
r	relaxivity
RF	radio frequency
ROI	region of interest
SE	spin echo
SPIO	superparamagnetic iron oxide
TE	echo time
TI	inversion time
TR	repetition time
T_1	longitudinal relaxation
T_2	transverse relaxation
T_2^*	transverse star relaxation
USPIO	ultra-small superparamagnetic iron oxide

List of original publications

This thesis is based on the following publications, which are referred to throughout the text by their Roman numerals:

- I Korpi, R., Alestalo, K., Ruuska, T., Lammentausta, E., Borra, R., Yannopoulos, F., Lehtonen, S., Korpi, J., Lappi-Blanco, E., Anttila, V., Lehenkari, P., Juvonen, T., & Blanco Sequeiros R. (2017) Two novel direct SPIO labels and in vivo MRI detection of labeled cells after acute myocardial infarct. *Acta Radiologica Open*, 6(8), 1-10.
- II Alestalo, K., Korpi, R., Mäkelä, J., Lehtonen, S., Mäkelä, T., Yannopoulos, F., Ylitalo, K., Haapea, M., Juvonen, T., Anttila, V., Lappi-Blanco, E., Blanco Sequeiros, R.*, & Lehenkari, P.* (2015) High number of transplanted stem cells improves myocardial recovery after AMI in a porcine model. *Scandinavian Cardiovascular Journal*, 49, 82-94.
- III Rosenholm, J., Korpi, R., Lammentausta, E., Lehtonen, S., Lehenkari, P., Niemi, R., Xiao, W., Zhang, J., Lindberg, D., Gu, H., Sahlgren, C., & Blanco Sequeiros, R. (2015) Novel, fast-processed crystalline and amorphous manganese oxide nanoparticles for stem cell labeling. *Inorganic Chemistry Frontier*, 2, 640-48.
- IV Korpi, R.*, Ahola, S.*, Behrouz, G., Lammentausta, E., Karhula, S., Saarakkala, S., Rieppo, L., Finnilä, M., Stapf, S., Rosenholm, J., Blanco Sequieros, R., Nieminen, M., & Telkki, V. Diffusion of amorphous manganese oxide nanoparticles into articular cartilage. *Manuscript*.

*Equal contribution

Contents

Abstract	
Tiivistelmä	
Acknowledgements	9
Abbreviations	11
List of original publications	13
Contents	15
1 Introduction	17
2 Review of the literature	19
2.1 Nanoparticles in magnetic resonance imaging.....	19
2.1.1 General aspects of contrast agents for MR imaging.....	19
2.1.2 The longitudinal relaxation (T_1) contrast agents	21
2.1.3 The transverse relaxation (T_2) contrast agents.....	24
2.1.4 Dual and other contrast agents.....	26
2.1.5 Techniques for stem cell labelling with magnetic nanoparticles.....	28
2.2 Acute myocardial infarction.....	29
2.2.1 Pathogenesis and pathophysiology of acute myocardial infarction	29
2.2.2 Stem cells in myocardial infarction.....	30
2.3 Osteoarthritis.....	40
2.3.1 Pathophysiology of osteoarthritis	40
2.3.2 MR imaging of proteoglycan content.....	41
3 Aims of the present study	45
4 Materials and methods	47
4.1 Study animals and human samples (I, II, IV).....	47
4.1.1 Porcine infarction model (I, II).....	48
4.1.2 Articular cartilage sample preparation (IV).....	48
4.2 Nanoparticles and cell labelling (I-IV).....	48
4.2.1 Preparation and characterization of nanoparticles (III)	49
4.2.2 Isolation and culturing of cells (I, II).....	49
4.2.3 Labelling of cells (I, II, III)	50
4.3 MR imaging and image analysis.....	51
4.3.1 Relaxivity measurements of nanoparticles in vitro (III, IV).....	51
4.3.2 MR imaging of nanoparticles in vitro (I, III).....	51
4.3.3 MR imaging of myocardial infarction (I, II)	52

4.3.4	Imaging of articular cartilage (IV).....	53
4.4	Echocardiography (II)	54
4.5	Biochemical analysis (I-II).....	54
4.6	Histopathology (I, II, IV)	55
4.6.1	Myocardial tissue samples (I, II)	55
4.6.2	Cartilage tissue samples (IV).....	55
4.7	Ethical considerations (I-IV).....	55
5	Results	57
5.1	Cellular proliferation of BMMNCs <i>in vitro</i> is not altered when labelling with SPIO using a rotation incubation method (I).....	57
5.2	Cellular relaxation values correlated with the SPIO label concentration <i>in vitro</i> (I).....	57
5.3	Spatial correspondence of labelled BMMNCs between MRI and histology were observed <i>in vivo</i> (I, II)	57
5.4	BMMNC transplantation seems to have a therapeutic effect after AMI <i>in vivo</i> (I, II).....	58
5.5	Characterization of manganese particles (III, IV)	59
5.6	Relaxiometric properties of amorphous MnO nanoparticles are displayed better than in crystalline MnO particles	60
5.7	The relaxivity of MnO _x is high and higher than the relaxivity of Gd-DTPA (IV).....	60
5.8	MnO _x diffuses faster than Gd-DTPA into the cartilage and the behaviour mimic dGEMRIC imaging.	60
6	Discussion	63
6.1	The role of cell tracking and experimental model in cellular treatment of AMI (I, II)	63
6.2	Amorphous manganese oxide as a contrast agent (III, IV)	67
6.3	Future aspects of nanoparticles	70
7	Summary and conclusions	73
	References	75
	Original publications	99

1 Introduction

Acute myocardial infarction (AMI) and osteoarthritis (OA) can be considered as examples of an acute and a chronic ulcer and share many similarities including low self-renewal capacity of the damaged tissues. Both diseases manifest typically in adulthood and are a significant burden to public health and are responsible for high costs. Regardless of the current therapies, AMI is the number one leading cause of mortality (Yusuf et al., 2017), while OA is one of the common diseases causing chronic pain and a major cause of disability (From Centers for Disease Control and Prevention, 1994; Felson et al., 1995; Losina et al., 2015). Regenerative stem cell therapies ideally should be able to restore the tissue however currently stem cell therapies post-AMI are considered to be therapeutic although they exert only a minor effect on the damaged tissue (Clifford, Fisher, Brunskill, Doree, Mathur, Clarke et al., 2012; Jeong et al., 2018; Ward, Abadeh, & Connelly, 2018). It would be beneficial to be able to track the post-transplantation fate of the cells in order to understand the mechanisms of the provided therapy and possibly to enhance it. Similarly, in osteoarthritis, the ability to monitor the early changes of the disease might enhance the current therapies or even achieve a curative treatment since it is known that the later structural changes of OA are incurable.

Magnetic resonance (MR) imaging is currently the pre-eminent non-invasive, non-toxic *in vivo* imaging method with superior endogenous tissue contrast. Paramagnetic or superparamagnetic nanoparticles possess a high magnetic moment which enables the shortening of the T_1 or T_2 relaxation time and thus enables additional contrast and allows them to be used as contrast agents for MR imaging (Han, Xu, Taratula, & Farsad, 2019). In general, nanoparticles are metal ions and thus toxic in their free ionic form and therefore typically they are bound into a chelate in biomedical imaging applications. Furthermore, surface modification may enhance their properties and these alterations allow for the development of numerous innovative applications.

In this work, the usability of nanoparticle labels for cell imaging and for imaging proteoglycan content was investigated. The usability of a novel fast superparamagnetic iron oxide (SPIO) labelling method for bone marrow mononuclear cell (BMMNC) labelling and cell tracking using MR imaging was assessed. The feasibility of novel amorphous and crystalline manganese oxide (MnO) labels for labelling mesenchymal stem cell (MSC) was studied. Moreover, the role of amorphous MnO in determining the proteoglycan content of articular

cartilage was investigated. Finally, the role of therapy with BMMNCs in an experimental AMI model was assessed.

2 Review of the literature

2.1 Nanoparticles in magnetic resonance imaging

2.1.1 General aspects of contrast agents for MR imaging

Magnetic resonance imaging, characterized by its good soft tissue contrast and spatial and temporal resolution, is based on the relaxation of spinning protons in an external magnetic field after they have been excited by a given radio frequency (RF) pulse (Han et al., 2019; Lauterbur, 1973; Odeblad & Lindstrom, 1955; Odeblad, Bhar, & Lindstrom, 1956). After the RF pulse, the realignment of the magnetic moment of proton nuclei to their original alignment, parallel to the external magnetic field, is called a longitudinal relaxation (T_1) (Estelrich, Sanchez-Martin, & Busquets, 2015). Simultaneously to T_1 relaxation, there is a transverse relaxation (T_2), which in turn characterizes the time taken for the in-phase magnetization of the proton nuclei, that occur in a perpendicular manner to the external magnetic field, to lose coherence after the given pulse. The T_2 relaxation time is determined by interactions of random fashion spinning proton nuclei. The time taken for dephasing may also depend on non-homogeneities of the external magnetic field and together these result in an even more rapid relaxation than pure T_2 spin-spin relaxation, a phenomenon referred to as transverse star relaxation (T_2^*). (Ridgway, 2010)

There are a few key elements that are important in determining a soft tissue contrast on MR image. Firstly, divergences in the hydrogen proton density in tissues, thus the amount of protons, result in differences in T_1 and T_2 relaxation times (Bottomley, *et al.*, 1984; Crooks, *et al.*, 1984; Fullerton, Potter, & Dornbluth, 1982, Kiviniitty, 1984). Secondly, given the nature of longitudinal and transverse relaxation parameters; in living tissue, the T_2 relaxation is much faster (Rumenapp, Gleich, & Haase, 2012). Thirdly, in MR imaging, there are subsequent RF pulses and therefore the relaxation rate of water protons before another RF pulse determines the signal intensity of the image. In other words, the molecules or tissues where protons may relax more rapidly before another RF pulse have a high T_1 signal intensity, thus appear as bright, on the T_1 MR image. Subsequently, tissues where protons do not reach relaxation before another RF pulse show the appearance of a lower signal intensity, i.e. they appear darker on the T_1 image. (Stephen, Kievit, & Zhang, 2011) On the contrary, because of the differences in relaxation physics,

a shorter T_2 relaxation time results in a decrease in the signal intensity in the T_2 image (Czeyda-Pommersheim, Martin, Costello, & Kalb, 2017). Furthermore, by using a computational contrast which makes it possible to select the favourable time points for image creation, then an additional endogenous contrast may be achieved, for example fat saturation and water sensitive sequences (Brateman, 1986; Moore & Chung, 2017; Yousaf, Dervenoulas, & Politis, 2018).

In order to achieve better differentiation of tissue pathology in the MR image a wide variety of contrast agents have been developed (Han et al., 2019). When using a contrast agent, the diseased tissue has to possess higher vascularity than the surrounding tissue or in some other way permit a higher uptake of contrast agent in order to stand out (Geraldès & Laurent, 2009). In molecular and cellular imaging, the cells or molecules of interest may be labelled with contrast agent before delivery to the host tissue to be distinguishable from surrounding tissue (Cromer Berman, Walczak, & Bulte, 2011). In MR imaging, the contrast enhancement can be achieved by reducing either to a greater extent of T_1 or T_2 relaxation. Those contrast agents that mainly shorten T_1 relaxation time are usually utilized to increase signal on MR images and therefore called as positive contrast agents. Similarly, the contrast agents that mainly shorten T_2 relaxation time are utilized to decrease signal on MR images and therefore called as negative contrast agents. (Shokrollahi, 2013).

Magnetic nanoparticles have unpaired electrons and possess a strong magnetic moment which allows them to be used as contrast agents for MR imaging (Cromer Berman et al., 2011). Nanoparticles can be characterized as either paramagnetic or super-paramagnetic according to their chemical properties (Shokrollahi, 2013). Other significant requirements for MR contrast agents when one is aiming at clinical use such as low toxicity, optimal dissolution or elimination, and good tolerance. Therefore, the paramagnetic metal ions, gadolinium (Gd^{3+}), manganese (Mn^{2+}), and iron (Fe^{3+}), agents that are highly toxic in their free ionic form can only be accepted when bound to chelate if they are to be used as a contrast agent (Bellin & Van Der Molen, A J, 2008; Bulte, J. W. & Kraitchman, 2004; Gilad et al., 2008). Furthermore, when trying to achieve multivalency, higher relaxivity, and/ or targeted drug or gene delivery, further coating and surface modification and encapsulation of the chelate compound have been developed (Veisèh, Gunn, & Zhang, 2010). The characteristic trajectory of an MR imaging contrast agent is presented in a pictorial form in figure 1.

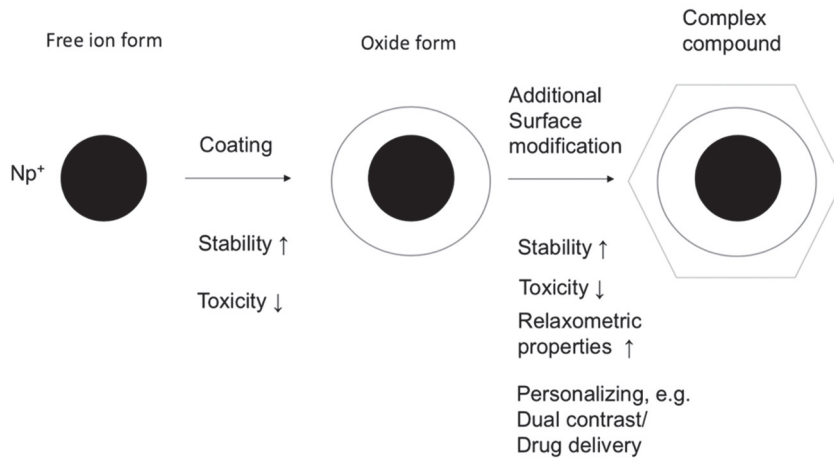


Fig. 1. Schematic illustration of the structural formation of an MR imaging contrast agent.

2.1.2 The longitudinal relaxation (T_1) contrast agents

Gadolinium based contrast agents

Gadolinium based contrast agents (GBCAs) accelerate T_1 relaxation and create a bright contrast in T_1 weighted images. GBCAs have been the most widely used T_1 contrast agents and several types of gadolinium chelates have been approved by the European Medicines Agency and the US Food and Drug Administration (FDA) for use as contrast agents in humans (Estelrich et al., 2015). Gadolinium chelates can be classified into linear and macrocyclic forms according to their ligands, the most usual compounds are gadopentetate dimeglumine (Gd-DTPA), which is a linear, and gadoterate (Gd-DOTA), which is a macrocyclic agent (Czeyda-Pommersheim et al., 2017). Furthermore, GBCAs can be classified based on their biodistribution into extracellular, hepatocyte-specific, and blood-pool agents (Aime & Caravan, 2009). These agents differ in terms of tissue behavior, their plasma half-life, and excretion. Most GBCAs are considered as non-specific agents because due to their low molecular weight they leak rapidly from the vascular space to the extravascular

space. They are eliminated through the kidneys with a half-life of 1.5 hours in patients with normal renal function (Bellin & Van Der Molen, A J, 2008). The rapid plasma half-life excludes their application in long-term cellular or molecular tracking studies (Estelrich et al., 2015).

Blood-pool agents created for vascular imaging, have slower extravasation from the vascular space because they have a larger molecular size due to their complexation with polymers and because they non-covalently bind with serum albumin (Estelrich et al., 2015). They are excreted primarily through the kidneys, however with longer plasma half-lives because of interactions with albumin (Czeyda-Pommersheim et al., 2017).

Hepatobiliary agents are designated according to their name, for hepatobiliary imaging and are based on the uptake of the contrast agent by hepatocytes (Aime & Caravan, 2009). Up to half of the administered dose is excreted via hepatic clearance with the rest excreted through the kidneys (Czeyda-Pommersheim et al., 2017).

A prolonged plasma half-life, mostly because of renal insufficiency, is associated with gadolinium ion release from the chelating agent and is likely to be the major reason why these agents have been claimed to cause the development of nephrogenic systemic fibrosis (NSF) (Czeyda-Pommersheim et al., 2017). The disease has been linked to linear, and to a lesser extent also to macrocyclic GBCAs (Beam et al., 2017). The difference between the linear and the macrocyclic agents may be due to the fact that the macrocyclic agents appear to be more stable which reduces the chances for exposure to gadolinium ion and thus toxicity (Schmitt-Willich, 2007). In addition, GBCAs have been recently associated with the accumulation of gadolinium into the human brain, and again linear agents appear to be more of a risk (Kanda, Ishii, Kawaguchi, Kitajima, & Takenaka, 2014; Kanda, Oba, Toyoda, Kitajima, & Furui, 2016; Kanda et al., 2017; Radbruch et al., 2015; Radbruch, 2018). In contrast, this phenomenon has been observed also with patients with normal renal function (Murata, Murata, Gonzalez-Cuyar, & Maravilla, 2016). The effects of this type of accumulation are however unclear and at the present time, there are no publications depicting brain toxicity (Kanda et al., 2017). Furthermore, as with practically all medicines or exogenous substances administered into the human body, GBCAs may cause immediate hypersensitivity reactions and other side effects, although the incidence of this phenomenon appears to be low (Jung et al., 2012).

Manganese based contrast agents

Manganese accelerates to a greater extent T_1 relaxation time than T_2 relaxation time and similarly to gadolinium, provides a bright contrast on T_1 weighted MR images. The published literature describes a few approaches using manganese in its different forms as a contrast agent or a cell label. For example, manganese chloride (MnCl_2) has been used to study neural and brain function of both healthy and Parkinson's disease animals, to study cardiac function (Pelled, Bergman, Ben-Hur, & Goelman, 2007; Silva, Lee, Aoki, & Koretsky, 2004; Soria et al., 2011), and for labelling white blood cells *in vitro*, suggesting that MnCl_2 could be used to study cell migration (Aoki et al., 2006). Crystalline manganese oxide (MnO) nanoparticles encapsulated in a polyethylene glycol (PEG)-phospholipid shell have been used for cellular imaging of breast cancer cells of brain metastases in rats (Na et al., 2007), and for cellular labelling of rat glioma cells with a double-labelling design with SPIO (Gilad et al., 2008). Manganese nanoparticles, in the form of a PEGylated ultra-small MnO, have been studied for determining the diagnosis of malignancy (Huang, H. et al., 2015; Liu, Song, & Tang, 2013) or PEGylated KMnF_3 particles for contrast agent for *in vivo* brain imaging of mice (Liu et al., 2013).

While studies using MnCl_2 have focussed on the yet unresolved toxicity (Silva et al., 2004), MnO appears to be biocompatible and tolerable with respect to toxicity (Gilad et al., 2008; Na et al., 2007). However, those MnO nanoparticles which have been developed have faced some challenges with rather low relaxivity, which reduces the observed signal (Gilad et al., 2008; Na et al., 2007). PEGylated MnO has shown higher relaxivity and appears to be biocompatible and with low toxicity, but in its present form, it does not appear to be suitable for longer cellular tracking experiments as it is excreted from animals within 24 hours (Liu et al., 2013). Nonetheless, Huang et al. did remark on the good contrast and the suitability of PEGylated MnO for long-term tracking (Huang et al., 2015).

Further studies have examined novel manganese oxide forms, for example silica coated hollow MnO nanoparticles, which have achieved improvements in relaxivity (Bae et al., 2011; Kim et al., 2011; Shin et al., 2009), as well as in the toxicity rate (Kim et al., 2011), an improved payload of therapeutic agents (Bae et al., 2011; Shin et al., 2009), and long term viability (Kim et al., 2011).

In summary, the major benefits of MnO complexes appear to be their positive contrast ability and sufficient surface modification and apparently low toxicity. In addition, Mn^{2+} is able to enter cells through calcium channels and thus it can pass

through the blood brain barrier, which means that manganese complexes may have feasibility in neuroimaging applications (Estelrich et al., 2015). While advances are made in terms of both usability and safety, at present the published literature mainly describes novel methods with large variations in terms of both study designs and the used form of manganese nanoparticles.

2.1.3 The transverse relaxation (T_2) contrast agents

Ferromagnetic or superparamagnetic nanoparticles, characterized by their shortening of T_2 and T_2^* relaxation, have been used as negative contrast agents for over two decades, mainly for research purposes as cellular contrast agents (Bulte & Kraitchman, 2004). Other applications include identification of lymph nodes (Geraldes & Laurent, 2009; Heesackers et al., 2008), cancer cell detection (Bakhtiary et al., 2016) and drug delivery applications (Mahmoudi, Sahraian, Shokrgozar, & Laurent, 2011) to name only a few.

Superparamagnetic iron oxide nanoparticles

Superparamagnetic iron oxide nanoparticles can be divided into three subgroups according to their size: 1, superparamagnetic iron oxide (SPIO) particles; 2, ultra-small superparamagnetic iron oxide (USPIO) nanoparticles (Weissleder et al., 1990), which are both in the nanometer size range; and 3, micron-sized paramagnetic iron oxide (MPIO) nanoparticles (Shapiro, Skrtic, & Koretsky, 2005). The structure of these compounds contains a highly crystalline core including multiple Fe^{2+} and Fe^{3+} ions and a stabilizing coating substrate, most commonly dextran or carboxydextran, which are biodegradable through uptake by Kupffer cells and macrophages, i.e. the metabolism pathway of endogenous iron in humans (Weissleder et al., 1989). There have been a few FDA approved SPIO nanoparticles which have been used in imaging of the mononuclear phagocyte system, lymph node imaging, hepatocellular carcinoma imaging, and for cell labelling in humans (Thakor et al., 2016). Three dextran coated SPIO contrast agents were even recently briefly evaluated in clinical trials (de Vries et al., 2005; Karussis et al., 2010; Toso et al., 2008; Zhu, Zhou, & XingWu, 2006) before the substances were subsequently withdrawn from the market and from clinical use because of concerns over fatal anaphylaxis and potential toxicity (Estelrich et al., 2015). Currently, only ferumoxytol is an FDA approved SPIO label, however its use is restricted to the treatment of iron deficiency anemia in patients with renal failure (Thakor et al.,

2016). Furthermore, a solution of dextran-coated USPIO nanoparticles, ferumoxtran-10, which was previously withdrawn from the market, is now again in clinical use for diagnosing lymph node metastases by using magnetic resonance lymphography in patients with prostate cancer in the Netherlands (Fortuin et al., 2018), although it previously showed moderate false positive rates (Heesakkers et al., 2008; Heesakkers et al., 2009). Several other SPIO and USPIO solutions using dextran or carboxydextran have been developed, with some being commercially available for experimental use (Shokrollahi, 2013). There are other coating options e.g. polyethylene glycol (Basly, Felder-Flesch, Perriat, Pourroy, & Begin-Colin, 2011), polystyrene (Seymour, Schacht, & Duncan, 1991), and silica (Laurent et al., 2008). In addition, chitosan and polyethyleneimine are used for coating, however those substances are mainly used as delivery carriers or for targeted delivery (Veiseh et al., 2010). MPIOs coated with polystyrene, have displayed higher relaxivity as compared to nanometer sized SPIO particles (Hinds et al., 2003) and even have been demonstrated to be sufficiently sensitive to allow single cell detection both *in vitro* (Hinds et al., 2003; Shapiro et al., 2004; Shapiro et al., 2005) and *in vivo* in mouse/ rat brain (Heyn et al., 2006; Shapiro, Sharer, Skrtic, & Koretsky, 2006). However, polystyrene is not biocompatible (Seymour et al., 1991) and thus the use of MPIO is restricted to experimental settings. Nonetheless, by exploiting additional shell modifications, SPIO nanoparticles may be customised for further biological and targeting purposes (Veiseh et al., 2010).

In the design of a stem cell label, the effects of labeling with SPIO nanoparticles are rather well described in terms of cellular viability, migration, and differentiation capacity of labeled cells and in general SPIO labeling appears to be safe at clinically relevant doses (Arbab et al., 2003; Arbab et al., 2004; Frank et al., 2003; Kostura, Kraitchman, Mackay, Pittenger, & Bulte, 2004; Suzuki et al., 2007). The differentiation capacity of stem cells to the host tissue cell lineage/ lineages are of importance when designing stem cell therapy, and interestingly, the SPIO label has been found to block chondrogenesis of mesenchymal stem cells (Kostura et al., 2004). In another publication, *in vitro* SPIO labeling was shown to dose-dependently reduce osteogenesis and chondrogenesis of mesenchymal stem cells (Chen, Y. C. et al., 2010).

Other iron oxide contrast agents

In addition to SPIO particles, the published literature describes a few other ferrous contrast agents with preliminary promising results. Firstly, magnetite iron

nanoparticles (Fe_3O_4), which have initially displayed high relaxivity but also appreciable cytotoxicity (Rasouli et al., 2018; Wei et al., 2018). Secondly, cross-linked iron oxides (CLIOs) (Senpan et al., 2009) and monocrystalline iron oxide nanoparticles (MIONs), which in its smallest form ($<5\text{nm}$), has shown potential also as a positive contrast agent (Shen, Wu, & Chen, 2017). Other options include ferrites, where T_2 relaxivity of iron oxide nanoparticles is significantly enhanced by replacing one Fe^{2+} with a transition-metal dopant, usually manganese, nickel, or cobalt (Sun, S. et al., 2004). These agents appear to be biocompatible (Bauer & Schulten, 1992; Hadjipanayis et al., 2008) unlike metal-alloy metal nanoparticles, which possess significantly higher relaxivity than SPIO particles, but unfortunately also toxic or mutagenic (Maenosono, Suzuki, & Saita, 2008) at least if not further stabilized by an additional coating (Lacroix, Ho, & Sun, 2010).

Several disadvantages encountered when exploiting ferrous nanoparticles. Firstly, the susceptibility artifacts (Terreno, Castelli, Viale, & Aime, 2010) and also difficulties in distinguishing the signal from signals emitted by endogenous tissue components and from some pathological processes that result in a decreased signal such as hemorrhage or gas accumulation. Secondly, the misinterpretation challenges, i.e. whether the cells are alive or dead since SPIO particles remain in the immediate vicinity of dead cells before normal dead cell clear-out (Bulte, J. W., 2009). Thirdly, a restricted long-term detection of highly proliferating cells (Walczak, Kedziorek, Gilad, Barnett, & Bulte, 2007), and finally, a trend towards self-aggregation (Karimi, Karimi, & Shokrollahi, 2013).

2.1.4 Dual and other contrast agents

When developing a novel contrast agent for MR imaging, there is usually one or a few particular drawbacks in the current substances that the new agent tries to resolve. Gadolinium chelates are in clinical use and thus offer a point of reference. For example, one major limitation with gadolinium chelates is that they do not pass through the blood-brain-barrier without invasive techniques (Ding et al., 2010). Some new compounds can overcome this disadvantage, for instance gold nanoparticles that can pass through the blood brain barrier, (Meola, Rao, Chaudhary, Sharma, & Chang, 2018), or dual contrast agents, for example gadolinium chelate, coated with SPIO polymer which is being investigated as a possible contrast agent for brain tumour imaging (Yang, H. et al., 2011). However, more commonly, there are two aims for simultaneous T_1 and T_2 contrast: to resolve possible uncertain signals due to artefacts and to enable more than one substance to be tracked at the

same time. There are some novel stem cell labelling techniques being designed and reports of a few dual MR imaging contrast agent studies have been published. The advantages of dual contrast using the combination of SPIO and gadolinium chelates, have been evaluated in two studies; it was found that it was possible to distinguish living from dead cells (Ngen et al., 2015; Ngen, Kato, & Artemov, 2017), which is known to be difficult to achieve with the SPIO label (Bulte, J. W., 2009). A study examined gadolinium hybrid iron oxide nanocomposites; it was found that the labelling did not exert any significant effect on the viability, proliferation, or differentiation of mesenchymal stem cells *in vitro*, with a high T_1 and T_2 contrast in both *in vitro* and *in vivo* mice brain being observed (Zeng et al., 2016).

Magneto liposomes or micelles are often characterized as a distinct contrast agent group although in fact, they are typically encapsulated gadolinium chelates or SPIO/USPIO particles. In these amphiphilic molecular aggregates, the encapsulation should improve the biological stability (Bulte, J. W., de Cuyper, Despres, & Frank, 1999; Langereis, Geelen, Grull, Strijkers, & Nicolay, 2013). The research using liposomes or micelles has focused on targeted drug or gene delivery because of their advantages such as the straightforward means of surface modification and convenient preservation of pharmaceuticals, and the method has even reached clinical use as a way to improve drug delivery (Faria et al., 2013; German et al., 2015; Khaleghi, Rahbarizadeh, Ahmadvand, Malek, & Madaah Hosseini, 2016; Langereis et al., 2013; Martinez-Gonzalez, Estelrich, & Busquets, 2016; Soenen, Hødenius, & De Cuyper, 2009). Instead, there are only a few publications using liposomes which have focused on studying cell labelling and cell homing using a variety of cells, including endothelial cells, pancreatic islet cells, and hepatocellular cancer cells (Garcia Ribeiro, Ketkar-Atre et al., 2018; Garcia Ribeiro et al., 2018; Garcia Ribeiro, Gysemans et al., 2018; Soenen, Brisson et al., 2011; Soenen, De Meyer et al., 2011). Another study examined liposomes incorporating mesenchymal stem cell (MSCs) and progenitor cells (Ketkar-Atre et al., 2013). However, the study raised concerns about cell-contrast agent interactions that may lead to toxic responses. One concern related to micelles and liposomes is not the risk of coating the individual SPIO particles but instead with the formation SPIO particle agglomerates which would lessen the magnetic properties and alter the physiochemical features of the contrast agent (Dagata et al., 2008).

2.1.5 Techniques for stem cell labelling with magnetic nanoparticles

At present, no stem cells are transplanted with a label in clinical settings. Nonetheless, before the cell therapies can become clinical routine, it will be important to be able to have a capacity to track the cells. This will be crucial not only in understanding the therapeutic effect of transplanted cells in more detail and to evaluate therapy related effects but also to detect possible side-effects of the label or transplanted cells in the host tissue. Further, when developing a novel cell label, it is important to remember that if one wishes to fully understand the effects the label has on humans, it may still be necessary to monitor cells also *in vivo* in humans even though *in vitro* and *in vivo* studies have been conducted in laboratory animals. In this context, perhaps the most difficult perhaps even impossible task is to estimate the long-term effect of the compound as the life expectancy of humans is much longer than that of the laboratory-animals used in the initial studies. Further, when treatment should be initiated without delay, the labelling procedure should not postpone the treatment.

There are three different methods used for cellular labelling. A direct labelling, where a label is added to cells during their expansion in culture, and indirect labelling methods via a reporter gene, or a receptor. (Kircher, Gambhir, & Grimm, 2011). However, labelling cells by causing changes in the cell genome gives rise to concerns over safety and there are also ethical issues, and therefore the latter approach is less favourable for use in humans, and furthermore labelling via a receptor would require a specific cellular marker (Fu & Kraitchman, 2010). Therefore, despite the many potential advantages of indirect techniques i.e. long-term tracking of cells, evaluation of cell viability, cell migration, and possibly emerging cell populations (Kircher et al., 2011), the vast majority of cardiovascular *in vivo* studies have exploited direct techniques (Fu & Kraitchman, 2010). During the incubation, the endocytosis of the contrast agent occurs when the cells are suspended in culture medium (Hsiao et al., 2007; Yeh, Zhang, Ildstad, & Ho, 1993). The incubation process may be either too inefficient or too slow, but in these situations, the endocytosis process may be enhanced and hastened by the use of permeabilization agents, for example poly-L-lysine, lipofectamine, or protamine sulfate (Cromer Berman et al., 2011). In magnetofection, a cationic permeabilization agent makes possible an electrostatic interaction which increases the amount of contrast agent crossing the cell membrane (Wang & Jøkerst, 2016). However, these agents might be toxic (Arbab et al., 2004) and furthermore, the labelling times may last up to 48h. (Fu & Kraitchman, 2010). Alternatively, the

endosomal uptake of the label may be enhanced and speeded up by electroporation, which involves the application a low voltage (Walczak, Kedziorek, Gilad, Lin, & Bulte, 2005; Walczak et al., 2006).

2.2 Acute myocardial infarction

2.2.1 Pathogenesis and pathophysiology of acute myocardial infarction

According to the World Health Organization, an acute myocardial infarction, the leading cause of morbidity and mortality worldwide (Yusuf et al., 2017), is defined as “*myocardial cell necrosis due to significant and sustained ischemia*” (Mendis et al., 2011). The pathogenesis may be characterized by an obstruction of a coronary artery or arteries often because of an obstructing plaque or plaques in an atherosclerotic coronary artery or arteries, thrombosis, or less frequently, a spasm in a plaque-free coronary artery or arteries (Mendis et al., 2011). The pathophysiology of AMI consists of a series of metabolically related diverse aetiologies which ultimately result in pathological hypertrophic remodelling (Hill & Olson, 2008). Briefly, the pathway can be described as a three-step cascade involving inflammation, cell proliferation, and remodelling phases. In these overlapping phases, cells undergo apoptosis and necrosis, various immunomodulatory responses and proinflammatory cytokine secretion, granular tissue formation and fibroblast proliferation, scar tissue formation, cardiomyocyte dysfunction, fibrosis and ventricular stiffening (Lister, Rayner, & Suuronen, 2016). The end results are left ventricular (LV) dilatation and impaired cardiac muscle contractibility, reduced left ventricular ejection fraction, and possibly even cardiac failure (Zamilpa, Navarro, Flores, & Griffey, 2014)(Lister et al., 2016).The term adverse LV remodelling refers to the resulting pathological changes (Lund et al., 2007; Pfeffer & Braunwald, 1990).

Magnetic resonance imaging in the myocardial infarction

Cardiovascular (MR) imaging is a good way to assess mechanisms and efficiency of novel cell therapies in the treatment of AMI, (Ahmed, Carrick, Layland, Oldroyd, & Berry, 2013; Bulluck, Dharmakumar, Arai, Berry, & Hausenloy, 2018) and is currently considered the gold-standard in evaluating the size of the myocardial

infarction (MI) (Schulz-Menger et al., 2013). The MI size is proposed to be associated only to some degree with adverse LV remodelling (Bulluck et al., 2017; Westman et al., 2016) but strongly associated with mortality (Stone et al., 2016). Furthermore, MR imaging makes it possible to assess other pathophysiological processes including haemorrhage and microvascular obstruction, which have a prognostic value when assessing adverse LV remodelling (Bulluck et al., 2017; Carberry et al., 2017; van Kranenburg et al., 2014). Myocardial salvage refers to the reversibly-injured myocardium and thus the myocardial salvage index is the ratio of myocardial salvaged area of the final area of infarcted myocardium (final infarct size – myocardial salvage/ final infarct size) and is considered a more sensitive measure than MI size alone for evaluating the outcome of novel therapies (Botker, Kalltoft, Pedersen, & Kim, 2012). However, there are a few challenges encountered when estimating the salvaged myocardium. During the first week after reperfusion of an AMI, myocardial oedema is considered to occur in both salvaged and infarcted myocardium (Dall'Armellina et al., 2011). Furthermore, there is currently no consensus either on which sequence should be used in evaluation of the oedema (Bulluck et al., 2018) or on the optimal timing of the MR imaging for determining the MI size or the area of salvaged myocardium (Fernandez-Jimenez et al., 2017). Cardiovascular MR sequences for evaluating the above-mentioned prognostic related variables are listed in table 1.

2.2.2 Stem cells in myocardial infarction

Characterization of stem cells

Traditionally, stem cells have been classified as either embryonic or adult stem cells or as pluripotent or multipotent according to their origin/ differentiation capacity. In simplified terms, stem cell therapies are based on self-renewal and the differentiation capacity of the cells possibly to achieve some regeneration of the damaged tissue. Induced pluripotent stem cells are reprogrammed so that they are embryonic-like but nonetheless, they are adult origin stem cells (Takahashi & Yamanaka, 2006) (Takahashi & Yamanaka, 2013). A general characterization of stem cells and their advantages and disadvantages concerning the AMI therapy are summarized in table 2.

Table 1. Cardiovascular MR sequences for evaluating prognostic related variables of AMI.

Variables	Pathophysiology	Conventional Imaging sequence	Optional sequence/ sequence under research	Appearance	Prognostic significance
MI size	The mass volume of infarcted myocardium	Delayed enhancement***	Native T1 mapping, Post-contrast T1 mapping***	Infarcted myocardium appears more hyperenhanced than well-perfused myocardium	↑
Microvascular obstruction	Inability of the coronary microcirculation to re-perfuse despite reperfusion of previously occluded vessel				↑
Early obstruction	Early obstruction	First-pass perfusion*, High T1, Early enhancement*	T2 mapping, Native T1 mapping, Early enhancement**, Post-contrast CINE**	Hypointense area within the infarcted area	
Late obstruction	Late obstruction	Delayed enhancement***		Hypointense core within the areas of hyperenhancement	Persistent microvascular obstruction is associated with adverse LV remodelling
Intramycocardial haemorrhage	Extravasation of red blood cells into the myocardium				
Myocardial oedema	Increased water content in the myocardium				

Variables	Pathophysiology	Conventional Imaging sequence	Optional sequence/sequence under research	Appearance	Prognostic significance
Area at risk	Irreversibly and reversibly injured myocardium supplied by the infarction-related artery	T2 mapping, T1 mapping	Early enhancement*, Post-contrast CINE, Early enhancement mapping****		
Extracellular volume fraction	Calculated by equation which uses haematocrit, native and postcontrast T1 of blood and myocardium	Early enhancement mapping**** (native+post-contrast T1 of blood and myocardium+haematocrit)			Persistent elevation is associated with adverse LV remodelling

(¹), delay after contrast agent administration <4 min; (**), delay after contrast administration 4-10 min; (***), delay after contrast agent administration 10-20 min; (****), nat+delay after contrast agent administration 10-20 min; (†), prognostic significance; (††), major prognostic significance. Modified from Bulluck et al., 2018.

Table 2. Characterization of stem cells and their feasibility for stem cell therapy of myocardial infarction.

Origin/ cell type	Isolated from	Differentiation capacity	Advantages for AMI therapy	Disadvantages for AMI therapy	Clinical AMI trials
Embryonic					
Embryonic stem cells	Inner cell mass of the blastocysts during embryonic development	Pluripotent	Pluripotent	Ethical, Political, Regulatory problems	Single
Progenitor cells					
Bone marrow mononuclear cells*	Bone marrow	Multipotent	Most studied, Therapeutic	Heterogeneous	Many
Hematopoietic stem cells	Bone marrow	Multipotent; hematopoietic lineages	Peripheral blood could offer easy isolation	Therapeutic effect unclear	A few
Stromal cells					
Mesenchymal stem cells	Various; often bone marrow and adipose tissue	Multipotent	Second most widely studied, Therapeutic, Immunomodulatory – allogenic use, Safe, Easy isolation	Poor post-engraftment and survival, Invasive harvesting	Many
Skeletal myoblasts	Muscle	Skeletal myoblasts	Easy isolation, Survival capacity	Differentiation, Non-therapeutic in clinical trials, Arrhythmias	Single

Origin/ cell type	Isolated from	Differentiation capacity	Advantages for AMI therapy	Disadvantages for AMI therapy	Clinical AMI trials
Endothelial progenitor cells	Hematopoietic and non-hematopoietic (vessel walls)	Mature endothelial cells	Isolation from peripheral blood, Enhance neovascularization, Reduced tumorigenicity risk	Requirement of large blood pool/ expanding, Cardiac enzyme elevation when mobilizing	Single
Cardiac stem cells	Atrial appendages, endo/epicardial biopsies, pericardial	Multipotent; cardiac lineages	Immunomodulatory, May allow for allogenic use, Superior differentiation to cardiac lineages	Invasive isolation, Low availability, Require expansion in culture, Costly	A few
Differentiated tissue					
Induced pluripotent stem cells	Various adult somatic tissues	Pluripotent	Embryonic like pluripotency	Potentially tumorigenic, Mutations, Teratoma formation	None

*, BMMNCs consist of hematopoietic stem cells, mesenchymal stem cells, endothelial progenitor cells, monocytes, and lymphocytes. Modified from Chong, Ng, & Chan, 2016; Madigan & Atoui, 2018; Singh, Singh, & Sen, 2016.

Stem cell delivery for cardiac therapy

Stem cell delivery to the injured site is a complex process that aims to combine accurate delivery without any damage to either host tissue or the delivered cells. There are various routes of delivery for cardiac therapy: 1, intracoronary; 2, intravenous; 3, intramyocardial, which can be subdivided into a catheter-based and to a direct surgical intramyocardial injection; 4, retrograde venous; and 5, bioengineered tissue transplantation (Sheng, Zhou, & Hao, 2013). The first three techniques have been used in clinical trials (Jeong et al., 2018), although there are some major advantages and disadvantages related to the techniques. The intracoronary infusion is feasible, mini-invasive, inexpensive, and results in the delivery of a homogenous cell population in the injured tissue but is associated with the potential risk for microemboli (Wang & Jakerst, 2016). Although the direct intramyocardial injection is considered the most accurate and may avoid the issues of homing and mobilization of cells which are associated in general with vascular approaches, it is invasive, requiring thoracotomy which has its own complications (Sheng et al., 2013). The catheter-based intramyocardial injection can be performed either through a transc coronary venous or a transendocardial approach. The advantages are the low-invasive protocol and it is suitable for high-risk patients but requires further imaging guidance to reach the injured site (Sheng et al., 2013). The intravenous injection is the least invasive, and it is very straightforward and repeatable, however it has been associated with a low delivery rate and potential of cell leakage to other organs and elimination by the reticuloendothelial system (Barbash et al., 2003).

Stem cell therapy in myocardial infarction

The mortality and morbidity from AMI is high even with the current medical therapy (Ward et al., 2018), which is intended to achieve revascularization (Reddy, Khaliq, & Henning, 2015). The high mortality is explained by the low self-renewal capacity of myocardial tissue (van Berlo & Molkentin, 2014). Stem cell therapies aim to regenerate the damaged tissue and achieve a structural remodelling of the myocardium. The therapeutic mechanism is thought to be multifactorial e.g. stem cell differentiation into cardiac cell lineages (Zamilpa et al., 2014), paracrine regulation (Dixit & Katare, 2015) (Madigan & Atoui, 2018), enhancement of neovascularization (Angoulvant, Fazel, & Li, 2004), and endogenous cardiac precursor cell stimulation (Vrijnsen et al., 2016).

In the published literature, there are both clinical and preclinical stem cell AMI studies which have utilized a variety of stem cell lineages (Jeong et al., 2018; Madigan & Atoui, 2018; van der Spoel, T I et al., 2011; Ward et al., 2018; Wollert et al., 2017). The cell lineages and their advantages and disadvantages are summarized in table 2. To date, most of the research has focused on two cell lineages; mesenchymal stem cells (MSCs) (Jeong et al., 2018); and bone marrow mononuclear cells (BMMNCs) (Clifford et al., 2012; Janssens et al., 2006; Wollert et al., 2016). BMMNCs consist of MSCs and hematopoietic stem cells (HSCs), monocytes, lymphocytes, and endothelial progenitor cells (Micheu & Dorobantu, 2017).

Clinical evaluations as well as pre-clinical work done in laboratory animal models have revealed similar results with respect to the mechanism of action, regenerative, and functional properties. In clinical trials, the usual end points have been left ventricle end systolic volume, ejection fraction (EF), ventricular volumes, wall thickness, and scar size (Mathiasen et al., 2012). The following statistically significant changes have been reported in the clinical trials: 1, improvements in EF; 2, a decrease in left ventricular end systolic and end diastolic volume, and 3, a decrease in infarction size (Clifford, Fisher, Brunskill, Doree, Mathur, Watt et al., 2012). However, the published results have been inconsistent with respect to mortality. One meta-analysis reported significant lower all-cause and cardiac related mortality in BMMNC-treated patients as compared to control patients (Jeevanantham et al., 2012). More commonly, stem cell therapies have exerted no significant impact on mortality, although this has been claimed to be due to the low mortality rate in clinical trials (Clifford et al., 2012; Jeong et al., 2018). In summary, the provision of stem cell therapy after acute myocardial infarction seems to be undeniably beneficial when one assesses parameters that determine the condition of the myocardium in AMI patients, although, it does seem that the benefits seem small or at most moderate, and the observed differences with controls usually are within a few percentage points (Clifford et al., 2012; Jeong et al., 2018). However, the extensive variations between the published studies make it difficult to draw any definitive conclusions.

In fact, the behaviour and effects of stem cells in the infarcted myocardium are still not fully understood and thus, preclinical studies are still very much needed to clarify the therapeutic mechanism in a detailed way not possible in clinical settings. The reproducibility advantages of *in vitro* studies are undeniable and significant, but it is difficult to extrapolate *in vitro* results to human physiology; more similarities can be achieved by examining the effects of the cells in large animal

models. Additionally, the therapeutic outcome is also affected by several technical factors such as the timing of therapy, the number of transplanted cells, monitoring time points, as well as the delivery route (Clifford et al., 2012; Jeong et al., 2018). For example, in clinical trials, cell doses above 10^8 have achieved better outcomes (Clifford et al., 2012). Furthermore, it is almost inevitable that there will be a delay in cell delivery in clinical trials, typically of several days (Mathiasen et al., 2012).

Stem cell therapy in experimental acute myocardial infarction

Experimental AMI is usually induced by occluding one of the coronary arteries followed by reperfusion (Crisostomo et al., 2015; Fan et al., 2014; Lai, P. F. et al., 2013). In *in vivo* large animal studies, stem cell therapies have been shown to improve EF (Amado et al., 2005; Fan et al., 2014; Qi et al., 2008) and reduce scar size (Amado et al., 2005; Fan et al., 2014; Hashemi et al., 2008; Hatzistergos et al., 2010; Qi et al., 2008) as detected by MR imaging similarly to clinical trials. Furthermore, in two studies conducted in rats or rabbits, therapy with MSCs was shown to promote angiogenesis (Lai et al., 2013; Pennella et al., 2017) and also to improve electrophysiological remodelling by altering the expression of ion channels (Lai et al., 2013).

Similarly to the problem encountered in clinical trials, the timing of stem cell transplantation has varied in experimental settings. A meta-analysis evaluating intracoronary BMMSC transfer in patients found transfer 3-7 days post-AMI was optimal in achieving an improvement in left ventricular function, improvement on EF, and decrease on LV dimensions (Xu, Liu, Zhong, & Huang, 2017). Crisostomo *et al.* found no statistical difference between the groups that received stem cell therapy within 7 days post-AMI (Crisostomo et al., 2015). As in the clinical trials, the cell amount has varied between the experimental models, and still today no *in vivo* experimental studies have reported that there would be any significant correlation between the therapeutic outcome and the number of transplanted cells. As well as the above described differences between clinical trials and experimental models, there have been major differences in follow-up times; these are often due to regulations that are imposed for the use of laboratory animals, as well as due to the costs. In human trials, a long follow-up is already often determined by the course of the disease and that some additional novel therapy has been given.

Furthermore, in experimental models, despite the above-mentioned promising results, the engraftment and migration of transplanted cells are yet unclear even though one would think that this knowledge is crucial for understanding the

therapeutic mechanism (Chavakis, Urbich, & Dimmeler, 2008; Fan et al., 2014). One study conducted in mice found that the transplanted BMMNCs did not express cardiac tissue specific markers but rather haematopoietic or myeloid markers suggesting that the cells had undergone a haematopoietic engraftment (Balsam et al., 2004). The finding is in line with another work in mice where no differentiation into cardiomyocytes could be detected in mouse heart by using either genetic techniques or by comparing the number of cardiomyocytes in engrafted mouse hearts (Murry et al., 2004). Another study suggested that bone marrow derived hematopoietic cells could generate cardiomyocytes only by cell fusion (Nygren et al., 2004). In a mouse study using reporter gene imaging, fewer than 0.1% of transplanted BMMNCs had migrated to the injured myocardium after 2 weeks, however, in that study, the cells had been delivered intravenously (Sheikh et al., 2007). In the same study, there was no statistically significant improvement observed in cardiac function (Sheikh et al., 2007). More recently, Cai *et al.* (2016) demonstrated a significant myocardial recovery after BMMNCs transplantation in pigs (Cai et al., 2016). In this work, there was evidence of up-regulation of glucose metabolism-related enzymes in the areas injected with BMMSCs at 4 weeks' post-transplantation and it was postulated that the therapeutic effect could be mediated by activation of mammalian target of rapamycin signalling pathways, which together with microRNAs are considered major regulators of both physiological and pathological cardiovascular processes (Samidurai, Kukreja, & Das, 2018).

Stem cell tracking in myocardial infarction

In humans, PET imaging has indicated that the homing of intracoronary transplanted bone marrow cells after AMI varies from a few percent to 14-39% depending on whether the cells were or were not CD34-enriched, with the latter being more efficient (Hofmann et al., 2005). Those cells were mainly detected in the border zone. Moreover, when the biodistribution of bone marrow cells was examined, it seemed that the cells were detected primarily in liver and spleen (Hofmann et al., 2005). This may be explained with the hypothesis that the therapeutic effect of BMMSCs would be mainly mediated through paracrine pathways (Cai et al., 2016).

In order to be able to evaluate cell tracking *in vivo* with MR imaging, a map is required to ensure the accurate anatomical location of cells and to allow subsequent spatial comparison with histology. In heart imaging, the myocardium is usually divided into segments (Cerqueira et al., 2002) illustrated in figure 2.

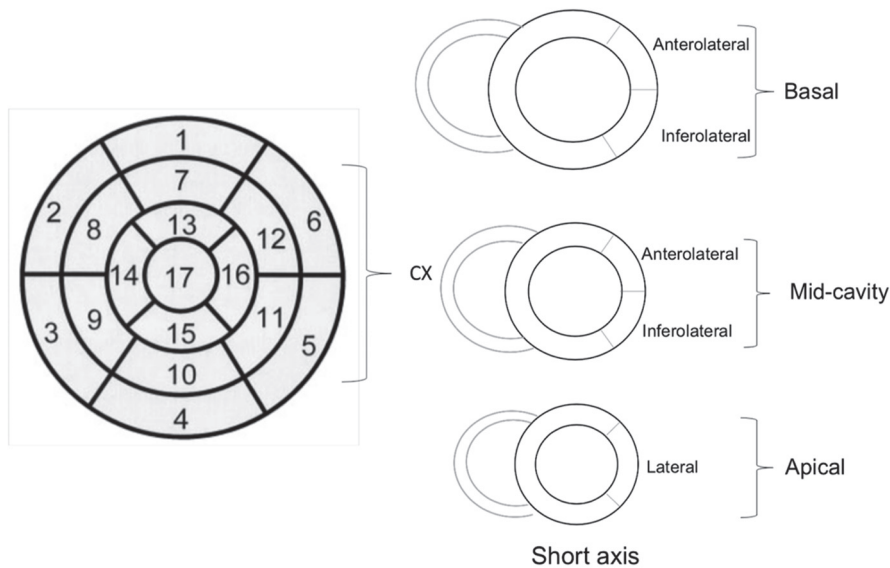


Fig. 2. Schematic illustration of left ventricle cardiac segments, modified from (Cerqueira et al., 2002).

In addition, the cells of interest must be labelled to assess their viability (Cromer Berman et al., 2011; Srinivas et al., 2010). Despite the considerable clinical interest towards stem cell therapies in AMI, interestingly there are only a few large animal studies published evaluating cell homing *in vivo* using SPIO labelling (He et al., 2007; Ma, G. S., Qi, Liu, Shen, Chen, Liu, Hu, Zhang, Teng, Ju, Ma, & Tang, 2011; Peng et al., 2013; Qi et al., 2008; Yang, K. et al., 2011). He et al. (2007) used minipigs, in which SPIO labelled cells were transplanted by myocardial injections at 10 days' post-AMI. The cells were viable in MR imaging throughout the 4 weeks' follow-up, with the results confirmed by histology. It is noteworthy that these investigators used an incubation time of 48 hours (He et al., 2007). There are two other studies using regular size pigs, with SPIO or USPIO, SPIO and MPIO labelled cells being delivered by intracoronary infusion at 3- 7d post-AMI; it was found that the cells were visible in the MR imaging at 4 weeks and in 5 out of 7 pigs still at 8 weeks. (Ma et al., 2011; Qi et al., 2008). The label was detected both in the infarction zone and peri-infarcted zone. Probably because of the transplantation route, the USPIO label that penetrates most easily because of its small size, was concluded to be the most suitable (Ma et al., 2011). Similarly, Peng *et al.*, (2011)

and Yang *et al.*, (2011) used intracoronary infusion and 8 weeks' follow-up, however the cell transplantation was performed at 7-12 days' or 12 days' post-AMI. In both experiments, the cells were dual labelled with SPIO and a lentiviral vector carrying the gene encoding green fluorescent protein (GFP). The first study found that the signal from the SPIO label did weaken over time, however the latter work reported that the hypointense signal from the SPIO label actually increased with time. One common finding in all these large-animal studies is that the labelled cells were detected mainly in the peri-infarction or border zone, but also that the stem cell therapy was observed to enhance myocardial recovery (He *et al.*, 2007; Ma *et al.*, 2011; Peng *et al.*, 2013; Qi *et al.*, 2008; Yang *et al.*, 2011). Another study used SPIO label with the swine AMI protocol, however instead of focusing on cell tracking, the work assessed the effects of MSCs overexpressing insulin-like growth factor-1 (IGF-1) and hepatocyte growth factor (HGF) transplantation (Gomez-Mauricio *et al.*, 2016). Interestingly, no significant synergistic therapy effect was observed with the MSC-IGF-1/MSC-IGF-HGF-treated groups, as compared to non-transplanted groups, however they found that both neovascularization and fibrosis was enhanced in the cell-transplanted groups.

The above works have been criticized; it has been claimed that MR imaging may not be suitable for long-term tracking of the SPIO label as there are studies suggesting that the long-term signal mimicking that from the SPIO label is actually emitted from extracellular iron particles (Huang, Z. *et al.*, 2015), and macrophages taking up the iron (Ma, N. *et al.*, 2015; Pawelczyk *et al.*, 2009; Terrovitis *et al.*, 2008). Interestingly Ma *et al.* (2015) used donor MSCs to identify the transplanted cells and after 4 weeks there were very few or no implanted cells in the myocardium but instead there was a rather progressive inflammatory response (Ma *et al.*, 2015).

2.3 Osteoarthritis

2.3.1 Pathophysiology of osteoarthritis

Osteoarthritis is a very common chronic disease, characterized by idiopathic or posttraumatic degeneration of articular cartilage (Bijlsma, Berenbaum, & Lafeber, 2011; Vina & Kwok, 2018). The weight loading joints i.e. hip and knee are the most common locations (Conaghan *et al.*, 2015) and in good agreement, mechanical loading of the joint has been associated with possible damage of articular cartilage (Yucesoy, Charles, Baker, & Burchfiel, 2015). Other common risk factors include

excess weight, biomechanical problems, joint trauma, and age (Rosenberg, J. H., Rai, Dilisio, & Agrawal, 2017).

About 4% of the net wet weight of articular cartilage consists of chondrocytes and an extracellular matrix, which is made up of about 65-85% of water, 15-20% of collagen, mainly type II collagen, and 3-10% of proteoglycans (PGs) (Maroudas & Venn, 1977; Pearle, Warren, & Rodeo, 2005; Venn & Maroudas, 1977). Articular cartilage can be divided into histologic zones according to its cellular components and collagen structure as follows: 1, superficial zone; 2, middle or transitional zone; 3, deep or radial zone; and 4, calcified zone (Pearle et al., 2005). The structure and biomechanics of articular cartilage are characterized in figure 3. The mechanical strength of the collagen network is orientation dependent and decreases with zone deepness until the deep zone, while the PG concentration on the contrary is elevated with zone deepness (Mow, V. C., Ratcliffe, & Poole, 1992). The collagen network largely determines the dynamic strength and the PGs account for the compressive strength of articular cartilage by interacting with the interstitial water of the extracellular matrix (Laasanen et al., 2003). In the extracellular matrix, large PG aggregates are formed which have been shown to inhibit PG depletion during mechanical loading (Roughley, 2006). The structure and biomechanics of articular cartilage are characterized in figure 3. While the articular cartilage is avascular and sustained by synovial fluid, the calcified zone has vascular channels originating from subchondral bone, with the interface commonly named as the tidemark (Hoemann, Lafantaisie-Favreau, Lascau-Coman, Chen, & Guzman-Morales, 2012).

The pathophysiology of OA is a multifactorial metabolically active cascade where there are two characteristic phenomena: the proteoglycan depletion due disruption of the collagen fibrillar network and morphological changes in the collagen network (Kempson, Muir, Swanson, & Freeman, 1970; Saarakkala et al., 2010). While the structural changes are considered irreversible, the molecular compositional changes that occur at the very beginning are possibly thought still to be reversible (Choi & Gold, 2011; Link, Stahl, & Woertler, 2007).

2.3.2 MR imaging of proteoglycan content

Although the morphological features of OA such as a narrowing of the joint width space, the presence of osteophytes, cartilage thickness/ surface area changes, and other cartilage characteristics like integrity, roughness, and inflammation can be assessed at least partly with a variety of imaging modalities other than MR imaging, MR imaging is currently considered to be the gold standard non-invasive method

to assess the molecular composition of articular cartilage (Hani et al., 2015). MR imaging is considered an accurate way of assessing a decrease in the PG concentration or an increase in water content (Bashir, Gray, & Burstein, 1996; Bashir, Gray, Boutin, & Burstein, 1997; Bashir, Gray, Hartke, & Burstein, 1999; Hani et al., 2015; Kang, Choi, Yoo, Hong, & Kang, 2017; Nieminen et al., 2002; Salo et al., 2012). The increase in the water content occurs as a result of the reduction in the PG content (Mankin & Thrasher, 1975; Saarakkala et al., 2010). The published literature describes three main methods to measure PG content in articular cartilage: 1, delayed gadolinium-enhancement magnetic resonance imaging of articular cartilage (dGEMRIC); 2, sodium MR imaging; and 3, T_1 rho mapping (Choi & Gold, 2011; Kijowski & Chaudhary, 2014). The first two approaches are based on the fixed charge density of articular cartilage which is due to the negatively charged glycosaminoglycan side chains of aggrecan, the main PG component in the articular cartilage (Aspberg, 2012). In dGEMRIC imaging, the decreased PG content within articular cartilage increases Gd-DTPA⁻² uptake as Gd-DTPA is negatively charged and therefore it is distributed throughout the PGs store. This inverse proportionality has been proven to be a highly sensitive and specific method to evaluate PG concentration in articular cartilage (Kijowski & Chaudhary, 2014). In sodium MR imaging, the negative charge of articular cartilage attracts positively charged ions like sodium and thus the decrease in the PG concentration results in a decreased intake of sodium ions and the method, like dGEMRIC, has been proven to be a sensitive way to assess the PG content (Shapiro, Borthakur, Gougoutas, & Reddy, 2002). In fact, both methods have been applied in human trials (Burstein et al., 2001; Multanen et al., 2009; Wheaton et al., 2004). The T_1 weighted rho mapping, based on a long-term RF pulse and the ability to detect the slow motions of macromolecular have been initially shown to be sensitive at detecting the early PG depletion and furthermore, it can reveal some other biochemical and biomechanical changes in OA (Choi & Gold, 2011). In addition to a lesser extent, T_2 mapping has been applied in the evaluation of the PG content but more often it has been used to assess the changes in collagen matrix and water (Choi & Gold, 2011).

The known problems for the dGEMRIC imaging include contrast agent related problems. Firstly, the time delay prior to MR imaging because of slow diffusion of contrast agent into the cartilage. Secondly, the risk of a nephrogenic systemic fibrosis (Beam et al., 2017), and thirdly, accumulation into the central nervous system (Kanda et al., 2017; Radbruch et al., 2015; Radbruch, 2018). The problems encountered in sodium imaging include the challenges of identifying the signal

origin (Kijowski & Chaudhary, 2014), the need for a high RF power which could cause tissue warming or even burning, and specific absorption rate related issues (Choi & Gold, 2011).

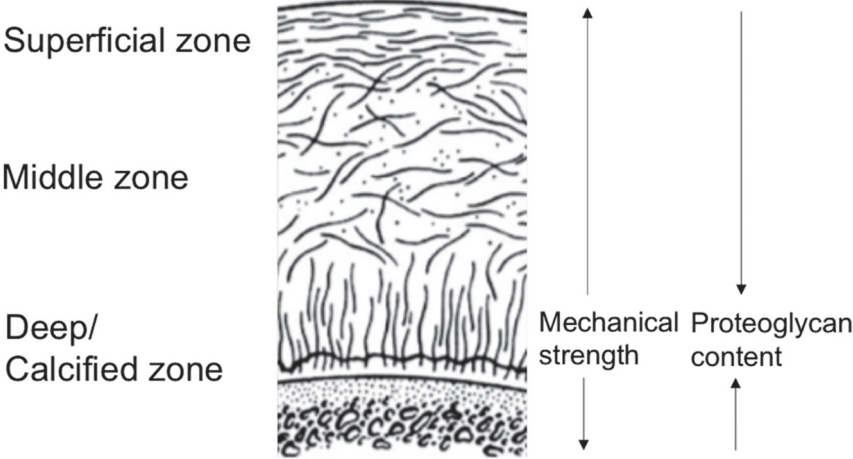


Fig. 3. The structure and biophysics of the articular cartilage (Mow, V. & Huskes, 2015).

3 Aims of the present study

The main purpose of this work was to develop magnetic contrast agents for cellular and other labelling purposes. An improved label could lead to a better understanding of pathological processes and the mechanisms behind regenerative therapy and eventually lead to a better understanding of diseases and improved therapeutic designs.

The specific aims of this study were:

1. To evaluate the usability of a novel, fast SPIO labelling method for BMMNCs labelling and for tracking stem cells by MR imaging in an experimental AMI model.
2. To investigate the usability of the novel, fast SPIO labelling method for long-term tracking of transplanted BMMNCs in an experimental AMI model and to evaluate the effectiveness of BMMNC therapy in cardiac regeneration after AMI.
3. To process novel MnO labels for magnetic resonance imaging and furthermore, to observe the usability of the labels for mesenchymal stem cell labelling.
4. To evaluate the role of a novel amorphous MnO label in measuring proteoglycan content in articular cartilage.

4 Materials and methods

The detailed methods used are presented in papers I-IV.

4.1 Study animals and human samples (I, II, IV)

Table 3. Characteristics of *in vivo* and *ex vivo* research assessments.

Variables	I	II	IV
Animals (<i>n</i>)			
Porcine	3	31	-
Bovine	-	-	12
Human samples (<i>n</i>)	-	-	11
Infarction model			
AMI	3	31	-
AMI+BMMNC	3	18	-
AMI+BMMNC+label	3	7	-
Imaging			-
MRI 0d	3	7	-
MRI 21d	-	7	-
MRI <i>ex vivo</i>	3	-	-
Electrocardiography	-	31	-
Blood samples	3	31	-
Cytokine levels, baseline	-	31	
Cytokine levels, 24h			
AMI	-	14	-
AMI+BMMNC	-	8	-
Cytokine levels, 21d			-
AMI	-	11	-
AMI+BMMNC	-	4	-
Histopathology	3	31	-
Cartilage model (<i>n</i>)			
Label			
MnOx Gd-DTPA	-	-	12
MnOx	-	-	11
Histopathology	-	-	11

4.1.1 Porcine infarction model (I, II)

AMI was induced according to a previously described method (Makela et al., 2007). Briefly, the pigs were anesthetized with midazolam (Pfizer AB, Solletuna Sverige) and ketamine hydrochloride (Pfizer AB), and anesthesia maintained with midazolam (Pfizer AB), fentanyl (Hameln, Hameln, Germany) pancuronium (Hameln, Hameln, Germany), and inhaled isoflurane (Orion Pharma, Turku, Finland). The circumflex coronary artery (CX) was surgically coiled (Scanlan, St. Paul, MN, USA) for 90 minutes. Subsequently, the labelled BMMNCs were transplanted within the area vascularized by CX by using direct intramuscular injections. The pigs were MR imaged *in vivo* at 1-2 hours' post-AMI (I, II) and at 21 days' (II) post-AMI. Biochemical analyses were performed at the baseline, and at 90 minutes after reperfusion, and in study II also at 24 hours' and at 21 days' post-AMI. In study II, in addition to the MR imaging, echocardiography was performed at the same time points as the biochemical analyses. After sacrifice, the formalin-fixed cardiac tissue was MR imaged *ex vivo* (I), and the left ventricle divided according to a standardized myocardial segmentation scheme (Cerqueira et al., 2002) for histology.

4.1.2 Articular cartilage sample preparation (IV)

Cylindrical 5 mm diameter osteochondral plugs, prepared from knee articular cartilage samples obtained from the local abattoir (bovine samples) or after total knee replacement surgery (human samples), were immersed in phosphate-buffered saline (PBS) and frozen at -18°C.

4.2 Nanoparticles and cell labelling (I-IV)

Table 4. Nanoparticles used and cell labelling in the study.

Variables	I	II	III	IV
Nanoparticles				
SPIO	yes	yes	-	-
MnOc	-	-	yes	-
MnOx	-	-	yes	yes
Gd-DTPA	-	-	-	yes

Variables	I	II	III	IV
Cells				
Human MSCs	-	-	yes	-
Porcine	yes	yes	-	-
BMMNCs				
Labelling method				
Rotating incubation method	yes	yes	-	-
Incubation and microwave	-	-	yes	yes
Electroporation	yes	-	-	-
Label toxicity evaluation	yes	-	yes	-

4.2.1 Preparation and characterization of nanoparticles (III)

A microwave reactor (Discover SClass, CEM, USA) with controllable time and temperature/heating was used for the synthesis of manganese oxide. By using heating, stirring, and ultrasonication, 12 mmol of sodium acetate was ethylene-glycol-dissolved. After adding 4 mmol $MnCl_2 \cdot 4H_2O$, the dissolving with the ethylene-glycol was repeated.

Dissolution of MnOx particles

A plasma mass spectrometry (ICP-MS, PerkinElmer, Elan 6100 DRC Plus) with a commercial multielement standard (PerkinElmer, Multi-Element Calibration Standard 3, N9300233) for calibration were used to study MnOx dissolution at an extracellular pH value = 7.4 and an intracellular pH value = 5 by using 4-(2-hydroxyethyl)piperazine-1-ethanesulfonic acid (HEPES) and morpholine-4-ethanesulfonic acid (MES) buffers.

4.2.2 Isolation and culturing of cells (I, II)

BMMNCs were isolated from the bone marrow aspirate gathered from the tibial tuberosity. After density-gradient centrifugation (Ficoll-Paque Plus, GE Healthcare Bio-Sciences AB; Uppsala, Sweden), which removed the granulocytes and

erythrocytes, the harvested BMMNCs were washed with PBS and plated. BMMNCs were then gathered and expanded in culture.

4.2.3 Labelling of cells (I, II, III)

SPIO labelling (I, II)

SPIO labelling was performed using 0.1 and 0.2 mg/mL concentrations of contrast agent (I; *in vitro* assessment) or in 39 mg/mL ferucarbotran corresponding to 36 mM iron (Resovist, Bayer Heathacre, Berlin, Germany) (I, II; the AMI models) and 1, a rotating incubation method (1hour incubation combined with continuous rotation to prevent aggregation) (I; *in vitro* and AMI model); 2, electroporation (two square wave protocols at 100V) (I; *in vitro* assessment); or 3, a rotation incubation method (37°C for 3 hours) (II). Later, the BMMNCs were washed with PBS and suspended into an agarose gel (I) or a saline solution (II) at a density of 10^8 cells/ 2 mL). Control BMMNCs were incubated with basal medium without label (I; *in vitro* assessment).

MnO labelling (III)

MnO labelling was performed by incubating the hMSCs for 2 hours in 10, 20, or 40 µg/ml concentrations of crystalline manganese oxide (MnO_c) or amorphous manganese oxide (MnO_x).

Proliferation and viability of labelled cells (I, III)

The cellular proliferation rate of labelled BMMNCs was analysed by measuring MTT absorbance with the (3-(4,5-dimethylthiazol-2-yl)-2,5-)diphenyltetrazolium bromide assay (Tetrazole, Sigma-Aldrich, St. Louis, MO, USA) and spectrophotometry 1-7 days after labelling. The MTT absorbance of cultured control cells was used as a reference.

4.3 MR imaging and image analysis

4.3.1 Relaxivity measurements of nanoparticles in vitro (III, IV)

The relaxivity (r) of MnOc (III) and MnOx (III, IV) at various particle suspensions were measured with a nuclear magnetic resonance (NMR) spectrometer (Minispec mq 60 (III) or DPX200, Avance III 300, and AVANCE III 600 (IV) (Bruker BioSpin, Rheinstetten Germany) by using the spin echo (III) and the spectroscopic saturation recovery (III, IV) sequences. Furthermore, the R of MnOx at various low field strengths between $2.34 \cdot 10^{-4}$ and $4.7 \cdot 10^{-1}$ were measured with a fast field cycling relaxometer (Stelar SPINMASTER FFC2000 1T C/CD, Mede, Italy) (IV). The relaxation of the Gd-DTPA in water (Magnevist, Bayer Schering Pharma AG, Berlin, Germany) at 7.1 T was determined for reference (IV).

The relaxivity of contrast agents for all of the field strengths were calculated by fitting T_1 and particle concentration data to the equation

$$[CA] = \frac{1}{r} \left(\frac{1}{T_{1CA}} - \frac{1}{T_1} \right), \quad (1)$$

where contrast agent (CA) is the concentration of the contrast agent and T_1 and T_{1CA} are the relaxation times of water in the presence or absence of the contrast agent.

4.3.2 MR imaging of nanoparticles in vitro (I, III)

T_1 , T_2 and T_2^* relaxation times of SPIO labelled BMMNCs were assessed using a 9.4 T NMR vertical magnet (Oxford Instruments, Abingdon, UK) and a 10 nm spectroscopic probe (I). An inversion recovery sequence with repetition time (TR) 700ms, echo time (TE) = 2 ms, inversion time (TI) 5-500 ms was used to assess T_1 relaxation by calculating the values/ areas of spectra. A spin echo (SE) sequence with TR 700 ms, eleven TEs between 2-40 ms was used to assess T_2 relaxation. A gradient echo sequence with TR 100 ms, seven TEs between 2-40 ms was used for T_2^* relaxation evaluation.

T_1 and T_2 relaxation times of MnOc and MnOx labelled MSCs were acquired using a 3T small MR scanner and an animal coil (RAPID Biomedical GmbH, Rimpar, Germany) (III). A single slice inversion recovery fast SE sequence with TR 1000 ms, TE 8.6 ms, ten TIs between 50-9500 ms, field of view (FOV) 120 ms, matrix 256^2 , yielding an in-plane resolution of 0.47 mm, slice thickness 3 mm, echo train length 8 and NEX 1 was used for the T_1 relaxation time. A multi-slice multi

echo spin echo sequence with TR 1680, twelve TEs between 11.5-138 ms, echo train length 5, FOV, matrix and slice thickness unchanged was used to assess T_2 relaxation times.

At 9.4 T (I) and 3 T (III), the region of interests (ROIs) were manually segmented into samples and the relaxation times acquired were fitted with the exponential relaxation equations using the in-house application (MATLAB, The MathWorks Inc., Natick, MA, USA).

The change in the signal intensity due the SPIO label was characterized at 1.5 T (GE Signa Twinspeed, GE Healthcare, Milwaukee, WI, USA) using a four-channel cardiac coil and the following imaging sequences: T_2 fast spin echo (FSE) sequence with TR 5400 ms, TE 96 ms, FOV 200 mm, FA 90°, NEX 1, AT 3min 47s, slice thickness/ interval 3/1 mm); T2 fluid-attenuated inversion recovery (FLAIR) sequence with TR 8802 ms, TE 133 ms, AT 3min 31s, slice thickness interval 3/1.5 mm, and unchanged FA, NEX, and FOV (I). ROIs were manually drawn on each specimen containing SPIOs as well as control specimens and the signal intensities of SPIO specimens were reported as a percentage of the signal intensities of the controls.

4.3.3 MR imaging of myocardial infarction (I, II)

The pigs were MR imaged with 1.5 T (GE Healthcare) using a four-channel cardiac coil and combined electrocardiogram and respiratory gating. The 2D CINE short axis sequence were imaged using the following imaging parameters: TR 4.2 ms, TE 1.8 ms, FOV 340, matrix size 256 x 256 mm, FOV 340, slice thickness 8-11 mm. Prior contrast enhancement sequences, a contrast agent, 0.2 mmol/ kg gadopentetate dimeglumine (Magnevist, Schering AG, Berling, Germany or Magnevist, Bayer Healthcare, Berlin, Germany), was intravenously injected. The perfusion sequence (T_1 multishot gradient-echo planar inversion-recovery) were obtained using the following parameters: TR 8 ms, TE 3.2 ms, matrix size 256 x 256 mm, FOV 340, slice thickness 11 ms. The delayed enhancement (DE) sequence (segmented inversion recovery fast gradient echo) was obtained 10 min after the contrast agent injection using the following parameters: TR 6.8 ms, TE 3.2 ms, matrix size 256 x 256 mm, FOV 340, slice thickness 10 mm, TI 200-150 ms.

For *ex vivo* imaging, a T_2 weighted fat saturation sequence (FSE) and a T_2^* weighted sequence were used with the following acquisition parameters: T_2^* using TE of 15 ms, TR of 660 ms, matrix size of 256 x 256 mm, FOV of 140, and slice

thickness of 3 mm; and T_2 FSE using TE of 86.5 ms, TR of 5400 ms, matrix size of 256 x 256 mm, and FOV of 140 mm.

The extent of AMI was evaluated from the 2D CINE (short axis), DE images (*in vivo*) and from T_2 FSE and T_2^* weighted images (*ex vivo*) and recorded as the number of affected cardiac segments (Cerqueira et al., 2002). The level of change in segmental intensity caused by the iron label was qualitatively classified into the following grades: 0 = no change, 1 = moderate change, and 2 = strong change). The relative percentage change in the signal was quantitatively counted by placing segmental ROIs on each 2D CINE slice within the segment in the systolic and diastolic phases by using an open-source viewer software (Osirix v.6.5, Pixmeo, Bernex, Switzerland). In the correlation analysis of imaging results with histology, the segmental mean values were used. EF was calculated from 2D CINE images by using a ROI-based method and in-house software (GE advantage workstation, GE Healthcare) with the data presented as mean values from two readings. Abnormal myocardial kinetics were determined segmentally as follows: 0 = normal, 1 = hypokinesia, 2 = akinesia, and 3 = dyskinesia.

The segmental volume of segment 16 was hard to draw and therefore this segment was excluded from the MRI analysis.

4.3.4 Imaging of articular cartilage (IV)

T₁ maps

Bovine and human samples were placed in 5 mm sample tubes and 2-3 different concentrations between 0.05 and 0.2 mM of MnOx contrast agent were allowed to diffuse into cartilage samples through the superficial cartilage. The diffusion was monitored until 24 hours' post-contrast by repeatedly assaying T_1 relaxation maps. Later, the contrast agent solution was replaced by PBS and the washout was monitored until 48 hours post-contrast. For reference, the procedure was repeated in bovine samples with 1 mM of Gd-DTPA contrast agent. A 7.1 T Bruker Avance III 300 NMR spectrometer (Bruker, Rheinstetten, Germany) with a Micro 2.5 gradient system, a 10 mm RF coil, a saturation recovery spin-echo imaging sequences (FOV 8 mm x 10 mm, resolution 250 μ m x 78 μ m, TE 5 ms, TR times between 44 and 5120 ms, and slice thickness 1 mm. The Paravision software was used to acquire the T_1 relaxation maps.

Concentration maps

By fitting the T_1 maps and measured relaxivities of contrast agents to the equation (section 4.3.1., appendix 1) then it was possible to obtain the spatial contrast agent concentration maps. A MatLab (Math-Works Inc., Natick, MA, USA) was used for calculations of concentration versus time at three different zones of articular cartilage: 1, superficial zone (P1); 2, middle zones (P2-3); and 3, deep zone or calcified region). To achieve exact spatial correlation between pre- and post-contrast images, the first post-contrast image was used as a reference.

4.4 Echocardiography (II)

A 3.5MHz transthoracic echocardiography (Acuson Sequia 512, Siemens AG, Munich, Germany) was used to determine the thicknesses of interventricular septum and posterior wall of LV, LV mass using the method described by Reichek and Devereux, (1977) (Devereux & Reichek, 1977). EF was estimated using the Teichholz formula. Furthermore, the cardiac output was measured using the velocity-time integral of the pulsed-wave Doppler and the trans-mitral flow peaks and the isovolumetric relaxation of the aortic valve were determined with Doppler scanning.

4.5 Biochemical analysis (I-II)

Blood gases, pH, electrolytes, glucose, haemoglobin, haematocrit, ionized calcium (i-STAT analyser, Abbot, Santa Clara, CA, USA), basic blood count, leukocyte differential count (Cell-Dyn analyser, Abbot), and troponin I (Immunoassay, Innotrac, AIO, Turku, Finland) were assayed at the baseline (I, II), at 90 min post-AMI (I, II), at 120 min post-AMI (II) with the latter three values also measured at 21 days' (II) post-AMI.

Cytokine levels were analysed at the baseline, 1 day, and 21 days with a Bio-Plex Pro Human Cytokine Assay (Bio-Rad Laboratories Inc., Hercules, CA, USA) (II). Briefly, the samples were centrifuged, diluted, and analysed. Five-parameter logistic equations were used for automatic calculation of the results.

4.6 Histopathology (I, II, IV)

4.6.1 Myocardial tissue samples (I, II)

Samples were formalin-fixed, paraffin embedded, cut and stained with hematoxylin-eosin (HE) (II) and Prussian blue (30 min incubation in 2% potassium ferrocyanide) (I, II).

Prussian blue positively stained BMMNCs were assessed according to the colour intensity, size, and shape. The number of cells were calculated using a three-scale classification: 0 = no BMMNCs, 1 = a few BMMNCs, and 2 = a large number of BMMNCs. Individual values from sections were summed for segmental grade so that grade 1 in 2-3/3 sections was classified as grade 2.

The characterization of myocardial damage was assessed by analysing HE stained sections and was classified as follows: 0 = normal tissue, 1 = granulation tissue, 2 = necrotic areas, and 3 = fibrotic areas (II).

4.6.2 Cartilage tissue samples (IV)

Safranin O-staining, a light microscopy system (Axio Scope A1, Carl Zeiss MicroImaging GmbH, Gottingen, Germany) and a digital camera (Retiga 4000R, OImaging, Surrey, BC, Canada) were used to evaluate PG distribution in human samples, with the method previously described by Kiviranta et al. (Kiviranta, Jurvelin, Tammi, Saamanen, & Helminen, 1985). Briefly, after staining and sectioning, neutral density filters with four optical density (OD) values between 0.3 and 1.5 (Edmund optics, Barrington, NJ, USA) were used to obtain calibration images with various OD values between 0.0 and 2.5. During the calibration, the grey-level values of images were converted to OD values using the equation of Rodbard with Image J (v.1.5b, National Institutes of Health, USA).

The Osteoarthritis Research Society International (OARSI) grading system (Pritzker et al., 2006) and a modified Mankin score (Mankin, Dorfman, Lippiello, & Zarins, 1971) were used to determine the severity of OA.

4.7 Ethical considerations (I-IV)

The animal experiments (I-II) were approved by the Animal Care and Use Committee, University of Oulu, Finland (ESLH-2007 09818/YM-23). Bovine samples (IV) were obtained from the local abattoir (Atria Oyj, Kuopio, Finland)

and thus no ethical authorization was required. The use of human samples (IV) was approved by the ethics committee of Northern Ostrobothnia Hospital District (permit no: 78/2013).

5 Results

The detailed results are presented in studies I-IV.

5.1 Cellular proliferation of BMMNCs *in vitro* is not altered when labelling with SPIO using a rotation incubation method (I)

Cellular proliferation (viability) as measured by MTT absorbance of cells on days one and four was not statistically significant different between SPIO labelled and control BMMNCs *in vitro* (I, Fig 4). However, after 7 days, a statistically significant ($p < 0.001$) difference was evident between the cells labelled by electroporation and control cells (I, Fig 4).

5.2 Cellular relaxation values correlated with the SPIO label concentration *in vitro* (I)

In accordance with the iron content of samples, there were changes observed in relaxation values at 9.4 T. At 1.5 T, when comparing the T_1 SE, T_2 SE, and T_2 FLAIR sequences, the FLAIR sequence showed the clearest reduction in signal intensity between the labelled cells and controls (I, Fig 4). Furthermore, in a comparison of the labelling methods which had used, the rotating incubation method showed the highest signal reduction.

5.3 Spatial correspondence of labelled BMMNCs between MRI and histology were observed *in vivo* (I, II)

Qualitatively evaluated signal loss in CINE sequences were determined to reflect SPIO label which was detected in one to four of the five segments supplied by the CX in each animal; this corresponded to the histological evaluation (I, Table 1). In the positive segments, a 24 to 64% signal intensity loss was observed in quantitative analyses whereas in the negative segments, the observed signal intensity change varied from a 1% loss to a 3% increase (I, Fig 2). In histology, the percentages of the surface area covered by labelled BMMNCs were 0.002-0.927% in the cell positive segments (I, Fig 2).

In study II, the qualitative segmental correspondence was similar between the MR imaging and the histology, although the correlation was not so clear as found

in study I (II, Fig 3). At 21days' post-AMI, no label was detected with the MR imaging.

In the histological evaluation, most BMMNCs showed no changes in morphology. However, a few BMMNCs had become elongated and flattened and were positioned in a parallel fashion along myocytes or endothelial cells (I, Fig 3).

5.4 BMMNC transplantation seems to have a therapeutic effect after AMI *in vivo* (I, II)

Table 5. Effects of AMI and BMMNC transplantation (I, II).

Variable	0-24 hours post-AMI		21 days post-AMI	
	BMMNCs	Control	BMMNCs	Control
Echocardiography				
Fractional shortening	↓	↓	↑↑*	↑*
EF	↓	↓	↑↑*	↑*
MRI				
EF	↓		↑#	
Abnormal myocardial kinetics	↑↑		↑	
Delayed enhancement	↑		↑	
Abnormal perfusion	↑		↑	
Histology				
Hemorrhage	↑		↑	↑
Necrosis	↑		↑	↑
Granulation tissue	no		↑	↑
Fibrosis	no		↑/no	↑/no
Calcification				
Metabolic changes				
Troponin	↑	↑	↓	↓
Cytokine levels				
IL-1ra	+/-	+/-	↑↑	↑
PDGF	↓	↓↓	↑	↓
IFN-γ	+/-	↓	↑	↓
G-CSF				

IL-1ra, interleukin-1 receptor antagonist; PDGF, platelet-derived growth factor; IFN-γ, interferon gamma; G-CSF, granulocyte colony-stimulating factor; (*), statistical difference (p<0.05); (#) n = 7

5.5 Characterization of manganese particles (III, IV)

In order to obtain the characteristic crystalline MnO phase, it was found sufficient to heat the pale green synthesis mixture without capping agents for 30 min at 240°C (III, Fig 1a). After ethanol purification, the stable suspension appeared to be black and the TEM analysis showed the presence of nanocrystals (III, Fig 1b). This, together with the determined reaction temperature and different reaction times (10, 20, and 30 min) used for manganese oxide syntheses, were evaluated together with the polymeric agents poly(acrylic acid) (PAA) and poly(vinyl pyrrolidone) (PVP) (III, Table 1). With the PVP-addition, the suspensions resulted in a similar black product after purification. In contrast, with the PAA-addition the suspensions resulted in the formation of a white product (III, Fig 1c). TEM analysis of the white suspensions suggested that they had an amorphous structure (III, Fig 1d). The phenomenon can be explained by the two-step formation of crystalline MnO: 1, the hydrolysis of Mn^{2+} to $Mn(OH)_2$ and 2, the dehydration of $Mn(OH)_2$. The hydrolysis requires alkaline conditions and the PAA is a polyacid and thus no crystalline MnO is formed in the presence of PAA.

In order to characterize the behaviour in solution, the hydrodynamic size and net surface charge at neutral pH of the water/ buffer suspensions of the MnO_c and MnO_x were assessed by using dynamic light scattering and electrokinetic measurements (III, Fig 2). MnO_c samples had a narrow size distribution and low polydispersity values which were indicative of well-dispersed particles. MnO samples showed less discrete and less well-defined particles but they could be readily dispersed in an aqueous solvent and thus possessed preferable hydrodynamic characteristics. The net surface charge of MnO_x at neutral pH was negative due to the carboxylic acid groups resulting from the PAA used (III, Table 1). In contrast, the crystalline sample exhibited a net neutral charge, strengthening the hypothesis that PVP does not contain chargeable groups. Furthermore, the net neutral charge at neutral pH is also reflected in the less favourable hydrodynamic size results.

To obtain PVP- or PAA-stabilized MnO particles, a reaction time of 20 min was found to be sufficient according to the dynamic light scattering data (III, Table I). The crystalline phase was confirmed by X-ray diffraction (III, Fig 3).

The samples produced using microwave digestion without any polymer showed diffraction patterns reflecting the MnO_x phase in accordance with TEM characterization, where the same pattern was observed for PVP-stabilized sample but not for PAA-stabilized sample.

TEM analysis showed some differences in morphology and size, also suggesting that there was more coherent morphology with 30 min reaction time than with 20 min reaction time. Further, the morphology and size became even more coherent with PVP addition. TEM analysis showed the coexistence of nanoclusters together with single nanoparticles in the PVP-stabilized sample. This is thought to explain the somewhat large hydrodynamic size of PVP-stabilized particles despite that their particle diameter is about 10nm. Here, the PVP seemed to cause more undesirable effects i.e. it appeared rather a morphology inducer and/or growth regulator.

MnOx was shown to dissolve over time and no signs of accumulation were evident in either neutral or acidic conditions (IV, Fig 4).

5.6 Relaxiometric properties of amorphous MnO nanoparticles are displayed better than in crystalline MnO particles

Relaxation times T_1 and T_2 as a function of the MnO concentration of MnOx were significantly shorter than the MnOc samples measured in the spectrometer (III, Fig 5, Fig 6). Similarly, MR imaging at 3 T displayed slightly higher relaxivity (shorter relaxation times) of amorphous particles as compared to crystalline particles (III, Fig 8). However, the difference between the samples was not so significant when measured in agar and not in aqueous suspension (III, Fig 5). The T_1 and T_2 relaxation times for MnOx labelled hMsCs showed similarly shorter relaxation times as compared to MnOc labelled hMsCs (III, Table 2).

5.7 The relaxivity of MnOx is high and higher than the relaxivity of Gd-DPTA (IV)

The T_1 relaxivity of MnOx decreases with an increasing field strength (IV, Fig 1). At 7.1 T, the relaxivity of MnOx in water was $15 \text{ mM}^{-1}\text{s}^{-1}$ and the corresponding relaxivity of Gd-DTPA was $4.04 \text{ mM}^{-1}\text{s}^{-1}$ (IV, Fig 1).

5.8 MnOx diffuses faster than Gd-DTPA into the cartilage and the behaviour mimic dGEMRIC imaging.

The diffusion of MnOx into the articular cartilage is faster than that of Gd-DTPA (IV, Fig 2). In contrast to Gd-DTPA complexes that reach a stable level within 24 hours in the superficial cartilage, in both human and bovine samples, the MnOx

concentration increased until 2 hours, after which it started to decline. The concentration of MnOx in the calcified zone was observed to increase within 24 hours. After washout, MnOx particles or their dissociation products were still present in the calcified zone. In human samples however, the signal to noise ratio in the deep zone was weaker, however with the signal received, no such accumulative behavior was observed.

In each human sample, T_1 profiles were in parallel to the OD profiles and furthermore, the concentration profiles were found to follow in the reverse order of the gathered OD profiles (IV, Fig 5) mimicking the dGEMRIC behavior. However, no inverse correlation between those T_1 profiles and OD profiles was observed when looking at all samples together. High variability on OA gradings was observed when these were analyzed by Mankin and OARSI and no statistically significant correlation was observed between the observed grades and the estimated proteoglycan concentration. However, because of the technical issues raised in the pilot study, the number of samples assessed in the final correlation analyses was restricted to five.

6 Discussion

6.1 The role of cell tracking and experimental model in cellular treatment of AMI (I, II)

Interestingly, despite numerous on-going and completed clinical trials of stem cell therapy, with most frequently the MSC and BMMNCs therapies being given post-AMI (Ward et al., 2018), the mechanisms underpinning stem cell therapies, are still subject to on-going research. Originally, the migration and differentiation of transplanted cells (Kawada et al., 2004) were considered to be key elements, however at the present time, it seems evident that the engraftment of transplanted cells remains low and the observed therapeutic effect is also due to other properties; actions through paracrine pathways, enhancement of neovascularization, and endogenous cardiac precursor cell stimulation (Angoulvant et al., 2004; Dixit & Katare, 2015; Hatzistergos et al., 2010; Madigan & Atoui, 2018; Vrijisen et al., 2016). Even though the therapy involves various mechanisms, it is important to understand the mechanisms of actions of cell homing in more detail. In other words, tracking of cells makes it possible to follow the pathway and that may clarify which signaling cascades are up- or down-regulated post-transplantation and thus to understand more fully the regeneration process.

The SPIO label is currently the most commonly used and the most effective contrast agent for cellular MR imaging (Bulte, J. W., Vymazal, Brooks, Pierpaoli, & Frank, 1993; Rosenberg, J. T., Yuan, Grant, & Ma, 2016). Here, both novel direct *in vitro* SPIO labeling methods were found to be functionally feasible. A rotating incubation method appeared to be more sensitive and less toxic than electroporation and even a statistically significant difference was observed in cellular proliferation rate at 7 days between the labelling methods, although it should be stated that both methods exerted no significant impact on proliferation or cellular viability. This is in line with previous findings where direct labeling using SPIO particles has been shown to be both feasible and safe (Balakumaran et al., 2010; Mailander et al., 2008; Walczak, Kedziorek, Gilad, Lin, & Bulte, 2005). Here with both methods, the labeling time was only one hour, which is a major achievement especially as most reported incubation methods usually have a duration of several hours (Arbab et al., 2005; Hinds et al., 2003). In the published literature, the only direct labeling method that has reached a comparable time window is magnetoelectroporation (Walczak, Kedziorek, Gilad, Lin, & Bulte, 2005). The labelling time could have

been shortened further by increasing the concentration of the label. However, the labelling time was already clinically convenient and on *in vitro* imaging, the signal intensity values at 1.5 T and T_1 and T_2 relaxation times at 9.4 T correlated well with the concentration of the label. Additionally, by increasing the label dose, this could have led to increased aggregation, which has been associated with toxicity and the risk for microemboli (Karimi, Karimi, & Shokrollahi, 2013). The possibility that there would be free aggregates would naturally have led to less specific imaging. Furthermore, although as it is currently an experimental model, the lowest possible label concentration is desirable in terms of toxicity and possible side effects.

A rotation incubation method was chosen for the labeling technique in the *in vivo* studies because of its sensitivity, and at an hour post-AMI, the histologically confirmed label viability conducted with MR imaging reached a 100 % value in terms of sensitivity and specificity. Additionally, the qualitative cell-count grading showed a good correlation between MR imaging and histology. The quantitative correlation did not show a statistically significant correlation; this might be because of the difficulties in analyzing the volumetric MR imaging data and histological 2D data simultaneously. In a longitudinal study conducted at 2 hours post-AMI, the radiological-pathological correlation was not so high or so coherent. However, there were technical difficulties related to the condition of the animals when they were being imaged, mainly arrhythmias, which introduced additional artifacts in the images. The standardized myocardial segmentation scheme (Cerqueira et al., 2002) was found to be feasible to allow correlation with histology. However, the observed non-coherence between MR imaging and histology at 2 hours might be partly also due problems with the segmental borders. For example, the morphology in the *in vivo* MR images may differ from their appearance when they are prepared for histology and it is impossible to achieve absolute equivalence if no wire marking or other marking method has been applied. As far as we know, there are no such methods published in related articles. Additionally, the evaluation of MR images was conducted at 2 hours' post-AMI and the histology performed after 21 days. Therefore, there may have occurred some migration of transplanted cells between days 0 and 21. This is supported by the observation in the acute phase, where the histology did observe changes in both the location and morphology of BMMNCs similarly to our previous cardiac explant model (Alestalo et al., 2013), suggesting active migration. Additionally, in previous similar longitudinal works, the cells have been located mainly in a peri-infarcted zone irrespective of the delivery route (Ma et al., 2011; Ma, G. S., Qi, Liu, Shen, Chen, Liu, Hu, Zhang, Teng, Ju, Ma, & Tang, 2011; Peng et al., 2013; Qi et al., 2008; Yang et al., 2011).

This may refer to the active migration of cells. On 0 days post-AMI, hemorrhage could have caused interpretational difficulties as endogenous sources like iron deposits cause a similar decrease in the signal (Cromer Berman et al., 2011). However here, the histology in the acute phase did not show any signs of massive hemorrhage.

On 21 days' post-AMI, no label was reliably detected with MR imaging. This divergence with other large-animal studies (He et al., 2007; Ma et al., 2011; Peng et al., 2013; Yang et al., 2011) may be due concurrent signal loss by trans-mural necrosis and fibrosis. Additionally, histological analysis showed cartilage and calcification in the infarcted area in both control and BMMNC treated animals in agreement with our previous work (Makela et al., 2012). This might further increase the signal loss in the MR images at the site of infarction and thus introduce even greater interpretational challenges. The phenomenon of cartilage and calcific formation is nonspecific although it has been associated with inadequate wound healing (Aho et al., 2013). Here it is worthwhile noting that the transplantation of BMMNCs did not seem to promote any calcification but instead it tended to reduce it. Interestingly, in *in vitro* studies, the SPIO label has been shown to inhibit osteogenesis and chondrogenesis of MSCs in a dose-dependent manner (Chen et al., 2010). On the other hand, the fact that the label did not appear reliably at 21 days is in line with other studies suggesting that SPIO labelling may not be suitable for longitudinal tracking through non-specific uptake by phagocytic cells and moreover, the signal loss over time may occur due to cell proliferation and biodegradation (Ferrucci & Stark, 1990; Huang et al., 2015; Ma et al., 2015). It remains unclear at which level the iron-containing macrophages, which are capable of mimicking the labelled cells (Amsalem et al., 2007; Bulte, J. W. M., 2019b; Pawelczyk et al., 2009; Terrovitis et al., 2008), were present as no macrophage specific antibodies were available in this study. The possibility for significant leakage of transplanted cells after intramyocardial transplantation with multiple injections to the beating heart has also been speculated in the published literature (Teng, Luo, Chiu, & Shum-Tim, 2006), despite the fact that at present this method of cell delivery is considered to be the most accurate (Sheng et al., 2013).

Abnormal kinetics were observed in both the intramural area of infarction and the peri-infarcted zone at 1-2 hours and at 21 days' post-AMI, however the extent did decline over time. EF, analyzed from MR images, was found to be low at 0 days' post-AMI and it increased by 21 days. Similarly, a statistically significant difference in EF recovery between BMMNCs treated group and controls was observed with echocardiography. These findings are consistent with previous

outcomes with similar study designs (Amado et al., 2005; Fan et al., 2014; Zhou et al., 2009). MR imaging showed small areas of hypoenhancement within the hyperenhanced regions on DE images at 0 days which may refer to the presence of persistent microvascular obstruction (PMO). However, the label did cause susceptibility artifacts that did confuse the analysis and thus the observed phenomenon was left unresolved. PMO has been associated with an increased complication rate, subsequent cardiovascular events, and a poor prognosis (Hombach et al., 2005).

Cytokine levels at 24 hours and at 21 days both BMMNC and control animals showed extensive variability. No statistically significant difference was observed between the groups, however some trends were apparent; the clearest differences were the increase in the amounts of interferon gamma (IFN- γ), platelet-derived growth factor (PDGF), granulocyte colony-stimulating factor (G-CSF), and interleukin-1 receptor antagonist (IL-1Ra) levels in the BMMNC group at 21 days. Cytokines are characterized by their numerous, often overlapping effects (Lai, S. L., Marin-Juez, & Stainier, 2019). Furthermore, the mechanisms of paracrine regulation and cytokine secretion on stem cell therapy of AMI are also somewhat unclear, however the cytokine secretion of stem cells has been hypothesized to constitute a significant part of the therapeutic outcome (Li, Wang, Jia, & Du, 2014). For this reason, some cytokine-based therapies are now being developed (Dubnika et al., 2018). A prolonged inflammatory reaction post-AMI has been associated with poor healing (Frangogiannis, 2014). Furthermore, it seems that anti-inflammatory cytokines play a major role in the timely resolution of the inflammatory response (Lai et al., 2019). However, the pro-inflammatory cytokines, that have a more prominent role in early AMI, and those anti-inflammatory cytokines also regulate each other's secretion and moreover, the secretion of many other factors (Lai et al., 2019). MSCs have been shown to secrete PDGF and G-CSF, which are growth factors known to enhance neovascularization (Awada, Johnson, & Wang, 2015; Hao, Mansson-Broberg, Gustafsson et al., 2004; Hao, Mansson-Broberg, Blomberg et al., 2004; Takano et al., 2003). Interestingly, a histological study did reveal signs of angiogenesis at 21d post-AMI. However, some questions must be raised about the reliability of the assay of cytokine levels as the method was not designed for use in experimental animals.

There is an ongoing debate about how well the data from *in vitro* and animal experiments is applicable to humans when new therapy methods are being developed. It is believed that assessments done in large animals have better similarities with human physiology. The experimental AMI model used here

seemed to have been well standardized as the EF values were similar in all study animals prior to and until 24 hours' post-AMI. In addition, the results obtained are similar to those emerging from clinical trials (Clifford et al., 2012), which strengthens the belief that this large animal model may produce clinically relevant information. Future studies will still be needed to clarify the therapeutic effects of stem cells. For example, the homing of cells remains somewhat unclear. The major limitations of the study were the rather low number of samples, however within the bounds of ethical permission and hypothesis testing, we were able to demonstrate the initial feasibility of this novel labelling method in the *in vivo* study design. As predicted, longitudinal tracking of SPIO still remains controversial.

6.2 Amorphous manganese oxide as a contrast agent (III, IV)

Although ferrous agents, mainly SPIO, are currently the most widely utilized nanoparticles for cell labelling designs, the well-known interpretational challenges related to the signal loss of the label and endogenous processes that decrease the signal (Modo, Hoehn, & Bulte, 2005; Terreno et al., 2010), act as stimuli for researchers to develop improved signal enhancing paramagnetic compounds.

Recently, manganese oxide has been proposed as a positive contrast agent for MR imaging (Gilad et al., 2008; Kim et al., 2011; Na et al., 2007; Shin et al., 2009). Thus far, the research has been confusing because of the various forms of compounds and coating substrates that have been used, even MnO alone. However, in all those published studies, one common factor is that MnO has been utilized in its crystalline form. Here, in addition to the crystalline MnO, we investigated the features of amorphous MnO and its feasibility for application as a contrast agent and for *in vitro* labelling of hMSCs and further, the relaxometry properties were determined in agar at 3 T. Previously, no applications of this type using amorphous manganese oxide have been published although MnOx has been used in electrodes and as a catalyst. Interestingly it was found that that amorphous MnO exhibited greater relaxometric properties than crystalline MnO albeit both proved feasible. The differences between the relaxation times of amorphous and crystalline MnO may be a sum of many factors, including particle size, surface coating, saturation magnetizations, and degradability (Chen, D. et al., 2010; Duan et al., 2008; LaConte et al., 2007; Sun, N., Chen, Gu, & Wang, 2009). It is possible that there might have been the generation of linear aggregates because nanoparticles are able to attract nearby particles when aligned along the applied field, this being especially the case for large particles that are less stable in water and have a high saturation

magnetization; this phenomenon is well established for ferrous nanoparticles (Andreu, Calero, Camacho, & Faraudo, 2012; Odenbach & Muller, 2002). Along with these features, the polymer length of the stabilizing layer has been shown to have an impact on the inverse proportionality of T_2 relaxation and particle size (Saville et al., 2013). Therefore, a suitable surface functionalization could overcome these types of magnetic interactions of nanoparticles (Gulin-Sarfranz et al., 2014) and ideally there would then be no relaxation change over time.

A microwave irradiation was used with polyol process with the hydroxyl (-OH) group on the surface since this has been claimed to both synergistically enhance reactivity and shorten the labelling time (Bilecka, Djerdj, & Niederberger, 2008; Cheng, Xu, & Gu, 2011). Furthermore, the hydrophilic surface structure appeared to be biocompatible and stable in aqueous solutions at neutral pH and in physiological buffer (Wan, Cai, Meng, & Liu, 2007). Colloidal stability under aqueous conditions may have been enhanced by the polyelectrolyte similarly as can occur with an amphiphilic nonionic polymer (Ge et al., 2007; Graf, Vossen, Imhof, & van Blaaderen, 2003). In our study, amorphous formation was achieved by using a polyacid which caused a change in pH. As expected, changing the polyelectrolyte to PVP resulted in crystalline formation. However, PVP seemed to function as a morphology inducer or as a regulator of growth rather than a dissolution agent. In addition, when PVP was used, there was evidence of cluster formation, similar to the creation of aggregates.

The 3 T MR scanner was used to mimic the clinical equipment and in addition to labelling cells, the labels were imaged on agar as a means to evaluate the usability as a general contrast agent. The study of articular cartilage was designed not only to test the suitability of the amorphous MnO as a label but also to find faster and safer method to assess proteoglycan depletion in OA. This is because, despite dGEMRIC method is well described, it can't assess proteoglycan depletion in a reasonable time frame (Bashir et al., 1997; Kijowski & Chaudhary, 2014). The prolonged time required is due to the slow diffusion of gadolinium into the cartilage. Additionally, the dGEMRIC method, similarly to all forms of gadolinium enhanced imaging, has fallen from favour as gadopentate dimeglumine based contrast agents have recently been associated with nephrogenic systemic fibrosis (Haneder, Kucharczyk, Schoenberg, & Michaely, 2015; Thomsen et al., 2013) as well as an accumulation of the gadolinium into the brain (Kanda et al., 2014; Radbruch, 2018). The other relatively well described method to assess the proteoglycan concentration in articular cartilage utilizes sodium NM spectroscopy, however this method is also

time-consuming and needs specialized coils (Madelin, Lee, Regatte, & Jerschow, 2014).

The relaxivity of MnOx in water was found to be almost four times higher than that of Gd-DTPA at 7.1 T. Furthermore, the diffusion of MnOx into the articular cartilage was faster than that of Gd-DTPA. The difference in diffusion times may be due to the observed higher negative net surface charge of MnOx; this is higher than that present in molecular Gd-DTPA (Aime & Caravan, 2009), as the amorphous particles are actually larger in size. The net charge achieved with the PAA used is due to the label's carboxylic acid groups. It is noteworthy that crystalline MnO, in contrast to MnOx, exhibited a neutral net charge as the PVP does not possess chargeable groups. This difference again might mean that the diffusion into the articular cartilage might not be achieved with the crystalline MnO label. The time consumption is directly proportional to the cost and thus it is of importance if one considers the clinical use of these agents. Here, a clinically feasible two-hour labelling time in addition to the more rapid diffusion was achieved.

The negative association between concentration profiles of MnOx and OD was similar to the results typically obtained in dGEMRIC experiments in each articular human sample. Similarly, the T_1 relaxation time was observed to follow the OD profile in each human sample, leading to further testing of the feasibility of MnOx for the evaluation of the proteoglycan content. In the study, no statistical difference could be observed when analysing the correlation between the human samples. However, because of technical issues revealed in the pilot study, the small number of comparable samples was restricted and therefore no conclusions of the true nature of the possible mutual correlation may be drawn. No statistically significant correlation was observed between the MnOx concentration and histological scores evaluating the severity of OA (Mankin et al., 1971; Pritzker et al., 2006), however similarly the number of samples was not appropriate for statistical analysis. Those histological gradings are intended to determine the histological severity of OA, which pathophysiology and manifestations are multifactorial and multiple (Kempson et al., 1970; Pritzker et al., 2006). Performing a correlation analysis between proteoglycan content and OA severity may not be appropriate, despite the known decrease in the proteoglycan content within the progression of the disease (Mankin et al., 1971; Saarakkala et al., 2010). For example, it is possible that neither proteoglycan depletion nor the progression of the disease is linear and thus appropriate for this kind of statistical analysis. Furthermore, the human samples were gathered from both medial and lateral tibial plateau during arthroplasty. The

osteoarthritis of the knee is however characterized by its asymmetry. Thus, the obtained samples were probably with great-highly variability and some at degree of severe arthrosis, as was shown here. The interest towards proteoglycan content imaging has however arisen because the proteoglycan depletion starts in the early stage of arthrosis (Choi & Gold, 2011; Kempson et al., 1970) when possibly the disease is still at a reversible stage. Thus, in the future, gathering samples from the less diseased articular cartilage could be a better way for assessing the accuracy of the method to chase the early change of OA.

Interestingly, MnOx seemed to accumulate into the deep or calcified region in the bovine articular cartilage samples at 24 hours in contrast to human samples. However, in human samples, a low signal-to-noise ratio was observed in the calcified region and thus the phenomenon could remain undetected. After this finding, the dissociation was further studied in MES and HEPES buffer solutions that mimic intra- and extracellular conditions since if there was to be accumulation of contrast agent, this would lessen the value of the novel label and its possible usability. MnOx was noted to dissolve over time and there was no evidence to suggest that accumulation would take place. In the future, a longitudinal study would be needed to confirm this finding.

6.3 Future aspects of nanoparticles

Cellular imaging, and in particular tracking transplanted stem cells and evaluating cell homing *in vivo*, are crucial if we wish to understand the therapeutic phenomenon taking place post-transplantation. Furthermore, it will be important to learn more about how individual characteristics affect the manifestations of diseases, as well as ageing processes and the mutations that result within. These will form the basis for regenerative medicine; even today it is clear that therapies are becoming more individualized. One can envisage that there will be a need for a wide variety of safe, *in vivo* monitoring methods. Currently, MR resonance imaging is the gold-standard method for *in vivo* monitoring of transplanted cells; it allows us to follow cells in a non-invasive, non-toxic manner as well as providing additional information about the host tissue (Estelrich et al., 2015). However, at the present time, label detection is still mainly qualitative, although as described in some reports using MPIO, it may be becoming more quantitative (Heyn et al., 2006; Hinds et al., 2003; Shapiro et al., 2004; Shapiro et al., 2005; Shapiro et al., 2006). Yet again, it seems that these MPIO labels are toxic (Seymour et al., 1991), which for the time being reduces further interest in them. Further, as the labels become

more individualized depending on the desired action, they more often are developed in the form of a complex compound. However, it is the addition of these compounds to the oxide form of nanoparticles that has given rise to the concerns about additional side effects and even toxicity; these are topics that require further investigation. The search for better tolerability and good imaging contrast has led to a wide variety of contrast agents being developed and evaluated. Although this may seem to be beneficial, it has slowed down the gathering of sufficient research data of the individual contrast agents and thus delayed their possible introduction for human use.

In the future, therapies may undergo changes in their application e.g. stem cell therapies may either be supplemented with drugs or delivered as a mixture of different type stem cells and therefore, dual contrast agents could have a significant role in cell tracking (Ngen et al., 2015; Ngen et al., 2017). Thus far, major changes have been reported, which might be due the effects that the simultaneous assessment of T_1 and T_2 contrast have on each other. More recently, fluorine 19 MR imaging has been introduced as a method for multispectral imaging similarly to dual-contrast; this has been postulated to enable tracking of more than one source however at present its sensitivity is not considered to be sufficient (Bulte, J. W. M., 2019a; Chirizzi et al., 2019).

In addition to novel label designs, another novel, non-invasive imaging modality, magnetic particle imaging, has been developed (Bulte, 2019). Although magnetic particle imaging has many similarities to MR imaging, it does not gather endogenous signals and thus no signal is present prior to SPIO nanoparticle transplantation; in this respect, it resembles the situation with isotope imaging. This property might eliminate some of the interpretational challenges encountered with the SPIO label (Cromer Berman et al., 2011). Furthermore, one unique advantage of this technique is its ability for quantify cell detection, as well its ability to be applied in whole body imaging. It has already been speculated that many SPIO applications originally developed for MR imaging will be duplicated for magnetic particle imaging. Further hypotheses may be proposed towards the use of the paramagnetic nanoparticles by combining MR imaging and magnetic particle imaging in the future, which could achieve a better overall picture of the effects of stem cell therapy.

7 Summary and conclusions

The following conclusions may be drawn from these results:

1. The rotating incubation method appeared to be feasible and safe for fast labelling of BMMNCs with SPIO. *In vitro*, *in vivo* and *ex vivo* MR imaging showed high sensitivity and specificity for label detection in the acute phase. Cell tracking post-AMI using the SPIO label proved to be possible. However, the suitability of the SPIO label for long-term evaluation of cell homing in myocardial tissue remains unclear.
2. The delivery of BMMNCs post-AMI seems to be therapeutic and the results obtained in the experimental large-animal model are similar to those obtained in clinical trials; this suggests that the experimental model can be interpreted as functioning well.
3. The post-transplantation fate of stem cells remains somewhat unclear, however as the mechanisms of action are known to be multifactorial, it is clearly important to try to track the cells after transplantation in order to see which pathways contribute to the resulting effects.
4. The novel amorphous manganese oxide nanoparticles seemed to be feasible and safe for stem cell labelling and furthermore, they exhibited more favourable relaxivity than the crystalline particles and showed significantly higher relaxivity than can be obtained with Gd-DTPA.
5. Our pilot study revealed that amorphous MnO appeared to be feasible for assessing the proteoglycan content of articular cartilage. Further studies will be needed to define the accuracy and usability of the novel label for sensitive imaging of proteoglycans.

References

- Ahmed, N., Carrick, D., Layland, J., Oldroyd, K. G., & Berry, C. (2013). The role of cardiac magnetic resonance imaging (MRI) in acute myocardial infarction (AMI). *Heart, Lung & Circulation*, 22(4), 243-255. doi:10.1016/j.hlc.2012.11.016 [doi]
- Aho, O. M., Lehenkari, P., Ristiniemi, J., Lehtonen, S., Risteli, J., & Leskela, H. V. (2013). The mechanism of action of induced membranes in bone repair. *The Journal of Bone and Joint Surgery.American Volume*, 95(7), 597-604. doi:10.2106/JBJS.L.00310 [doi]
- Aime, S., & Caravan, P. (2009). Biodistribution of gadolinium-based contrast agents, including gadolinium deposition. *Journal of Magnetic Resonance Imaging : JMRI*, 30(6), 1259-1267. doi:10.1002/jmri.21969 [doi]
- Alestalo, K., Lehtonen, S., Yannopoulos, F., Makela, T., Makela, J., Ylitalo, K., . . . Lehenkari, P. (2013). Activity of mesenchymal stem cells in a nonperfused cardiac explant model. *Tissue Engineering.Part A*, 19(9-10), 1122-1131. doi:10.1089/ten.TEA.2012.0241 [doi]
- Amado, L. C., Saliaris, A. P., Schuleri, K. H., St John, M., Xie, J. S., Cattaneo, S., . . . Hare, J. M. (2005). Cardiac repair with intramyocardial injection of allogeneic mesenchymal stem cells after myocardial infarction. *Proceedings of the National Academy of Sciences of the United States of America*, 102(32), 11474-11479. doi:0504388102 [pii]
- Amsalem, Y., Mardor, Y., Feinberg, M. S., Landa, N., Miller, L., Daniels, D., . . . Leor, J. (2007). Iron-oxide labeling and outcome of transplanted mesenchymal stem cells in the infarcted myocardium. *Circulation*, 116(11 Suppl), 38. doi:116/11_suppl/I-38 [pii]
- Andreu, J. S., Calero, C., Camacho, J., & Faraudo, J. (2012). On-the-fly coarse-graining methodology for the simulation of chain formation of superparamagnetic colloids in strong magnetic fields. *Physical Review.E, Statistical, Nonlinear, and Soft Matter Physics*, 85(3 Pt 2), 036709. doi:10.1103/PhysRevE.85.036709 [doi]
- Angoulvant, D., Fazel, S., & Li, R. K. (2004). Neovascularization derived from cell transplantation in ischemic myocardium. *Molecular and Cellular Biochemistry*, 264(1-2), 133-142.
- Aoki, I., Takahashi, Y., Chuang, K. H., Silva, A. C., Igarashi, T., Tanaka, C., . . . Koretsky, A. P. (2006). Cell labeling for magnetic resonance imaging with the T1 agent manganese chloride. *NMR in Biomedicine*, 19(1), 50-59. doi:10.1002/nbm.1000 [doi]
- Arbab, A. S., Bashaw, L. A., Miller, B. R., Jordan, E. K., Lewis, B. K., Kalish, H., & Frank, J. A. (2003). Characterization of biophysical and metabolic properties of cells labeled with superparamagnetic iron oxide nanoparticles and transfection agent for cellular MR imaging. *Radiology*, 229(3), 838-846. doi:10.1148/radiol.2293021215 [doi]
- Arbab, A. S., Wilson, L. B., Ashari, P., Jordan, E. K., Lewis, B. K., & Frank, J. A. (2005). A model of lysosomal metabolism of dextran coated superparamagnetic iron oxide (SPIO) nanoparticles: Implications for cellular magnetic resonance imaging. *NMR in Biomedicine*, 18(6), 383-389. doi:10.1002/nbm.970 [doi]

- Arbab, A. S., Yocum, G. T., Wilson, L. B., Parwana, A., Jordan, E. K., Kalish, H., & Frank, J. A. (2004). Comparison of transfection agents in forming complexes with ferumoxides, cell labeling efficiency, and cellular viability. *Molecular Imaging*, 3(1), 24-32. doi:10.1162/153535004773861697 [doi]
- Aspberg, A. (2012). The different roles of aggrecan interaction domains. *The Journal of Histochemistry and Cytochemistry: Official Journal of the Histochemistry Society*, 60(12), 987-996. doi:10.1369/0022155412464376 [doi]
- Awada, H. K., Johnson, N. R., & Wang, Y. (2015). Sequential delivery of angiogenic growth factors improves revascularization and heart function after myocardial infarction. *Journal of Controlled Release: Official Journal of the Controlled Release Society*, 207, 7-17. doi:10.1016/j.jconrel.2015.03.034 [doi]
- Bae, K. H., Lee, K., Lee, J., Lee, I. S., Lee, J. H., & Park, T. G. (2011). Surface functionalized hollow manganese oxide nanoparticles for cancer targeted siRNA delivery and magnetic resonance imaging. *Journal of Controlled Release: Official Journal of the Controlled Release Society*, 152 Suppl 1, 133. doi:10.1016/j.jconrel.2011.08.044 [doi]
- Bakhtiary, Z., Saei, A. A., Hajipour, M. J., Raoufi, M., Vermesh, O., & Mahmoudi, M. (2016). Targeted superparamagnetic iron oxide nanoparticles for early detection of cancer: Possibilities and challenges. *Nanomedicine: Nanotechnology, Biology, and Medicine*, 12(2), 287-307. doi:10.1016/j.nano.2015.10.019 [doi]
- Balakumaran, A., Pawelczyk, E., Ren, J., Sworder, B., Chaudhry, A., Sabatino, M., . . . Robey, P. G. (2010). Superparamagnetic iron oxide nanoparticles labeling of bone marrow stromal (mesenchymal) cells does not affect their "stemness". *PLoS One*, 5(7), e11462. doi:10.1371/journal.pone.0011462 [doi]
- Balsam, L. B., Wagers, A. J., Christensen, J. L., Kofidis, T., Weissman, I. L., & Robbins, R. C. (2004). Haematopoietic stem cells adopt mature haematopoietic fates in ischaemic myocardium. *Nature*, 428(6983), 668-673. doi:10.1038/nature02460 [doi]
- Barbash, I. M., Chouraqui, P., Baron, J., Feinberg, M. S., Etzion, S., Tessone, A., . . . Leor, J. (2003). Systemic delivery of bone marrow-derived mesenchymal stem cells to the infarcted myocardium: Feasibility, cell migration, and body distribution. *Circulation*, 108(7), 863-868. doi:10.1161/01.CIR.0000084828.50310.6A [doi]
- Bashir, A., Gray, M. L., Boutin, R. D., & Burstein, D. (1997). Glycosaminoglycan in articular cartilage: In vivo assessment with delayed gd(DTPA)(2)-enhanced MR imaging. *Radiology*, 205(2), 551-558. doi:10.1148/radiology.205.2.9356644 [doi]
- Bashir, A., Gray, M. L., & Burstein, D. (1996). Gd-DTPA2- as a measure of cartilage degradation. *Magnetic Resonance in Medicine*, 36(5), 665-673.
- Bashir, A., Gray, M. L., Hartke, J., & Burstein, D. (1999). Nondestructive imaging of human cartilage glycosaminoglycan concentration by MRI. *Magnetic Resonance in Medicine*, 41(5), 857-865. doi:10.1002/(SICI)1522-2594(199905)41:53.0.CO;2-E [pii]
- Basly, B., Felder-Flesch, D., Perriat, P., Pourroy, G., & Begin-Colin, S. (2011). Properties and suspension stability of dendronized iron oxide nanoparticles for MRI applications. *Contrast Media & Molecular Imaging*, 6(3), 132-138. doi:10.1002/cmmi.416 [doi]

- Bauer, W. R., & Schulten, K. (1992). Theory of contrast agents in magnetic resonance imaging: Coupling of spin relaxation and transport. *Magnetic Resonance in Medicine*, 26(1), 16-39.
- Beam, A. S., Moore, K. G., Gillis, S. N., Ford, K. F., Gray, T., Steinwinder, A. H., & Graham, A. (2017). GBCAs and risk for nephrogenic systemic fibrosis: A literature review. *Radiologic Technology*, 88(6), 583-589. doi:88/6/583 [pii]
- Bellin, M. F., & Van Der Molen, A. J. (2008). Extracellular gadolinium-based contrast media: An overview. *European Journal of Radiology*, 66(2), 160-167. doi:101016/j.ejrad.2008.01.023 [doi]
- Bijlsma, J. W., Berenbaum, F., & Lafeber, F. P. (2011). Osteoarthritis: An update with relevance for clinical practice. *Lancet (London, England)*, 377(9783), 2115-2126. doi:10.1016/S0140-6736(11)60243-2 [doi]
- Bilecka, I., Djerdj, I., & Niederberger, M. (2008). One-minute synthesis of crystalline binary and ternary metal oxide nanoparticles. *Chemical Communications (Cambridge, England)*, (7):886-8. doi(7), 886-888. doi:10.1039/b717334b [doi]
- Botker, H. E., Kaltoft, A. K., Pedersen, S. F., & Kim, W. Y. (2012). Measuring myocardial salvage. *Cardiovascular Research*, 94(2), 266-275. doi:10.1093/cvr/cvs081 [doi]
- Bottomley, P. A., Foster, T. H., Argersinger, R. E., & Pfeifer, L. M. (1984). A review of normal tissue hydrogen NMR relaxation times and relaxation mechanisms from 1-100 Mhz: dependence on tissue type, NMR frequency, temperature, species, excision, and age. *Medical Physics*, 11(4), 425-48. doi:10.1118/1.595535 [doi]
- Brateman, L. (1986). Chemical shift imaging: a review. *American Journal of Roentgenology*, 146, 971-980. doi:10.2214/ajr.146.5.971[doi]
- Bulluck, H., Dharmakumar, R., Arai, A. E., Berry, C., & Hausenloy, D. J. (2018). Cardiovascular magnetic resonance in acute ST-segment-elevation myocardial infarction: Recent advances, controversies, and future directions. *Circulation*, 137(18), 1949-1964. doi:10.1161/CIRCULATIONAHA.117.030693 [doi]
- Bulluck, H., Go, Y. Y., Crimi, G., Ludman, A. J., Rosmini, S., Abdel-Gadir, A., . . . Hausenloy, D. J. (2017). Defining left ventricular remodeling following acute ST-segment elevation myocardial infarction using cardiovascular magnetic resonance. *Journal of Cardiovascular Magnetic Resonance: Official Journal of the Society for Cardiovascular Magnetic Resonance*, 19(1), 9. doi:10.1186/s12968-017-0343-9 [doi]
- Bulte, J. W. (2009). In vivo MRI cell tracking: Clinical studies. *AJR.American Journal of Roentgenology*, 193(2), 314-325. doi:10.2214/AJR.09.3107 [doi]
- Bulte, J. W. M. (2019a). Detecting different cell populations using multispectral (19)F MRI. *Radiology*, 291(2), 358-359. doi:10.1148/radiol.2019190377 [doi]
- Bulte, J. W. M. (2019b). Superparamagnetic iron oxides as MPI tracers: A primer and review of early applications. *Advanced Drug Delivery Reviews*, 138, 293-301. doi:S0169-409X(18)30311-9 [pii]
- Bulte, J. W., de Cuyper, M., Despres, D., & Frank, J. A. (1999). Short- vs. long-circulating magnetoliposomes as bone marrow-seeking MR contrast agents. *Journal of Magnetic Resonance Imaging*, 9(2), 329-335. doi:10.1002/(SICI)1522-2586(199902)9:23.0.CO;2-Z [pii]

- Bulte, J. W., & Kraitchman, D. L. (2004). Iron oxide MR contrast agents for molecular and cellular imaging. *NMR in Biomedicine*, 17(7), 484-499. doi:10.1002/nbm.924 [doi]
- Bulte, J. W., Vymazal, J., Brooks, R. A., Pierpaoli, C., & Frank, J. A. (1993). Frequency dependence of MR relaxation times. II. iron oxides. *Journal of Magnetic Resonance Imaging*, 3(4), 641-648.
- Burstein, D., Velyvis, J., Scott, K. T., Stock, K. W., Kim, Y. J., Jaramillo, D., . . . Gray, M. L. (2001). Protocol issues for delayed gd(DTPA)(2-)-enhanced MRI (dGEMRIC) for clinical evaluation of articular cartilage. *Magnetic Resonance in Medicine*, 45(1), 36-41. doi:10.1002/1522-2594(200101)45:13.0.CO;2-W [pii]
- Cai, M., Shen, R., Song, L., Lu, M., Wang, J., Zhao, S., . . . He, Z. X. (2016). Bone marrow mesenchymal stem cells (BM-MSCs) improve heart function in swine myocardial infarction model through paracrine effects. *Scientific Reports*, 6, 28250. doi:10.1038/srep28250 [doi]
- Carberry, J., Carrick, D., Haig, C., Ahmed, N., Mordi, I., McEntegart, M., . . . Berry, C. (2017). Persistent iron within the infarct core after ST-segment elevation myocardial infarction: Implications for left ventricular remodeling and health outcomes. *JACC.Cardiovascular Imaging*, doi:S1936-878X(17)30916-6 [pii]
- Cerqueira, M. D., Weissman, N. J., Dilsizian, V., Jacobs, A. K., Kaul, S., Laskey, W. K., . . . American Heart Association Writing Group on Myocardial Segmentation and Registration for Cardiac Imaging. (2002a). Standardized myocardial segmentation and nomenclature for tomographic imaging of the heart. A statement for healthcare professionals from the cardiac imaging committee of the council on clinical cardiology of the american heart association. *The International Journal of Cardiovascular Imaging*, 18(1), 539-542.
- Cerqueira, M. D., Weissman, N. J., Dilsizian, V., Jacobs, A. K., Kaul, S., Laskey, W. K., . . . American Heart Association Writing Group on Myocardial Segmentation and Registration for Cardiac Imaging. (2002b). Standardized myocardial segmentation and nomenclature for tomographic imaging of the heart. A statement for healthcare professionals from the cardiac imaging committee of the council on clinical cardiology of the american heart association. *Circulation*, 105(4), 539-542.
- Chavakis, E., Urbich, C., & Dimmeler, S. (2008). Homing and engraftment of progenitor cells: A prerequisite for cell therapy. *Journal of Molecular and Cellular Cardiology*, 45(4), 514-522. doi:10.1016/j.yjmcc.2008.01.004 [doi]
- Chen, D., Sun, N., Huang, Z., Cheng, C., Xu, H., & Gu, H. (2010). Experimental study on T2 relaxation time of protons in water suspensions of iron-oxide nanoparticles: Effects of polymer coating ; *Journal of Magnetism and Magnetic Materials*, 322(5), 548-556.
- Chen, Y. C., Hsiao, J. K., Liu, H. M., Lai, I. Y., Yao, M., Hsu, S. C., . . . Huang, D. M. (2010). The inhibitory effect of superparamagnetic iron oxide nanoparticle (ferucarbotran) on osteogenic differentiation and its signaling mechanism in human mesenchymal stem cells. *Toxicology and Applied Pharmacology*, 245(2), 272-279. doi:10.1016/j.taap.2010.03.011 [doi]

- Cheng, C., Xu, F., & Gu, H. (2011). Facile synthesis and morphology evolution of magnetic iron oxide nanoparticles in different polyol processes. *New Journal of Chemistry*, *35*, 1072-1079. doi:10.1039/C0NJ00986E
- Chirizzi, C., De Battista, D., Tirotta, I., Metrangolo, P., Comi, G., Bombelli, F. B., & Chaabane, L. (2019). Multispectral MRI with dual fluorinated probes to track mononuclear cell activity in mice. *Radiology*, *291*(2), 351-357. doi:10.1148/radiol.2019181073 [doi]
- Choi, J. A., & Gold, G. E. (2011). MR imaging of articular cartilage physiology. *Magnetic Resonance Imaging Clinics of North America*, *19*(2), 249-282. doi:10.1016/j.mric.2011.02.010 [doi]
- Chong, M. S., Ng, W. K., & Chan, J. K. (2016). Concise review: Endothelial progenitor cells in regenerative medicine: Applications and challenges. *Stem Cells Translational Medicine*, *5*(4), 530-538. doi:10.5966/sctm.2015-0227 [doi]
- Clifford, D. M., Fisher, S. A., Brunskill, S. J., Doree, C., Mathur, A., Clarke, M. J., . . . Martin-Rendon, E. (2012). Long-term effects of autologous bone marrow stem cell treatment in acute myocardial infarction: Factors that may influence outcomes. *PLoS One*, *7*(5), e37373. doi:10.1371/journal.pone.0037373 [doi]
- Clifford, D. M., Fisher, S. A., Brunskill, S. J., Doree, C., Mathur, A., Watt, S., & Martin-Rendon, E. (2012). Stem cell treatment for acute myocardial infarction. *The Cochrane Database of Systematic Reviews*, (2):CD006536. doi(2), CD006536. doi:10.1002/14651858.CD006536.pub3 [doi]
- Conaghan, P. G., Porcheret, M., Kingsbury, S. R., Gammon, A., Soni, A., Hurley, M., . . . Birrell, F. (2015). Impact and therapy of osteoarthritis: The arthritis care OA nation 2012 survey. *Clinical Rheumatology*, *34*(9), 1581-1588. doi:10.1007/s10067-014-2692-1 [doi]
- Crisostomo, V., Baez-Diaz, C., Maestre, J., Garcia-Lindo, M., Sun, F., Casado, J. G., . . . Sanchez-Margallo, F. M. (2015). Delayed administration of allogeneic cardiac stem cell therapy for acute myocardial infarction could ameliorate adverse remodeling: Experimental study in swine. *Journal of Translational Medicine*, *13*, 2. doi:10.1186/s12967-015-0512-2 [doi]
- Cromer Berman, S. M., Walczak, P., & Bulte, J. W. (2011). Tracking stem cells using magnetic nanoparticles. *Wiley Interdisciplinary Reviews.Nanomedicine and Nanobiotechnology*, *3*(4), 343-355. doi:10.1002/wnan.140 [doi]
- Crooks, L. E., Arakawa, M., Hoenninger, J., McCarten, M., Watts, J., & Kaufman, L. (1984). Magnetic resonance imaging: effects of magnetic field strength. *Radiology*, *151*(1), 127-133. doi:10.1148/radiology.151.1.6701302 [doi]
- Czeyda-Pommersheim, F., Martin, D. R., Costello, J. R., & Kalb, B. (2017). Contrast agents for MR imaging. *Magnetic Resonance Imaging Clinics of North America*, *25*(4), 705-711. doi:S1064-9689(17)30074-0 [pii]

- Dagata, J. A., Farkas, N., Dennis, C. L., Shull, R. D., Hackley, V. A., Yang, C., . . . Chang, E. H. (2008). Physical characterization methods for iron oxide contrast agents encapsulated within a targeted liposome-based delivery system. *Nanotechnology*, *19*(30), 4484/19/30/305101. Epub 2008 Jun 12. doi:10.1088/0957-4484/19/30/305101 [doi]
- Dall'Armellina, E., Karia, N., Lindsay, A. C., Karamitsos, T. D., Ferreira, V., Robson, M. D., . . . Choudhury, R. P. (2011). Dynamic changes of edema and late gadolinium enhancement after acute myocardial infarction and their relationship to functional recovery and salvage index. *Circulation Cardiovascular Imaging*, *4*(3), 228-236. doi:10.1161/CIRCIMAGING.111.963421 [doi]
- de Vries, I. J., Lesterhuis, W. J., Barentsz, J. O., Verdijk, P., van Krieken, J. H., Boerman, O. C., . . . Figdor, C. G. (2005). Magnetic resonance tracking of dendritic cells in melanoma patients for monitoring of cellular therapy. *Nature Biotechnology*, *23*(11), 1407-1413. doi:nbt1154 [pii]
- Devereux, R. B., & Reichek, N. (1977). Echocardiographic determination of left ventricular mass in man. anatomic validation of the method. *Circulation*, *55*(4), 613-618.
- Ding, D., Kanaly, C. W., Cummings, T. J., Herndon, J. E., Raghavan, R., & Sampson, J. H. (2010). Long-term safety of combined intracerebral delivery of free gadolinium and targeted chemotherapeutic agent PRX321. *Neurological Research*, *32*(8), 810-815. doi:10.1179/174367509X12581069052090 [doi]
- Dixit, P., & Katare, R. (2015). Challenges in identifying the best source of stem cells for cardiac regeneration therapy. *Stem Cell Research & Therapy*, *6*, 8. doi:10.1186/s13287-015-0010-8 [doi]
- Duan, H., Kuang, M., Wang, X., Wang, A., Mao, H., & Nie, S. (2008). Reexamining the effects of particle size and surface chemistry on the magnetic properties of iron oxide nanocrystals: New insights into spin disorder and proton relaxivity. *The Journal of Physical Chemistry*, *112*(22), 8127-8131. doi:10.1021/jp8029083
- Dubnika, A., Manoukian, M. A. C., Mohammadi, M. R., Parekh, M. B., Gurjarpadhye, A. A., Inayathullah, M., . . . Rajadas, J. (2018). Cytokines as therapeutic agents and targets in heart disease. *Cytokine & Growth Factor Reviews*, *43*, 54-68. doi:S1359-6101(18)30082-0 [pii]
- Estelrich, J., Sanchez-Martin, M. J., & Busquets, M. A. (2015). Nanoparticles in magnetic resonance imaging: From simple to dual contrast agents. *International Journal of Nanomedicine*, *10*, 1727-1741. doi:10.2147/IJN.S76501 [doi]
- Fan, C. Q., Leu, S., Sheu, J. J., Zhen, Y. Y., Tsai, T. H., Chen, Y. L., . . . Yip, H. K. (2014). Prompt bone marrow-derived mesenchymal stem cell therapy enables early porcine heart function recovery from acute myocardial infarction. *International Heart Journal*, *55*(4), 362-371. doi:DN/JST.JSTAGE/ihj/14-007 [pii]
- Faria, M. R., Cruz, M. M., Goncalves, M. C., Carvalho, A., Feio, G., & Martins, M. B. (2013). Synthesis and characterization of magnetoliposomes for MRI contrast enhancement. *International Journal of Pharmaceutics*, *446*(1-2), 183-190. doi:10.1016/j.ijpharm.2013.02.025 [doi]

- Felson, D. T., Zhang, Y., Hannan, M. T., Naimark, A., Weissman, B. N., Aliabadi, P., & Levy, D. (1995). The incidence and natural history of knee osteoarthritis in the elderly. the framingham osteoarthritis study. *Arthritis and Rheumatism*, 38(10), 1500-1505.
- Fernandez-Jimenez, R., Barreiro-Perez, M., Martin-Garcia, A., Sanchez-Gonzalez, J., Agüero, J., Galan-Arriola, C., . . . Ibanez, B. (2017). Dynamic edematous response of the human heart to myocardial infarction: Implications for assessing myocardial area at risk and salvage. *Circulation*, 136(14), 1288-1300. doi:10.1161/CIRCULATIONAHA.116.025582 [doi]
- Ferrucci, J. T., & Stark, D. D. (1990). Iron oxide-enhanced MR imaging of the liver and spleen: Review of the first 5 years. *AJR.American Journal of Roentgenology*, 155(5), 943-950. doi:10.2214/ajr.155.5.2120963 [doi]
- Fortuin, A. S., Bruggemann, R., van der Linden, J., Panfilov, I., Israel, B., Scheenen, T. W. J., & Barentsz, J. O. (2018). Ultra-small superparamagnetic iron oxides for metastatic lymph node detection: Back on the block. *Wiley Interdisciplinary Reviews.Nanomedicine and Nanobiotechnology*, 10(1), 10.1002/wnan.1471. Epub 2017 Apr 6. doi:10.1002/wnan.1471 [doi]
- Frangiannis, N. G. (2014). The inflammatory response in myocardial injury, repair, and remodelling. *Nature Reviews.Cardiology*, 11(5), 255-265. doi:10.1038/nrcardio.2014.28 [doi]
- Frank, J. A., Miller, B. R., Arbab, A. S., Zywicke, H. A., Jordan, E. K., Lewis, B. K., . . . Bulte, J. W. (2003). Clinically applicable labeling of mammalian and stem cells by combining superparamagnetic iron oxides and transfection agents. *Radiology*, 228(2), 480-487. doi:10.1148/radiol.2281020638 [doi]
- From the Centers for Disease Control and Prevention. Arthritis prevalence and activity limitations--United States, 1990. (1994). *Jama*, 272(5), 346-347.
- Fu, Y., & Kraitchman, D. L. (2010). Stem cell labeling for noninvasive delivery and tracking in cardiovascular regenerative therapy. *Expert Review of Cardiovascular Therapy*, 8(8), 1149-1160. doi:10.1586/erc.10.106 [doi]
- Fullerton, G. D., Potter, J. L., & Dornbluth, N. C. (1982) NMR relaxation of protons in tissues and other macromolecular water solutions. *Magnetic Resonance Imaging*, 1982(1), 209-228. doi:10.1016/0730-725x(82)90172-2 [doi]
- Garcia Ribeiro, R. S., Gysemans, C., da Cunha, J P M C M, Manshian, B. B., Jirak, D., Kriz, J., . . . Himmelreich, U. (2018). Magnetoliposomes as contrast agents for longitudinal in vivo assessment of transplanted pancreatic islets in a diabetic rat model. *Scientific Reports*, 8(1), 9. doi:10.1038/s41598-018-29136-9 [doi]
- Garcia Ribeiro, R. S., Ketkar-Atre, A., Yin, T., Louchami, K., Struys, T., Lambrichts, I., . . . Himmelreich, U. (2018). Improved labeling of pancreatic islets using cationic magnetoliposomes. *Journal of Personalized Medicine*, 8(1), 10.3390/jpm8010012. doi:E12 [pii]
- Ge, J., Hu, Y., Biasini, M., Dong, C., Guo, J., Beyermann, W. P., & Yin, Y. (2007). One-step synthesis of highly water-soluble magnetite colloidal nanocrystals. *Chemistry (Weinheim an Der Bergstrasse, Germany)*, 13(25), 7153-7161. doi:10.1002/chem.200700375 [doi]

- Geraldes, C. F., & Laurent, S. (2009). Classification and basic properties of contrast agents for magnetic resonance imaging. *Contrast Media & Molecular Imaging*, 4(1), 1-23. doi:10.1002/cmml.265 [doi]
- German, S. V., Navolokin, N. A., Kuznetsova, N. R., Zuev, V. V., Inozemtseva, O. A., Anis'kov, A. A., . . . Gorin, D. A. (2015). Liposomes loaded with hydrophilic magnetite nanoparticles: Preparation and application as contrast agents for magnetic resonance imaging. *Colloids and Surfaces.B, Biointerfaces*, 135, 109-115. doi:10.1016/j.colsurfb.2015.07.042 [doi]
- Gilad, A. A., Walczak, P., McMahon, M. T., Na, H. B., Lee, J. H., An, K., . . . Bulte, J. W. (2008). MR tracking of transplanted cells with "positive contrast" using manganese oxide nanoparticles. *Magnetic Resonance in Medicine*, 60(1), 1-7. doi:10.1002/mrm.21622 [doi]
- Gomez-Mauricio, G., Moscoso, I., Martin-Cancho, M. F., Crisostomo, V., Prat-Vidal, C., Baez-Diaz, C., . . . Bernad, A. (2016). Combined administration of mesenchymal stem cells overexpressing IGF-1 and HGF enhances neovascularization but moderately improves cardiac regeneration in a porcine model. *Stem Cell Research & Therapy*, 7(1), z. doi:10.1186/s13287-016-0350-z [doi]
- Graf, C., Vossen, D., Imhof, A., & van Blaaderen, A. (2003). A general method to coat colloidal particles with silica. *Langmuir*, 19(13), 6693-6700. doi:10.1021/la0347859
- Gulin-Sarfranz, T., Zhang, J., Desai Diti, Teuho, J., Sarfraz, J., Jiang, H., . . . Rosenholm, J. (2014). Combination of magnetic field and surface functionalization for reaching synergistic effects in cellular labeling by magnetic core-shell nanospheres. *Biomaterials Science*, 2, 1750-1760. doi:10.1039/C4BM00221K
- Hadjipanayis, C. G., Bonder, M. J., Balakrishnan, S., Wang, X., Mao, H., & Hadjipanayis, G. C. (2008). Metallic iron nanoparticles for MRI contrast enhancement and local hyperthermia. *Small (Weinheim an Der Bergstrasse, Germany)*, 4(11), 1925-1929. doi:10.1002/smll.200800261 [doi]
- Han, X., Xu, K., Taratula, O., & Farsad, K. (2019). Applications of nanoparticles in biomedical imaging. *Nanoscale*, doi:10.1039/c8nr07769j [doi]
- Haneder, S., Kucharczyk, W., Schoenberg, S. O., & Michaely, H. J. (2015). Safety of magnetic resonance contrast media: A review with special focus on nephrogenic systemic fibrosis. *Topics in Magnetic Resonance Imaging*, 24(1), 57-65. doi:10.1097/RMR.0b013e3182a14e79 [doi]
- Hani, A. F., Kumar, D., Malik, A. S., Ahmad, R. M., Razak, R., & Kiflie, A. (2015). Non-invasive and in vivo assessment of osteoarthritic articular cartilage: A review on MRI investigations. *Rheumatology International*, 35(1), 1-16. doi:10.1007/s00296-014-3052-9 [doi]
- Hao, X., Mansson-Broberg, A., Blomberg, P., Dellgren, G., Siddiqui, A. J., Grinnemo, K. H., . . . Sylven, C. (2004). Angiogenic and cardiac functional effects of dual gene transfer of VEGF-A165 and PDGF-BB after myocardial infarction. *Biochemical and Biophysical Research Communications*, 322(1), 292-296. doi:10.1016/j.bbrc.2004.07.101 [doi]

- Hao, X., Mansson-Broberg, A., Gustafsson, T., Grinnemo, K. H., Blomberg, P., Siddiqui, A. J., . . . Sylven, C. (2004). Angiogenic effects of dual gene transfer of bFGF and PDGF-BB after myocardial infarction. *Biochemical and Biophysical Research Communications*, 315(4), 1058-1063. doi:10.1016/j.bbrc.2004.01.165 [doi]
- Hashemi, S. M., Ghods, S., Kolodgie, F. D., Parcham-Azad, K., Keane, M., Hamamdzić, D., . . . Wilensky, R. L. (2008). A placebo controlled, dose-ranging, safety study of allogenic mesenchymal stem cells injected by endomyocardial delivery after an acute myocardial infarction. *European Heart Journal*, 29(2), 251-259. doi:ehm559 [pii]
- Hatzistergos, K. E., Quevedo, H., Oskouei, B. N., Hu, Q., Feigenbaum, G. S., Margitich, I. S., . . . Hare, J. M. (2010). Bone marrow mesenchymal stem cells stimulate cardiac stem cell proliferation and differentiation. *Circulation Research*, 107(7), 913-922. doi:10.1161/CIRCRESAHA.110.222703 [doi]
- He, G., Zhang, H., Wei, H., Wang, Y., Zhang, X., Tang, Y., . . . Hu, S. (2007). In vivo imaging of bone marrow mesenchymal stem cells transplanted into myocardium using magnetic resonance imaging: A novel method to trace the transplanted cells. *International Journal of Cardiology*, 114(1), 4-10. doi:S0167-5273(06)00153-7 [pii]
- Heesakkers, R. A., Hovels, A. M., Jager, G. J., van den Bosch, H C, Witjes, J. A., Raat, H. P., . . . Barentsz, J. (2008). MRI with a lymph-node-specific contrast agent as an alternative to CT scan and lymph-node dissection in patients with prostate cancer: A prospective multicohort study. *The Lancet.Oncology*, 9(9), 850-856. doi:10.1016/S1470-2045(08)70203-1 [doi]
- Heesakkers, R. A., Jager, G. J., Hovels, A. M., de Hoop, B., van den Bosch, H C, Raat, F., . . . Barentsz, J. O. (2009). Prostate cancer: Detection of lymph node metastases outside the routine surgical area with ferumoxtran-10-enhanced MR imaging. *Radiology*, 251(2), 408-414. doi:10.1148/radiol.2512071018 [doi]
- Heyn, C., Ronald, J. A., Mackenzie, L. T., MacDonald, I. C., Chambers, A. F., Rutt, B. K., & Foster, P. J. (2006). In vivo magnetic resonance imaging of single cells in mouse brain with optical validation. *Magnetic Resonance in Medicine*, 55(1), 23-29. doi:10.1002/mrm.20747 [doi]
- Hill, J. A., & Olson, E. N. (2008). Cardiac plasticity. *The New England Journal of Medicine*, 358(13), 1370-1380. doi:10.1056/NEJMra072139 [doi]
- Hinds, K. A., Hill, J. M., Shapiro, E. M., Laukkanen, M. O., Silva, A. C., Combs, C. A., . . . Dunbar, C. E. (2003). Highly efficient endosomal labeling of progenitor and stem cells with large magnetic particles allows magnetic resonance imaging of single cells. *Blood*, 102(3), 867-872. doi:10.1182/blood-2002-12-3669 [doi]
- Hoemann, C. D., Lafantaisie-Favreau, C. H., Lascau-Coman, V., Chen, G., & Guzman-Morales, J. (2012). The cartilage-bone interface. *The Journal of Knee Surgery*, 25(2), 85-97.
- Hofmann, M., Wollert, K. C., Meyer, G. P., Menke, A., Arseniev, L., Hertenstein, B., . . . Drexler, H. (2005). Monitoring of bone marrow cell homing into the infarcted human myocardium. *Circulation*, 111(17), 2198-2202. doi:01.CIR.0000163546.27639.AA [pii]

- Hombach, V., Grebe, O., Merkle, N., Waldenmaier, S., Hoher, M., Kochs, M., . . . Kestler, H. A. (2005). Sequelae of acute myocardial infarction regarding cardiac structure and function and their prognostic significance as assessed by magnetic resonance imaging. *European Heart Journal*, *26*(6), 549-557. doi:ehi147 [pii]
- Hsiao, J. K., Tai, M. F., Chu, H. H., Chen, S. T., Li, H., Lai, D. M., . . . Liu, H. M. (2007). Magnetic nanoparticle labeling of mesenchymal stem cells without transfection agent: Cellular behavior and capability of detection with clinical 1.5 T magnetic resonance at the single cell level. *Magnetic Resonance in Medicine*, *58*(4), 717-724. doi:10.1002/mrm.21377 [doi]
- Huang, H., Yue, T., Xu, K., Golzarian, J., Yu, J., & Huang, J. (2015). Fabrication and evaluation of tumor-targeted positive MRI contrast agent based on ultrasmall MnO nanoparticles. *Colloids and Surfaces.B, Biointerfaces*, *131*, 148-154. doi:10.1016/j.colsurfb.2015.04.047 [doi]
- Huang, Z., Li, C., Yang, S., Xu, J., Shen, Y., Xie, X., . . . Ge, J. (2015). Magnetic resonance hypointensive signal primarily originates from extracellular iron particles in the long-term tracking of mesenchymal stem cells transplanted in the infarcted myocardium. *International Journal of Nanomedicine*, *10*, 1679-1690. doi:10.2147/IJN.S77858 [doi]
- Janssens, S., Dubois, C., Bogaert, J., Theunissen, K., Deroose, C., Desmet, W., . . . Van de Werf, F. (2006). Autologous bone marrow-derived stem-cell transfer in patients with ST-segment elevation myocardial infarction: Double-blind, randomised controlled trial. *Lancet (London, England)*, *367*(9505), 113-121. doi:S0140-6736(05)67861-0 [pii]
- Jeevanantham, V., Butler, M., Saad, A., Abdel-Latif, A., Zuba-Surma, E. K., & Dawn, B. (2012). Adult bone marrow cell therapy improves survival and induces long-term improvement in cardiac parameters: A systematic review and meta-analysis. *Circulation*, *126*(5), 551-568. doi:10.1161/CIRCULATIONAHA.111.086074 [doi]
- Jeong, H., Yim, H. W., Park, H. J., Cho, Y., Hong, H., Kim, N. J., & Oh, I. H. (2018). Mesenchymal stem cell therapy for ischemic heart disease: Systematic review and meta-analysis. *International Journal of Stem Cells*, *11*(1), 1-12. doi:10.15283/ijsc17061 [doi]
- Jung, J. W., Kang, H. R., Kim, M. H., Lee, W., Min, K. U., Han, M. H., & Cho, S. H. (2012). Immediate hypersensitivity reaction to gadolinium-based MR contrast media. *Radiology*, *264*(2), 414-422. doi:10.1148/radiol.12112025 [doi]
- Kanda, T., Ishii, K., Kawaguchi, H., Kitajima, K., & Takenaka, D. (2014). High signal intensity in the dentate nucleus and globus pallidus on unenhanced T1-weighted MR images: Relationship with increasing cumulative dose of a gadolinium-based contrast material. *Radiology*, *270*(3), 834-841. doi:10.1148/radiol.13131669 [doi]
- Kanda, T., Nakai, Y., Hagiwara, A., Oba, H., Toyoda, K., & Furui, S. (2017). Distribution and chemical forms of gadolinium in the brain: A review. *The British Journal of Radiology*, *90*(1079), 20170115. doi:10.1259/bjr.20170115 [doi]
- Kanda, T., Oba, H., Toyoda, K., Kitajima, K., & Furui, S. (2016). Brain gadolinium deposition after administration of gadolinium-based contrast agents. *Japanese Journal of Radiology*, *34*(1), 3-9. doi:10.1007/s11604-015-0503-5 [doi]

- Kang, Y., Choi, J. Y., Yoo, H. J., Hong, S. H., & Kang, H. S. (2017). Delayed gadolinium-enhanced MR imaging of cartilage: A comparative analysis of different gadolinium-based contrast agents in an ex vivo porcine model. *Radiology*, *282*(3), 734-742. doi:10.1148/radiol.2016160367 [doi]
- Karimi, Z., Karimi, L., & Shokrollahi, H. (2013). Nano-magnetic particles used in biomedicine: Core and coating materials. *Materials Science & Engineering.C, Materials for Biological Applications*, *33*(5), 2465-2475. doi:10.1016/j.msec.2013.01.045 [doi]
- Karussis, D., Karageorgiou, C., Vaknin-Dembinsky, A., Gowda-Kurkalli, B., Gomori, J. M., Kassis, I., . . . Slavin, S. (2010). Safety and immunological effects of mesenchymal stem cell transplantation in patients with multiple sclerosis and amyotrophic lateral sclerosis. *Archives of Neurology*, *67*(10), 1187-1194. doi:10.1001/archneurol.2010.248 [doi]
- Kawada, H., Fujita, J., Kinjo, K., Matsuzaki, Y., Tsuma, M., Miyatake, H., . . . Fukuda, K. (2004). Nonhematopoietic mesenchymal stem cells can be mobilized and differentiate into cardiomyocytes after myocardial infarction. *Blood*, *104*(12), 3581-3587. doi:10.1182/blood-2004-04-1488 [doi]
- Kempson, G. E., Muir, H., Swanson, S. A., & Freeman, M. A. (1970). Correlations between stiffness and the chemical constituents of cartilage on the human femoral head. *Biochimica Et Biophysica Acta*, *215*(1), 70-77. doi:0304-4165(70)90388-0 [pii]
- Ketkar-Atre, A., Struys, T., Soenen, S. J., Lambrechts, I., Verfaillie, C. M., De Cuyper, M., & Himmelreich, U. (2013). Variability in contrast agent uptake by different but similar stem cell types. *International Journal of Nanomedicine*, *8*, 4577-4591. doi:10.2147/IJN.S51588 [doi]
- Khaleghi, S., Rahbarizadeh, F., Ahmadvand, D., Malek, M., & Madaah Hosseini, H. R. (2016). The effect of superparamagnetic iron oxide nanoparticles surface engineering on relaxivity of magnetoliposome. *Contrast Media & Molecular Imaging*, *11*(5), 340-349. doi:10.1002/cmmi.1697 [doi]
- Kijowski, R., & Chaudhary, R. (2014). Quantitative magnetic resonance imaging of the articular cartilage of the knee joint. *Magnetic Resonance Imaging Clinics of North America*, *22*(4), 649-669. doi:10.1016/j.mric.2014.07.005 [doi]
- Kim, T., Momin, E., Choi, J., Yuan, K., Zaidi, H., Kim, J., . . . Gilad, A. A. (2011). Mesoporous silica-coated hollow manganese oxide nanoparticles as positive T1 contrast agents for labeling and MRI tracking of adipose-derived mesenchymal stem cells. *Journal of the American Chemical Society*, *133*(9), 2955-2961. doi:10.1021/ja1084095 [doi]
- Kircher, M. F., Gambhir, S. S., & Grimm, J. (2011). Noninvasive cell-tracking methods. *Nature Reviews.Clinical Oncology*, *8*(11), 677-688. doi:10.1038/nrclinonc.2011.141 [doi]
- Kiviniitty, K. (1984). NMR relaxation times in NMR imaging. *Annals of Clinical Research*, *40*(16), 4-6.
- Kiviranta, I., Jurvelin, J., Tammi, M., Saamanen, A. M., & Helminen, H. J. (1985). Microspectrophotometric quantitation of glycosaminoglycans in articular cartilage sections stained with safranin O. *Histochemistry*, *82*(3), 249-255.

- Kostura, L., Kraitchman, D. L., Mackay, A. M., Pittenger, M. F., & Bulte, J. W. (2004). Feridex labeling of mesenchymal stem cells inhibits chondrogenesis but not adipogenesis or osteogenesis. *NMR in Biomedicine*, *17*(7), 513-517. doi:10.1002/nbm.925 [doi]
- Laasanen, M. S., Toyras, J., Korhonen, R. K., Rieppo, J., Saarakkala, S., Nieminen, M. T., . . . Jurvelin, J. S. (2003). Biomechanical properties of knee articular cartilage. *Biorheology*, *40*(1-3), 133-140.
- LaConte, L. E., Nitin, N., Zurkiya, O., Caruntu, D., O'Connor, C. J., Hu, X., & Bao, G. (2007). Coating thickness of magnetic iron oxide nanoparticles affects R2 relaxivity. *Journal of Magnetic Resonance Imaging: JMRI*, *26*(6), 1634-1641. doi:10.1002/jmri.21194 [doi]
- Lacroix, L. M., Ho, D., & Sun, S. (2010). Magnetic nanoparticles as both imaging probes and therapeutic agents. *Current Topics in Medicinal Chemistry*, *10*(12), 1184-1197. doi:BSP/CTMC/E-Pub/-0068-10-11 [pii]
- Lai, P. F., Panama, B. K., Masse, S., Li, G., Zhang, Y., Kusha, M., . . . Nanthakumar, K. (2013). Mesenchymal stem cell transplantation mitigates electrophysiological remodeling in a rat model of myocardial infarction. *Journal of Cardiovascular Electrophysiology*, *24*(7), 813-821. doi:10.1111/jce.12162 [doi]
- Lai, S. L., Marin-Juez, R., & Stainier, D. Y. R. (2019). Immune responses in cardiac repair and regeneration: A comparative point of view. *Cellular and Molecular Life Sciences : CMLS*, *76*(7), 1365-1380. doi:10.1007/s00018-018-2995-5 [doi]
- Langereis, S., Geelen, T., Grull, H., Strijkers, G. J., & Nicolay, K. (2013). Paramagnetic liposomes for molecular MRI and MRI-guided drug delivery. *NMR in Biomedicine*, *26*(7), 728-744. doi:10.1002/nbm.2971 [doi]
- Laurent, S., Forge, D., Port, M., Roch, A., Robic, C., Vander Elst, L., & Muller, R. N. (2008). Magnetic iron oxide nanoparticles: Synthesis, stabilization, vectorization, physicochemical characterizations, and biological applications. *Chemical Reviews*, *108*(6), 2064-2110. doi:10.1021/cr068445e [doi]
- Lauterbur, P. C. (1973). Image formation by induced local interactions: Examples of employing nuclear magnetic resonance. *Nature*, *242*(5394), 190-191.
- Li, N., Wang, C., Jia, L., & Du, J. (2014). Heart regeneration, stem cells, and cytokines. *Regenerative Medicine Research*, *2*(1), 6. eCollection 2014 Dec. doi:10.1186/2050-490X-2-6 [doi]
- Link, T. M., Stahl, R., & Woertler, K. (2007). Cartilage imaging: Motivation, techniques, current and future significance. *European Radiology*, *17*(5), 1135-1146. doi:10.1007/s00330-006-0453-5 [doi]
- Lister, Z., Rayner, K. J., & Suuronen, E. J. (2016). How biomaterials can influence various cell types in the repair and regeneration of the heart after myocardial infarction. *Frontiers in Bioengineering and Biotechnology*, *4*, 62. doi:10.3389/fbioe.2016.00062 [doi]

- Liu, Z. J., Song, X. X., & Tang, Q. (2013). Development of PEGylated KMnF₃ nanoparticles as a T1-weighted contrast agent: Chemical synthesis, in vivo brain MR imaging, and accounting for high relaxivity. *Nanoscale*, 5(11), 5073-5079. doi:10.1039/c3nr00721a [doi]
- Losina, E., Paltiel, A. D., Weinstein, A. M., Yelin, E., Hunter, D. J., Chen, S. P., . . . Katz, J. N. (2015). Lifetime medical costs of knee osteoarthritis management in the united states: Impact of extending indications for total knee arthroplasty. *Arthritis Care & Research*, 67(2), 203-215. doi:10.1002/acr.22412 [doi]
- Lund, G. K., Stork, A., Muellerleile, K., Barmeyer, A. A., Bansmann, M. P., Knefel, M., . . . Saeed, M. (2007). Prediction of left ventricular remodeling and analysis of infarct resorption in patients with reperfused myocardial infarcts by using contrast-enhanced MR imaging. *Radiology*, 245(1), 95-102. doi:245/1/95 [pii]
- Ma, G. S., Qi, C. M., Liu, N. F., Shen, C. X., Chen, Z., Liu, X. J., . . . Tang, Y. L. (2011). Efficiently tracking of stem cells in vivo using different kinds of superparamagnetic iron oxide in swine with myocardial infarction. *Chinese Medical Journal*, 124(8), 1199-1204.
- Ma, N., Cheng, H., Lu, M., Liu, Q., Chen, X., Yin, G., . . . Zhao, S. (2015). Magnetic resonance imaging with superparamagnetic iron oxide fails to track the long-term fate of mesenchymal stem cells transplanted into heart. *Scientific Reports*, 5, 9058. doi:10.1038/srep09058 [doi]
- Madelin, G., Lee, J. S., Regatte, R. R., & Jerschow, A. (2014). Sodium MRI: Methods and applications. *Progress in Nuclear Magnetic Resonance Spectroscopy*, 79, 14-47. doi:10.1016/j.pnmrs.2014.02.001 [doi]
- Madigan, M., & Atoui, R. (2018). Therapeutic use of stem cells for myocardial infarction. *Bioengineering (Basel, Switzerland)*, 5(2), 10.3390/bioengineering5020028. doi:E28 [pii]
- Maenosono, S., Suzuki, T., & Saita, S. (2008). Super-paramagnetic FePt nanoparticles as excellent MRI contrast agents. *Journal of Magnetism and Magnetic Materials*, 320(9), L83.
- Mahmoudi, M., Sahraian, M. A., Shokrgozar, M. A., & Laurent, S. (2011). Superparamagnetic iron oxide nanoparticles: Promises for diagnosis and treatment of multiple sclerosis. *ACS Chemical Neuroscience*, 2(3), 118-140. doi:10.1021/cn100100e [doi]
- Mailander, V., Lorenz, M. R., Holzapfel, V., Musyanovych, A., Fuchs, K., Wiesneth, M., . . . Schrezenmeier, H. (2008). Carboxylated superparamagnetic iron oxide particles label cells intracellularly without transfection agents. *Molecular Imaging and Biology : MIB : The Official Publication of the Academy of Molecular Imaging*, 10(3), 138-146. doi:10.1007/s11307-007-0130-3 [doi]
- Makela, J., Yannopoulos, F., Ylitalo, K., Makikallio, T., Lehtonen, S., Lappi-Blanco, E., . . . Anttila, V. (2012). Granulation tissue is altered after intramyocardial and intracoronary bone marrow-derived cell transfer for experimental acute myocardial infarction. *Cardiovascular Pathology : The Official Journal of the Society for Cardiovascular Pathology*, 21(3), 132-142. doi:10.1016/j.carpath.2011.06.002 [doi]

- Makela, J., Ylitalo, K., Lehtonen, S., Dahlbacka, S., Niemela, E., Kiviluoma, K., . . . Anttila, V. (2007). Bone marrow-derived mononuclear cell transplantation improves myocardial recovery by enhancing cellular recruitment and differentiation at the infarction site. *The Journal of Thoracic and Cardiovascular Surgery*, *134*(3), 565-573. doi:S0022-5223(07)00770-2 [pii]
- Mankin, H. J., Dorfman, H., Lippiello, L., & Zarins, A. (1971). Biochemical and metabolic abnormalities in articular cartilage from osteo-arthritic human hips. II. correlation of morphology with biochemical and metabolic data. *The Journal of Bone and Joint Surgery.American Volume*, *53*(3), 523-537.
- Mankin, H. J., & Thrasher, A. Z. (1975). Water content and binding in normal and osteoarthritic human cartilage. *The Journal of Bone and Joint Surgery. American Volume*, *57*(1), 76-80.
- Maroudas, A., & Venn, M. (1977). Chemical composition and swelling of normal and osteoarthrotic femoral head cartilage. II. swelling. *Annals of the Rheumatic Diseases*, *36*(5), 399-406.
- Martinez-Gonzalez, R., Estelrich, J., & Busquets, M. A. (2016). Liposomes loaded with hydrophobic iron oxide nanoparticles: Suitable T(2) contrast agents for MRI. *International Journal of Molecular Sciences*, *17*(8), 10.3390/ijms17081209. doi:10.3390/ijms17081209 [doi]
- Mathiasen, A. B., Jorgensen, E., Qayyum, A. A., Haack-Sorensen, M., Eklund, A., & Kastrup, J. (2012). Rationale and design of the first randomized, double-blind, placebo-controlled trial of intramyocardial injection of autologous bone-marrow derived mesenchymal stromal cells in chronic ischemic heart failure (MSC-HF trial). *American Heart Journal*, *164*(3), 285-291. doi:10.1016/j.ahj.2012.05.026 [doi]
- Mendis, S., Thygesen, K., Kuulasmaa, K., Giampaoli, S., Mahonen, M., Ngu Blackett, K., . . . Writing group on behalf of the participating experts of the WHO consultation for revision of WHO definition of myocardial infarction. (2011). World health organization definition of myocardial infarction: 2008-09 revision. *International Journal of Epidemiology*, *40*(1), 139-146. doi:10.1093/ije/dyq165 [doi]
- Meola, A., Rao, J., Chaudhary, N., Sharma, M., & Chang, S. D. (2018). Gold nanoparticles for brain tumor imaging: A systematic review. *Frontiers in Neurology*, *9*, 328. doi:10.3389/fneur.2018.00328 [doi]
- Micheu, M. M., & Dorobantu, M. (2017). Fifteen years of bone marrow mononuclear cell therapy in acute myocardial infarction. *World Journal of Stem Cells*, *9*(4), 68-76. doi:10.4252/wjsc.v9.i4.68 [doi]
- Modo, M., Hoehn, M., & Bulte, J. W. (2005). Cellular MR imaging. *Molecular Imaging*, *4*(3), 143-164.
- Moore, M. M., & Chung, T. (2017). Review of key concepts in magnetic resonance physics. *Pediatric Radiology*, *47*(5), 497-506. doi:10.1007/s00247-017-3791-3 [doi]
- Mow, V. C., Ratcliffe, A., & Poole, A. R. (1992). Cartilage and diarthrodial joints as paradigms for hierarchical materials and structures. *Biomaterials*, *13*(2), 67-97. doi:0142-9612(92)90001-5 [pii]

- Mow, V., & Huskes, R. (2015). *Basic orthopaedic biomechanics and mechano-biology* (3rd ed.) Lippincott Williams & Wilkins. doi:<https://doi.org/10.1186/1475-925X-4-28>
- Multanen, J., Rauvala, E., Lammentausta, E., Ojala, R., Kiviranta, I., Hakkinen, A., . . . Heinonen, A. (2009). Reproducibility of imaging human knee cartilage by delayed gadolinium-enhanced MRI of cartilage (dGEMRIC) at 1.5 tesla. *Osteoarthritis and Cartilage*, *17*(5), 559-564. doi:10.1016/j.joca.2008.12.001 [doi]
- Murata, N., Murata, K., Gonzalez-Cuyar, L. F., & Maravilla, K. R. (2016). Gadolinium tissue deposition in brain and bone. *Magnetic Resonance Imaging*, *34*(10), 1359-1365. doi:S0730-725X(16)30140-0 [pii]
- Murry, C. E., Soonpaa, M. H., Reinecke, H., Nakajima, H., Nakajima, H. O., Rubart, M., . . . Field, L. J. (2004). Haematopoietic stem cells do not transdifferentiate into cardiac myocytes in myocardial infarcts. *Nature*, *428*(6983), 664-668. doi:10.1038/nature02446 [doi]
- Na, H. B., Lee, J. H., An, K., Park, Y. I., Park, M., Lee, I. S., . . . Hyeon, T. (2007). Development of a T1 contrast agent for magnetic resonance imaging using MnO nanoparticles. *Angewandte Chemie (International Ed.in English)*, *46*(28), 5397-5401. doi:10.1002/anie.200604775 [doi]
- Ngen, E. J., Kato, Y., & Artemov, D. (2017). Direct cell labeling to image transplanted stem cells in real time using a dual-contrast MRI technique. *Current Protocols in Stem Cell Biology*, *42*, 5A.10.19. doi:10.1002/cpsc.33 [doi]
- Ngen, E. J., Wang, L., Kato, Y., Krishnamachary, B., Zhu, W., Gandhi, N., . . . Artemov, D. (2015). Imaging transplanted stem cells in real time using an MRI dual-contrast method. *Scientific Reports*, *5*, 13628. doi:10.1038/srep13628 [doi]
- Nieminen, M. T., Rieppo, J., Silvennoinen, J., Toyras, J., Hakumaki, J. M., Hyttinen, M. M., . . . Jurvelin, J. S. (2002). Spatial assessment of articular cartilage proteoglycans with gd-DTPA-enhanced T1 imaging. *Magnetic Resonance in Medicine*, *48*(4), 640-648. doi:10.1002/mrm.10273 [doi]
- Nygren, J. M., Jovinge, S., Breitbach, M., Sawen, P., Roll, W., Hescheler, J., . . . Jacobsen, S. E. (2004). Bone marrow-derived hematopoietic cells generate cardiomyocytes at a low frequency through cell fusion, but not transdifferentiation. *Nature Medicine*, *10*(5), 494-501. doi:10.1038/nm1040 [doi]
- Odeblad, E., Bhar, B. N., & Lindstrom, G. (1956). Proton magnetic resonance of human red blood cells in heavy-water exchange experiments. *Archives of Biochemistry and Biophysics*, *63*(1), 221-225. doi:0003-9861(56)90025-X [pii]
- Odeblad, E., & Lindstrom, G. (1955). Some preliminary observations on the proton magnetic resonance in biologic samples. *Acta Radiologica*, *43*(6), 469-476.
- Odenbach, S., & Muller, H. W. (2002). Stationary off-equilibrium magnetization in ferrofluids under rotational and elongational flow. *Physical Review Letters*, *89*(3), 037202. doi:10.1103/PhysRevLett.89.037202 [doi]
- Pawelczyk, E., Jordan, E. K., Balakumaran, A., Chaudhry, A., Gormley, N., Smith, M., . . . Frank, J. A. (2009). In vivo transfer of intracellular labels from locally implanted bone marrow stromal cells to resident tissue macrophages. *PloS One*, *4*(8), e6712. doi:10.1371/journal.pone.0006712 [doi]

- Pearle, A. D., Warren, R. F., & Rodeo, S. A. (2005). Basic science of articular cartilage and osteoarthritis. *Clinics in Sports Medicine*, 24(1), 1-12. doi:S0278-5919(04)00094-8 [pii]
- Pelled, G., Bergman, H., Ben-Hur, T., & Goelman, G. (2007). Manganese-enhanced MRI in a rat model of parkinson's disease. *Journal of Magnetic Resonance Imaging : JMRI*, 26(4), 863-870. doi:10.1002/jmri.21051 [doi]
- Peng, C., Yang, K., Xiang, P., Zhang, C., Zou, L., Wu, X., . . . Chen, L. (2013). Effect of transplantation with autologous bone marrow stem cells on acute myocardial infarction. *International Journal of Cardiology*, 162(3), 158-165. doi:10.1016/j.ijcard.2011.05.077 [doi]
- Pennella, S., Reggiani Bonetti, L., Migaldi, M., Manenti, A., Lonardi, R., Giuliani, E., . . . Mattioli, A. V. (2017). Does stem cell therapy induce myocardial neoangiogenesis? histological evaluation in an ischemia/reperfusion animal model. *Journal of Cardiovascular Medicine (Hagerstown, Md.)*, 18(4), 277-282. doi:10.2459/JCM.0000000000000357 [doi]
- Pfeffer, M. A., & Braunwald, E. (1990). Ventricular remodeling after myocardial infarction. experimental observations and clinical implications. *Circulation*, 81(4), 1161-1172.
- Pritzker, K. P., Gay, S., Jimenez, S. A., Ostergaard, K., Pelletier, J. P., Revell, P. A., . . . van den Berg, W. B. (2006). Osteoarthritis cartilage histopathology: Grading and staging. *Osteoarthritis and Cartilage*, 14(1), 13-29. doi:S1063-4584(05)00197-4 [pii]
- Qi, C. M., Ma, G. S., Liu, N. F., Shen, C. X., Chen, Z., Liu, X. J., . . . Tang, Y. L. (2008). Transplantation of magnetically labeled mesenchymal stem cells improves cardiac function in a swine myocardial infarction model. *Chinese Medical Journal*, 121(6), 544-550.
- Radbruch, A. (2018). Gadolinium deposition in the brain: We need to differentiate between chelated and dechelated gadolinium. *Radiology*, 288(2), 434-435. doi:10.1148/radiol.2018180294 [doi]
- Radbruch, A., Weberling, L. D., Kieslich, P. J., Eidel, O., Burth, S., Kickingereider, P., . . . Bendszus, M. (2015). Gadolinium retention in the dentate nucleus and globus pallidus is dependent on the class of contrast agent. *Radiology*, 275(3), 783-791. doi:10.1148/radiol.2015150337 [doi]
- Rasouli, E., Basirun, W. J., Rezayi, M., Shamel, K., Nourmohammadi, E., Khandanlou, R., . . . Khoshdel Sarkarizi, H. (2018). Ultrasmall superparamagnetic Fe₃O₄ nanoparticles: Honey-based green and facile synthesis and in vitro viability assay. *International Journal of Nanomedicine*, 13, 6903-6911. doi:10.2147/IJN.S158083 [doi]
- Reddy, K., Khaliq, A., & Henning, R. J. (2015). Recent advances in the diagnosis and treatment of acute myocardial infarction. *World Journal of Cardiology*, 7(5), 243-276. doi:10.4330/wjc.v7.i5.243 [doi]
- Ridgway, J. P. (2010). Cardiovascular magnetic resonance physics for clinicians: Part I. *Journal of Cardiovascular Magnetic Resonance: Official Journal of the Society for Cardiovascular Magnetic Resonance*, 12, 71. doi:10.1186/1532-429X-12-71 [doi]

- Rosenberg, J. H., Rai, V., Dilisio, M. F., & Agrawal, D. K. (2017). Damage-associated molecular patterns in the pathogenesis of osteoarthritis: Potentially novel therapeutic targets. *Molecular and Cellular Biochemistry*, 434(1-2), 171-179. doi:10.1007/s11010-017-3047-4 [doi]
- Rosenberg, J. T., Yuan, X., Grant, S., & Ma, T. (2016). Tracking mesenchymal stem cells using magnetic resonance imaging. *Brain Circulation*, 2(3), 108-113. doi:10.4103/2394-8108.192521 [doi]
- Roughley, P. J. (2006). The structure and function of cartilage proteoglycans. *European Cells & Materials*, 12, 92-101. doi:vol012a11 [pii]
- Rumenapp, C., Gleich, B., & Haase, A. (2012). Magnetic nanoparticles in magnetic resonance imaging and diagnostics. *Pharmaceutical Research*, 29(5), 1165-1179. doi:10.1007/s11095-012-0711-y [doi]
- Saarakkala, S., Julkunen, P., Kiviranta, P., Makitalo, J., Jurvelin, J. S., & Korhonen, R. K. (2010). Depth-wise progression of osteoarthritis in human articular cartilage: Investigation of composition, structure and biomechanics. *Osteoarthritis and Cartilage*, 18(1), 73-81. doi:10.1016/j.joca.2009.08.003 [doi]
- Salo, E. N., Nissi, M. J., Kulmala, K. A., Tiitu, V., Toyras, J., & Nieminen, M. T. (2012). Diffusion of gd-DTPA(2)(-) into articular cartilage. *Osteoarthritis and Cartilage*, 20(2), 117-126. doi:10.1016/j.joca.2011.11.016 [doi]
- Samidurai, A., Kukreja, R. C., & Das, A. (2018). Emerging role of mTOR signaling-related miRNAs in cardiovascular diseases. *Oxidative Medicine and Cellular Longevity*, 2018, 6141902. doi:10.1155/2018/6141902 [doi]
- Saville, S. L., Woodward, R. C., House, M. J., Tokarev, A., Hammers, J., Qi, B., . . . Mefford, O. T. (2013). The effect of magnetically induced linear aggregates on proton transverse relaxation rates of aqueous suspensions of polymer coated magnetic nanoparticles. *Nanoscale*, 5(5), 2152-2163. doi:10.1039/c3nr32979h [doi]
- Schmitt-Willich, H. (2007). Stability of linear and macrocyclic gadolinium based contrast agents. *The British Journal of Radiology*, 80(955), 5. doi:80/955/581 [pii]
- Schulz-Menger, J., Bluemke, D. A., Bremerich, J., Flamm, S. D., Fogel, M. A., Friedrich, M. G., . . . Nagel, E. (2013). Standardized image interpretation and post processing in cardiovascular magnetic resonance: Society for cardiovascular magnetic resonance (SCMR) board of trustees task force on standardized post processing. *Journal of Cardiovascular Magnetic Resonance: Official Journal of the Society for Cardiovascular Magnetic Resonance*, 15, 35. doi:10.1186/1532-429X-15-35 [doi]
- Senpan, A., Caruthers, S. D., Rhee, I., Mauro, N. A., Pan, D., Hu, G., . . . Lanza, G. M. (2009). Conquering the dark side: Colloidal iron oxide nanoparticles. *ACS Nano*, 3(12), 3917-3926. doi:10.1021/nn900819y [doi]
- Seymour, L., Schacht, E., & Duncan, R. (1991). The effect of size of polystyrene particles on their retention within the rat peritoneal compartment, and on their interaction with rat peritoneal macrophages in vitro. *Cell Biology International Reports*, 15(4), 277-286.
- Shapiro, E. M., Borthakur, A., Gougoutas, A., & Reddy, R. (2002). ²³Na MRI accurately measures fixed charge density in articular cartilage. *Magnetic Resonance in Medicine*, 47(2), 284-291. doi:10.1002/mrm.10054 [pii]

- Shapiro, E. M., Sharer, K., Skrtic, S., & Koretsky, A. P. (2006). In vivo detection of single cells by MRI. *Magnetic Resonance in Medicine*, 55(2), 242-249. doi:10.1002/mrm.20718 [doi]
- Shapiro, E. M., Skrtic, S., & Koretsky, A. P. (2005). Sizing it up: Cellular MRI using micron-sized iron oxide particles. *Magnetic Resonance in Medicine*, 53(2), 329-338. doi:10.1002/mrm.20342 [doi]
- Shapiro, E. M., Skrtic, S., Sharer, K., Hill, J. M., Dunbar, C. E., & Koretsky, A. P. (2004). MRI detection of single particles for cellular imaging. *Proceedings of the National Academy of Sciences of the United States of America*, 101(30), 10901-10906. doi:10.1073/pnas.0403918101 [doi]
- Sheikh, A. Y., Lin, S. A., Cao, F., Cao, Y., van der Bogt, K E, Chu, P., . . . Wu, J. C. (2007). Molecular imaging of bone marrow mononuclear cell homing and engraftment in ischemic myocardium. *Stem Cells (Dayton, Ohio)*, 25(10), 2677-2684. doi:2007-0041 [pii]
- Shen, Z., Wu, A., & Chen, X. (2017). Iron oxide nanoparticle based contrast agents for magnetic resonance imaging. *Molecular Pharmaceutics*, 14(5), 1352-1364. doi:10.1021/acs.molpharmaceut.6b00839 [doi]
- Sheng, C. C., Zhou, L., & Hao, J. (2013). Current stem cell delivery methods for myocardial repair. *BioMed Research International*, 2013, 547902. doi:10.1155/2013/547902 [doi]
- Shin, J., Anisur, R. M., Ko, M. K., Im, G. H., Lee, J. H., & Lee, I. S. (2009). Hollow manganese oxide nanoparticles as multifunctional agents for magnetic resonance imaging and drug delivery. *Angewandte Chemie (International Ed.in English)*, 48(2), 321-324. doi:10.1002/anie.200802323 [doi]
- Shokrollahi, H. (2013). Contrast agents for MRI. *Materials Science & Engineering.C, Materials for Biological Applications*, 33(8), 4485-4497. doi:10.1016/j.msec.2013.07.012 [doi]
- Silva, A. C., Lee, J. H., Aoki, I., & Koretsky, A. P. (2004). Manganese-enhanced magnetic resonance imaging (MEMRI): Methodological and practical considerations. *NMR in Biomedicine*, 17(8), 532-543. doi:10.1002/nbm.945 [doi]
- Singh, A., Singh, A., & Sen, D. (2016). Mesenchymal stem cells in cardiac regeneration: A detailed progress report of the last 6 years (2010-2015). *Stem Cell Research & Therapy*, 7(1), 0. doi:10.1186/s13287-016-0341-0 [doi]
- Soenen, S. J., Brisson, A. R., Jonckheere, E., Nuytten, N., Tan, S., Himmelreich, U., & De Cuyper, M. (2011). The labeling of cationic iron oxide nanoparticle-resistant hepatocellular carcinoma cells using targeted magnetoliposomes. *Biomaterials*, 32(6), 1748-1758. doi:10.1016/j.biomaterials.2010.11.005 [doi]
- Soenen, S. J., De Meyer, S. F., Dresselaers, T., Vande Velde, G., Pareyn, I. M., Braeckmans, K., . . . Vanhoorelbeke, K. I. (2011). MRI assessment of blood outgrowth endothelial cell homing using cationic magnetoliposomes. *Biomaterials*, 32(17), 4140-4150. doi:10.1016/j.biomaterials.2011.02.037 [doi]
- Soenen, S. J., Hodenius, M., & De Cuyper, M. (2009). Magnetoliposomes: Versatile innovative nanocolloids for use in biotechnology and biomedicine. *Nanomedicine (London, England)*, 4(2), 177-191. doi:10.2217/17435889.4.2.177 [doi]

- Soria, G., Aguilar, E., Tudela, R., Mullol, J., Planas, A. M., & Marin, C. (2011). In vivo magnetic resonance imaging characterization of bilateral structural changes in experimental parkinson's disease: A T2 relaxometry study combined with longitudinal diffusion tensor imaging and manganese-enhanced magnetic resonance imaging in the 6-hydroxydopamine rat model. *The European Journal of Neuroscience*, *33*(8), 1551-1560. doi:10.1111/j.1460-9568.2011.07639.x [doi]
- Srinivas, M., Aarntzen, E. H., Bulte, J. W., Oyen, W. J., Heerschap, A., de Vries, I. J., & Figdor, C. G. (2010). Imaging of cellular therapies. *Advanced Drug Delivery Reviews*, *62*(11), 1080-1093. doi:10.1016/j.addr.2010.08.009 [doi]
- Stephen, Z. R., Kievit, F. M., & Zhang, M. (2011). Magnetite nanoparticles for medical MR imaging. *Materials Today (Kidlington, England)*, *14*(7-8), 330-338. doi:10.1016/S1369-7021(11)70163-8 [doi]
- Stone, G. W., Selker, H. P., Thiele, H., Patel, M. R., Udelson, J. E., Ohman, E. M., . . . Ben-Yehuda, O. (2016). Relationship between infarct size and outcomes following primary PCI: Patient-level analysis from 10 randomized trials. *Journal of the American College of Cardiology*, *67*(14), 1674-1683. doi:10.1016/j.jacc.2016.01.069 [doi]
- Sun, N., Chen, D., Gu, H., & Wang, X. (2009). Experimental study on relaxation time of protons in water suspensions of iron-oxide nanoparticles: Waiting time dependence. *Journal of Magnetism and Magnetic Materials*, *321*(18), 2971-2975.
- Sun, S., Zeng, H., Robinson, D. B., Raoux, S., Rice, P. M., Wang, S. X., & Li, G. (2004). Monodisperse MFe₂O₄ (M = fe, co, mn) nanoparticles. *Journal of the American Chemical Society*, *126*(1), 273-279. doi:10.1021/ja0380852 [doi]
- Suzuki, Y., Zhang, S., Kundu, P., Yeung, A. C., Robbins, R. C., & Yang, P. C. (2007). In vitro comparison of the biological effects of three transfection methods for magnetically labeling mouse embryonic stem cells with ferumoxides. *Magnetic Resonance in Medicine*, *57*(6), 1173-1179. doi:10.1002/mrm.21219 [doi]
- Takahashi, K., & Yamanaka, S. (2006). Induction of pluripotent stem cells from mouse embryonic and adult fibroblast cultures by defined factors. *Cell*, *126*(4), 663-676. doi:S0092-8674(06)00976-7 [pii]
- Takahashi, K., & Yamanaka, S. (2013). Induced pluripotent stem cells in medicine and biology. *Development (Cambridge, England)*, *140*(12), 2457-2461. doi:10.1242/dev.092551 [doi]
- Takano, H., Ohtsuka, M., Akazawa, H., Toko, H., Harada, M., Hasegawa, H., . . . Komuro, I. (2003). Pleiotropic effects of cytokines on acute myocardial infarction: G-CSF as a novel therapy for acute myocardial infarction. *Current Pharmaceutical Design*, *9*(14), 1121-1127.
- Teng, C. J., Luo, J., Chiu, R. C., & Shum-Tim, D. (2006). Massive mechanical loss of microspheres with direct intramyocardial injection in the beating heart: Implications for cellular cardiomyoplasty. *The Journal of Thoracic and Cardiovascular Surgery*, *132*(3), 628-632. doi:S0022-5223(06)00962-7 [pii]
- Terreno, E., Castelli, D. D., Viale, A., & Aime, S. (2010). Challenges for molecular magnetic resonance imaging. *Chemical Reviews*, *110*(5), 3019-3042. doi:10.1021/cr100025t [doi]

- Terrovitis, J., Stuber, M., Youssef, A., Preece, S., Leppo, M., Kizana, E., . . . Abraham, M. R. (2008). Magnetic resonance imaging overestimates ferumoxide-labeled stem cell survival after transplantation in the heart. *Circulation*, *117*(12), 1555-1562. doi:10.1161/CIRCULATIONAHA.107.732073 [doi]
- Thakor, A. S., Jokerst, J. V., Ghanouni, P., Campbell, J. L., Mitra, E., & Gambhir, S. S. (2016). Clinically approved nanoparticle imaging agents. *Journal of Nuclear Medicine : Official Publication, Society of Nuclear Medicine*, *57*(12), 1833-1837. doi:jnumed.116.181362 [pii]
- Thomsen, H. S., Morcos, S. K., Almen, T., Bellin, M. F., Bertolotto, M., Bongartz, G., . . . ESUR Contrast Medium Safety Committee. (2013). Nephrogenic systemic fibrosis and gadolinium-based contrast media: Updated ESUR contrast medium safety committee guidelines. *European Radiology*, *23*(2), 307-318. doi:10.1007/s00330-012-2597-9 [doi]
- Toso, C., Vallee, J. P., Morel, P., Ris, F., Demuylder-Mischler, S., Lepetit-Coiffe, M., . . . Berney, T. (2008). Clinical magnetic resonance imaging of pancreatic islet grafts after iron nanoparticle labeling. *American Journal of Transplantation : Official Journal of the American Society of Transplantation and the American Society of Transplant Surgeons*, *8*(3), 701-706. doi:10.1111/j.1600-6143.2007.02120.x [doi]
- van Berlo, J. H., & Molkenkin, J. D. (2014). An emerging consensus on cardiac regeneration. *Nature Medicine*, *20*(12), 1386-1393. doi:10.1038/nm.3764 [doi]
- van der Spoel, T I, Jansen of Lorkeers, S J, Agostoni, P., van Belle, E., Gyongyosi, M., Sluijter, J. P., . . . Chamuleau, S. A. (2011). Human relevance of pre-clinical studies in stem cell therapy: Systematic review and meta-analysis of large animal models of ischaemic heart disease. *Cardiovascular Research*, *91*(4), 649-658. doi: 10.1093/cvr/cvr113 [doi]
- van Kranenburg, M., Magro, M., Thiele, H., de Waha, S., Eitel, I., Cochet, A., . . . van Geuns, R. J. (2014). Prognostic value of microvascular obstruction and infarct size, as measured by CMR in STEMI patients. *JACC.Cardiovascular Imaging*, *7*(9), 930-939. doi:10.1016/j.jcmg.2014.05.010 [doi]
- Veiseh, O., Gunn, J. W., & Zhang, M. (2010). Design and fabrication of magnetic nanoparticles for targeted drug delivery and imaging. *Advanced Drug Delivery Reviews*, *62*(3), 284-304. doi:10.1016/j.addr.2009.11.002 [doi]
- Venn, M., & Maroudas, A. (1977). Chemical composition and swelling of normal and osteoarthrotic femoral head cartilage. I. chemical composition. *Annals of the Rheumatic Diseases*, *36*(2), 121-129.
- Vina, E. R., & Kwoh, C. K. (2018). Epidemiology of osteoarthritis: Literature update. *Current Opinion in Rheumatology*, *30*(2), 160-167. doi:10.1097/BOR.0000000000000479 [doi]
- Vrijisen, K. R., Maring, J. A., Chamuleau, S. A., Verhage, V., Mol, E. A., Deddens, J. C., . . . Sluijter, J. P. (2016). Exosomes from cardiomyocyte progenitor cells and mesenchymal stem cells stimulate angiogenesis via EMMPRIN. *Advanced Healthcare Materials*, *5*(19), 2555-2565. doi:10.1002/adhm.201600308 [doi]

- Walczak, P., Kedziorek, D. A., Gilad, A. A., Barnett, B. P., & Bulte, J. W. (2007). Applicability and limitations of MR tracking of neural stem cells with asymmetric cell division and rapid turnover: The case of the shiverer dysmyelinated mouse brain. *Magnetic Resonance in Medicine*, *58*(2), 261-269. doi:10.1002/mrm.21280 [doi]
- Walczak, P., Kedziorek, D. A., Gilad, A. A., Lin, S., & Bulte, J. W. (2005). Instant MR labeling of stem cells using magnetoelectroporation. *Magnetic Resonance in Medicine*, *54*(4), 769-774. doi:10.1002/mrm.20701 [doi]
- Walczak, P., Ruiz-Cabello, J., Kedziorek, D. A., Gilad, A. A., Lin, S., Barnett, B., . . . Bulte, J. W. (2006). Magnetoelectroporation: Improved labeling of neural stem cells and leukocytes for cellular magnetic resonance imaging using a single FDA-approved agent. *Nanomedicine: Nanotechnology, Biology, and Medicine*, *2*(2), 89-94. doi:S1549-9634(06)00010-4 [pii]
- Wan, J., Cai, W., Meng, X., & Liu, E. (2007). Monodisperse water-soluble magnetite nanoparticles prepared by polyol process for high-performance magnetic resonance imaging. *Chemical Communications (Cambridge, England)*, (47):5004-6. doi(47), 5004-5006. doi:10.1039/b712795b [doi]
- Wang, J., & Jokerst, J. V. (2016a). Stem cell imaging: Tools to improve cell delivery and viability. *Stem Cells International*, *2016*, 9240652. doi:10.1155/2016/9240652 [doi]
- Ward, M. R., Abadeh, A., & Connelly, K. A. (2018). Concise review: Rational use of mesenchymal stem cells in the treatment of ischemic heart disease. *Stem Cells Translational Medicine*, doi:10.1002/sctm.17-0210 [doi]
- Wei, R., Zhou, T., Sun, C., Lin, H., Yang, L., Ren, B. W., . . . Gao, J. (2018). Iron-oxide-based twin nanoplates with strong T2 relaxation shortening for contrast-enhanced magnetic resonance imaging. *Nanoscale*, *10*(38), 18398-18406. doi:10.1039/c8nr04995e [doi]
- Weissleder, R., Elizondo, G., Wittenberg, J., Rabito, C. A., Bengel, H. H., & Josephson, L. (1990). Ultrasmall superparamagnetic iron oxide: Characterization of a new class of contrast agents for MR imaging. *Radiology*, *175*(2), 489-493. doi:10.1148/radiology.175.2.2326474 [doi]
- Weissleder, R., Stark, D. D., Engelstad, B. L., Bacon, B. R., Compton, C. C., White, D. L., . . . Lewis, J. (1989). Superparamagnetic iron oxide: Pharmacokinetics and toxicity. *AJR.American Journal of Roentgenology*, *152*(1), 167-173. doi:10.2214/ajr.152.1.167 [doi]
- Westman, P. C., Lipinski, M. J., Luger, D., Waksman, R., Bonow, R. O., Wu, E., & Epstein, S. E. (2016). Inflammation as a driver of adverse left ventricular remodeling after acute myocardial infarction. *Journal of the American College of Cardiology*, *67*(17), 2050-2060. doi:10.1016/j.jacc.2016.01.073 [doi]
- Wheaton, A. J., Borthakur, A., Shapiro, E. M., Regatte, R. R., Akella, S. V., Kneeland, J. B., & Reddy, R. (2004). Proteoglycan loss in human knee cartilage: Quantitation with sodium MR imaging--feasibility study. *Radiology*, *231*(3), 900-905. doi:10.1148/radiol.2313030521 [doi]

- Wollert, K. C., Meyer, G. P., Lotz, J., Ringes-Lichtenberg, S., Lippolt, P., Breidenbach, C., . . . Drexler, H. (2016). Intracoronary autologous bone-marrow cell transfer after myocardial infarction: The BOOST randomised controlled clinical trial. *Lancet (London, England)*, *364*(9429), 141-148. doi:10.1016/S0140-6736(04)16626-9 [doi]
- Wollert, K. C., Meyer, G. P., Muller-Ehmsen, J., Tschope, C., Bonarjee, V., Larsen, A. I., . . . Bauersachs, J. (2017). Intracoronary autologous bone marrow cell transfer after myocardial infarction: The BOOST-2 randomised placebo-controlled clinical trial. *European Heart Journal*, *38*(39), 2936-2943. doi:10.1093/eurheartj/ehx188 [doi]
- Xu, J. Y., Liu, D., Zhong, Y., & Huang, R. C. (2017). Effects of timing on intracoronary autologous bone marrow-derived cell transplantation in acute myocardial infarction: A meta-analysis of randomized controlled trials. *Stem Cell Research & Therapy*, *8*(1), 5. doi:10.1186/s13287-017-0680-5 [doi]
- Yang, H., Zhuang, Y., Sun, Y., Dai, A., Shi, X., Wu, D., . . . Yang, S. (2011). Targeted dual-contrast T1- and T2-weighted magnetic resonance imaging of tumors using multifunctional gadolinium-labeled superparamagnetic iron oxide nanoparticles. *Biomaterials*, *32*(20), 4584-4593. doi:10.1016/j.biomaterials.2011.03.018 [doi]
- Yang, K., Xiang, P., Zhang, C., Zou, L., Wu, X., Gao, Y., . . . Peng, C. (2011). Magnetic resonance evaluation of transplanted mesenchymal stem cells after myocardial infarction in swine. *The Canadian Journal of Cardiology*, *27*(6), 818-825. doi:10.1016/j.cjca.2011.07.633 [doi]
- Yeh, T. C., Zhang, W., Ildstad, S. T., & Ho, C. (1993). Intracellular labeling of T-cells with superparamagnetic contrast agents. *Magnetic Resonance in Medicine*, *30*(5), 617-625.
- Yousaf, T., Dervenoulas, G., & Politis, M. (2018). Advances in MRI methodology. *International Review of Neurobiology*, *141*, 31-76. doi:S0074-7742(18)30075-8 [pii]
- Yucesoy, B., Charles, L. E., Baker, B., & Burchfiel, C. M. (2015). Occupational and genetic risk factors for osteoarthritis: A review. *Work (Reading, Mass.)*, *50*(2), 261-273. doi:10.3233/WOR-131739 [doi]
- Yusuf, S., Hawken, S., Ounpuu, S., Dans, T., Avezum, A., Lanas, F., . . . INTERHEART Study Investigators. (2017). Effect of potentially modifiable risk factors associated with myocardial infarction in 52 countries (the INTERHEART study): Case-control study. *Lancet (London, England)*, *364*(9438), 937-952. doi:10.1016/S0140-6736(04)17018-9 [doi]
- Zamilpa, R., Navarro, M. M., Flores, I., & Griffey, S. (2014). Stem cell mechanisms during left ventricular remodeling post-myocardial infarction: Repair and regeneration. *World Journal of Cardiology*, *6*(7), 610-620. doi:10.4330/wjc.v6.i7.610 [doi]
- Zeng, Y., Wang, L., Zhou, Z., Wang, X., Zhang, Y., Wang, J., . . . Zhou, L. (2016). Gadolinium hybrid iron oxide nanocomposites for dual T1- and T2-weighted MR imaging of cell labeling. *Biomaterials Science*, *5*(1), 50-56. doi:10.1039/c6bm00706f [doi]
- Zhou, Y., Wang, S., Yu, Z., Hoyt, R. F., Sachdev, V., Vincent, P., . . . Horvath, K. A. (2009). Direct injection of autologous mesenchymal stromal cells improves myocardial function. *Biochemical and Biophysical Research Communications*, *390*(3), 902-907. doi:10.1016/j.bbrc.2009.10.074 [doi]

Zhu, J., Zhou, L., & XingWu, F. (2006). Tracking neural stem cells in patients with brain trauma. *The New England Journal of Medicine*, 355(22), 2376-2378. doi:355/22/2376 [pii]

Original publications

- I Korpi, R., Alestalo, K., Ruuska, T., Lammentausta, E., Borra, R., Yannopoulos, F., Lehtonen, S., Korpi, J., Lappi-Blanco, E., Anttila, V., Lehenkari, P., Juvonen, T., & Blanco Sequeiros R. (2017) Two novel direct SPIO labels and in vivo MRI detection of labeled cells after acute myocardial infarct. *Acta Radiologica Open*, 6(8), 1-10.
- II Alestalo, K., Korpi, R., Mäkelä, J., Lehtonen, S., Mäkelä, T., Yannopoulos, F., Ylitalo, K., Haapea, M., Juvonen, T., Anttila, V., Lappi-Blanco, E., Blanco Sequeiros, R.*, & Lehenkari, P.* (2015) High number of transplanted stem cells improves myocardial recovery after AMI in a porcine model. *Scandinavian Cardiovascular Journal*, 49, 82-94.
- III Rosenholm, J., Korpi, R., Lammentausta, E., Lehtonen, S., Lehenkari, P., Niemi, R., Xiao, W., Zhang, J., Lindberg, D., Gu, H., Sahlgren, C., & Blanco Sequeiros, R. (2015) Novel, fast-processed crystalline and amorphous manganese oxide nanoparticles for stem cell labeling. *Inorganic chemistry frontier*, 2, 640-48.
- IV Korpi, R.*, Ahola, S.*, Behrouz, G., Lammentausta, E., Karhula, S., Saarakkala, S., Rieppo, L., Finnilä, M., Stapf, S., Rosenholm, J., Blanco Sequieros, R., Nieminen, M., & Telkki, V. Diffusion of amorphous manganese oxide nanoparticles into articular cartilage. *Manuscript*.

Reprinted with permission from SAGE Publishing (License <http://www.creativecommons.org/licenses/by-nc/4.0/>) (I), Taylor & Francis (II), and Royal Society of Chemistry (III).

Original publications are not included in the electronic version of the dissertation.

1558. Merikukka, Marko (2020) Lapsuuden elinolojen yhteydet aikuisuuden hyvinvointiin : Kansallinen syntymäkohortti 1987 -rekisteritutkimus
1559. Ahonen-Siirtola, Mirella (2020) Surgical treatment of incisional ventral hernia : with a special reference to laparoscopic techniques
1560. Prusila, Roosa (2020) Clinical studies in adult lymphomas with special emphasis on late effects of treatments
1561. Kilpiö, Teemu (2020) Circulating factors in regulation of cardiac function and stress response
1562. Tiulpin, Aleksei (2020) Deep learning for knee osteoarthritis diagnosis and progression prediction from plain radiographs and clinical data
1563. Konstari, Sanna (2020) Systemic and dietary risk factors for knee osteoarthritis : associations of serum vitamin D, metabolic syndrome, dietary magnesium intake and serum C-reactive protein with the risk of knee osteoarthritis
1564. Julku, Johanna (2020) Early and later timed cervical headgear treatment : a randomized controlled trial
1565. Tonttila, Panu (2020) Multiparametric magnetic resonance imaging for the detection and characterisation of prostate cancer
1566. Tölli, Marja (2020) Identification and characterization of small molecule modulators of cardiac hypertrophy
1567. Heikkala, Eveliina (2020) Co-occurrence of unhealthy behaviours and psychosocial problems among adolescents, with special reference to low back and multisite musculoskeletal pains during adolescence and labour market exclusion in early adulthood
1568. Kinnunen, Sini (2020) The interaction of transcription factors GATA4 and NKX2-5 and the effect of interaction-targeted small molecules on the heart
1569. Yu, Jia (2020) Effects of loading, estrogen level, and aging on rat mandibular condylar cartilage
1570. Korhonen, Linda (2020) Pediatric forearm fractures with special reference to operatively treated shaft fractures and ulnar styloid process nonunion
1571. Similä, Toni (2020) Tooth loss among middle-aged adults in the Northern Finland Birth Cohort 1966 : associations with tobacco smoking and diabetes

S E R I E S E D I T O R S

A
SCIENTIAE RERUM NATURALIUM
University Lecturer Tuomo Glumoff

B
HUMANIORA
University Lecturer Santeri Palviainen

C
TECHNICA
Postdoctoral researcher Jani Peräntie

D
MEDICA
University Lecturer Anne Tuomisto

E
SCIENTIAE RERUM SOCIALIUM
University Lecturer Veli-Matti Ulvinen

E
SCRIPTA ACADEMICA
Planning Director Pertti Tikkanen

G
OECONOMICA
Professor Jari Juga

H
ARCHITECTONICA
University Lecturer Anu Soikkeli

EDITOR IN CHIEF
University Lecturer Santeri Palviainen

PUBLICATIONS EDITOR
Publications Editor Kirsti Nurkkala

ISBN 978-952-62-2612-5 (Paperback)
ISBN 978-952-62-2613-2 (PDF)
ISSN 0355-3221 (Print)
ISSN 1796-2234 (Online)